The Effects of XIAP Gene Therapy in a Murine Model of Leber's Hereditary Optic Neuropathy and a Feline Model of Retinal Detachment

Sarah Jeannette Wassmer

Thesis submitted to the Faculty of Graduate and Postdoctoral Studies

in partial fulfillment of the requirements for the

Ph.D. degree in Cellular and Molecular Medicine

Department of Cellular and Molecular Medicine

Faculty of Medicine

University of Ottawa

September 30, 2016

AUTHORIZATIONS

This Agreement between Sarah Wassmer ("You") and Springer ("Springer") consists of your license details and the terms and conditions provided by Springer and Copyright Clearance Center.

License Number 3956140984257
License date Sep 25, 2016
Licensed Content Publisher Springer
Licensed Content Publication Springer eBook
Licensed Content Title The Development of a Cat Model of Retinal Detachment and Re-attachment
Licensed Content Author Sarah Wassmer
Licensed Content Date Jan 1, 2016
Type of Use Thesis/Dissertation
Portion Full text
Number of copies 1
Author of this Springer article
Yes and you are the sole author of the new work
Order reference number
Title of your thesis / dissertation
The x-linked inhibitor of apoptosis (XIAP) gene therapy protects the optic nerve in a mouse model of leber's hereditary optic neuropathy and the retina in a feline model of retinal detachment
Expected completion date Oct 2016
Estimated size(pages) 50
Requestor Location Sarah Wassmer
95 Bronson Avenue
Unit 803
Ottawa, ON K1R1E2
Canada
Attn: Sarah Wassmer
Billing Type Invoice
Attn: Sarah Wassmer
Total 0.00 CAD

Dear Dr. Wassmer,

Thank you for your email.

Congratulations for your published paper entitled "Chitosan microparticles for delivery of proteins to the
retina".

I wish to inform you that you can use it for your thesis.

Meanwhile, you may find this link helpful.

What Rights Do I Retain as an Author?
http://service.elsevier.com/app/answers/detail/a_id/565/

Please ensure that the reference number remains in the subject line when responding to this email.

Should you require further assistance please visit Researcher Support where you will find 24/7 support
contact details, including live chat

Kind regards,
Joanna Mae Hermida
Researcher Support
Response Via Email (Jenalyn Balbedina)

This Agreement between Sarah Wassmer ("You") and Nature Publishing Group ("Nature Publishing Group") consists of your license details and the terms and conditions provided by Nature Publishing Group and Copyright Clearance Center.

License Number 3957090279943
License date Sep 27, 2016
Licensed Content Publisher Nature Publishing Group
Licensed Content Publication Nature Reviews Molecular Cell Biology
Licensed Content Title Mitochondria and cell death: outer membrane permeabilization and
beyond
Licensed Content Author Stephen W. G. Tait and Douglas R. Green
Licensed Content Date Sep 1, 2010
Licensed Content Volume Number
11
Licensed Content Issue Number
9
Type of Use reuse in a dissertation / thesis
Requestor type academic/educational
Format print and electronic
Portion figures/tables/illustrations
Number of figures/tables /illustrations
1
High-res required no
Figures Figure 1.
Author of this NPG article no
Your reference number
Title of your thesis / dissertation
The x-linked inhibitor of apoptosis (XIAP) gene therapy protects the optic nerve in a mouse model of leber's hereditary optic neuropathy and the retina in a feline model of retinal detachment
Expected completion date Oct 2016
Estimated size (number of pages)
50
Requestor Location Sarah Wassmer
Billing Type Invoice

This Agreement between Sarah Wassmer ("You") and Nature Publishing Group ("Nature Publishing Group") consists of your license details and the terms and conditions provided by Nature Publishing Group and Copyright Clearance Center.

License Number 3957090443015
License date Sep 27, 2016
Licensed Content Publisher Nature Publishing Group
Licensed Content Publication Nature Reviews Molecular Cell Biology
Licensed Content Title Regulated necrosis: the expanding network of non-apoptotic cell death pathways
Licensed Content Author Tom Vanden Berghe, Andreas Linkermann, Sandrine Jouan-Lanhouet, Henning Walczak, Peter Vandenabeele
Licensed Content Date Jan 23, 2014
Licensed Content Volume Number
15
Licensed Content Issue Number
2
Type of Use reuse in a dissertation / thesis
Requestor type academic/educational
Format print and electronic
Portion figures/tables/illustrations
Number of figures/tables /illustrations
1
High-res required no
Figures Figure 2.
Author of this NPG article no
Your reference number
Title of your thesis / dissertation
The x-linked inhibitor of apoptosis (XIAP) gene therapy protects the optic nerve in a mouse model of leber's hereditary optic neuropathy and the retina in a feline model of retinal detachment
Expected completion date Oct 2016
Estimated size (number of pages)
50
Requestor Location Sarah Wassmer
Billing Type Invoice

FULL TITLE

The X-linked Inhibitor of Apoptosis (XIAP) gene therapy protects the optic nerve in a mouse model of Leber's hereditary optic neuropathy and the retina in a feline model of retinal detachment.

ABSTRACT

In Canada alone, there were an estimated 800,000 visually impaired people in 2007, costing the federal government an annual amount of $15.8 billion in services, treatments and lost revenue. These costs are estimated to double by the year 2032, as the population ages. The leading causes of visual impairment and blindness is retinal degeneration, characterized by the progressive death of retinal cells. The research presented in this PhD thesis aimed to prevent retinal degeneration by over-expressing the X-linked Inhibitor of Apoptosis (XIAP) in retinal cells using plasmid and adeno-associated viral vectors. The work is divided into four sequential chapters targeted at developing an anti-apoptotic gene therapy strategy to prevent retinal cell death. The first chapter examines XIAP gene therapy in the treatment of Leber's Hereditary Optic Neuropathy (LHON). *In vitro* studies using the 661W cone-photoreceptor cell line showed that XIAP over-expression significantly lowers cell death when 661W cells are exposed to a number of apoptotic stimuli. In a mouse model of Leber's Hereditary Optic Neuropathy (LHON), XIAP expression in retinal ganglion cells (RGCs) protected the ultrastructure of the RGC axons within the optic nerve, in addition to providing evidence of functional protection. The second and third chapters further examine the potential for XIAP gene therapy in the treatment of retinal disease by developing an *in vivo* model of retinal detachment in cats,

followed by evaluating the efficacy of XIAP gene therapy intervention. When XIAP was over-expressed in the photoreceptor cells, there was significant structural protection and trends in preservation of function in this model of degeneration. Finally, the fourth chapter explores an alternate method to viral gene therapy by evaluating the efficacy and toxicity of chitosan microparticles as a protein delivery system to the retina. Results show that chitosan microparticles are mucosal-adhesive and are non-toxic at low concentrations *in vitro* in 661W cells and *in vivo* in rats. This thesis work provides strong evidence that XIAP gene therapy is an effective method for preventing retinal degeneration, and works as a broad spectrum gene therapy strategy that can be applied to different forms of retinal degeneration.

TABLE OF CONTENTS

LIST OF FIGURES

Figures (F) and supplemental figures (SF) in order of appearance

LIST OF TABLES

ABBREVIATIONS

2D	2-dimensional
661W	Immortalized mouse cone photoreceptor cell line
AAV	Adeno-associated virus
AIF	Apoptosis inducing factor
Apaf	Apoptotic protease-activating factor
Apo1/Fas/CD95	Fas ligand
BAD	BCL-2-associated death promoter
BAX	BCL-2-associated x protein
BCL	B-cell lymphoma
BIR	Baculovirus inhibitor of apoptosis protein Repeat
C_3F_8	Perfluoropropane
Cd/m^2	Candela per meter squared
$Cd\ m/s^2$	Candela meter per second squared
cIAP	Cellular inhibitor of apoptosis
CMP	Chitosan microparticle
COMMD	Copper metabolism domain containing
COX	Cytochrome c oxidase
Cybrids	Cellular hybrids
CYLD	cylindromatosis
DAPI	4',6-diamidino-2-phenylindole
Diablo	Direct inhibitor of apoptosis-binding
DISC	Death-inducing signaling complex

ERG	Electroretinogram
F	Phenylalanine
FADD	Fas-associated death domain
$FLIP_L$	FLICE-like inhibitory protein long isoform
GFP	Green Fluorescent Protein
GSH	glutathione
H	Histidine
H_2O_2	Hydrogen peroxide
H&E	Hematoxylin and eosin
Hz	Hertz
IAP	Inhibitor of apoptosis
IKK-β	Inhibitor of nuclear factor kappa-B kinase
INL	Inner nuclear layer
JNK	JUN N-terminal kinase
LC	Lamina cribrosa
LCA	Leber's congenital amaurosis
LHON	Leber's hereditary optic neuropathy
MEKK	Mitogen-activated protein kinase kinase
MIMP	Mitochondrial inner membrane potential
MLKL	Mixed lineage kinase domain-like
MOMP	Mitochondrial outer membrane permeabilization
MP	Microparticle
MRI	Magnetic resonance imaging

NADH	Nicotinamide adenine dinucleotide
ND4	NADH dehydrogenase Subunit 4
Nec1	Necrostatin 1
NF-κB	Nuclear factor kappa-B
NFL	Nerve fiber layer
ONL	Outer nuclear layer
PERG	Pattern electroretinogram
PhRc	Photoreceptor
R	Arginine
RD	Retinal detachment
RGC	Retinal ganglion cell layer
RING	Really interesting new gene
RIPK	Receptor interacting protein kinase
ROS	Reactive Oxygen Species
RPE	Retinal pigmented epithelium
RT-qPCR	Reverse transcriptase quantitative polymerase chain reaction
SD	Standard deviation
SE	Standard error
Smac	Second mitochondria-derived activator of caspase
SV40	Simian vacuolating virus 40
TAK	TGF-β-activated kinase
TB	Toluidine blue
TRADD	TNF receptor-associated death domain

TRAF	TNF receptor-associated factor
TRAIL	TNF-related apoptosis-inducing ligand
TNF-α	Tumor necrosis factor alpha
TNFR	Tumor Necrosis Factor Receptor
μ	Micro
UBA	Ubiquitin binding domain
WB	Western blot
XAF	XIAP-associated factor
XIAP	X-linked inhibitor of apoptosis
Y	Tyrosine
Z-VAD-FMK	arbobenzoxy-valyl-alanyl-aspartyl-[O-methyl]-fluoromethylketone

Dedicated to all those suffering from vision impairment.

ACKNOWLEDGEMENTS

"If I have seen further it is by standing on the shoulders of Giants." – Isaac Newton

To all the giants in my life, thank you for taking me further than I ever thought possible. There are so many people to thank and I do not want to make the thesis any longer than it already is, so to the following, I express my sincerest appreciation:

First and foremost, I would like to thank my dedicated supervisor, Dr. Catherine Tsilfidis. Thank you for your guidance, support and friendship over the past years. Your leadership and direction have made me want to pursue a career in science, and hopefully one day follow in your footsteps. Thank you for always encouraging me to take chances on new ideas and directions. I've had such a wonderful time learning from you! I have had a remarkable experience because of you.

I would also like to thank Adam Baker, Dr. Wai Gin Fong and Dr. Alan Mears for all of their help and instruction in the laboratory. Thank you for always answering my endless stream of questions and being so patient. Also thank you to Dr. Robert Korneluk, Dr. David Park and Dr. Erik Suuronen for guiding me throughout this thesis and making every TAC meeting a positive learning experience.

A sincere thank you to Dr. Buhrmann and Dr. Hincke for being my supervisors as I explored positions working in the Ophthalmic Surgical Simulation Center and the anatomy laboratory. Your never-ending kindness and faith in me has cultivated the passionate teacher that I am today. Thank you for helping me to develop as a medical educator.

To my wonderful friends, Heather Goldthorpe, Mirabelle and Miriel Ho, Alexa Hryniuk, Sarah Kawesa, Roshan Kumar and Pamela Lagali, without whom I could not

have completed this process. It helped so much to have such incredible people surround me throughout the day. Thanks for the stimulating conversation and all of the troubleshooting.

To my dad, my favorite geneticist, who sparked my interest in science at a young age—I would not be here without you. Thank you for continually answering my math questions and reading over my work. I always treasure our deep conversations about science and the world. And to my incredible mother, thanks for always making me laugh and showing me what it means to earn a PhD. Your work ethic is one I will always try to live up to. I am so proud to be your daughter and hope I can touch people's lives the way you do.

To my siblings and grandparents, thank you for sticking with me through this journey and for all of your love and encouragement along the way. I look forward to continuing my career and making you proud.

Last but not least, thank you to my husband, Brendan, who has been through it all, every step of the way. You've attended every WIP and Ophthalmology Research Day, listened to every practice presentation and helped me prepare for each lab meeting. I could not have done this without you. Thank you for your unwavering love, patience when one hour at the lab on a Saturday turns into four, understanding when I'm in a bad mood because something unexplainable happened to my science, and caring about my work when you don't understand a word. We often joke you're a "Science widow", but truly, thanks for believing in what I do, supporting me and knowing that I will make a difference.

CHAPTER 1: INTRODUCTION

The Retina

The vertebrate retina is composed of seven specialized cell types that are segregated into three main layers: the retinal ganglion cell (RGC) layer, the inner nuclear layer (INL) and the outer nuclear layer (ONL) (Dyer and Cepko, 2001) (Figure 1.1). The ONL is composed of rod and cone photoreceptors, which convert light into electrical energy that is propagated to the interneurons (bipolar, amacrine and horizontal cells) within the INL (Crescitelli, 1972; Dyer and Cepko, 2001). This electrical signal is subsequently transmitted to the brain by RGCs within the ganglion cell layer (Crescitelli, 1972; Levitan and Buchsbaum, 1993). Specifically, it is the nerve fiber layer (NFL) composed of the axons from each RGC that ultimately forms the optic nerve to send the information to the brain. Also within the neural retina are the support glia called Müller cells, which span all three layers (Livesey and Cepko, 2001). Müller cells interact with the retinal neurons to control the extracellular environment (Newman and Reichenbach, 1996). The "feet" or basement membrane of the Müller cells make up the inner limiting membrane (ILM) which creates the boundary between the retina and the vitreous cavity (Semeraro et al., 2015).

Rod cells, comprising 95% of the photoreceptor cells, are responsible for peripheral vision and vision in dim light whereas cone cells are responsible for central vision, colour vision in bright light and detailed visual acuity (Marieb, 2007). Both the cone and rod photoreceptor outer segments face the retinal pigmented epithelium (RPE) layer. RPE cells form a monolayer between the neural retina and the outer vasculature (Strauss, 2005). The RPE is essential for photoreceptor viability as it provides nutrition and ion transport, protection against photo-oxidation, molecule recycling (essential for

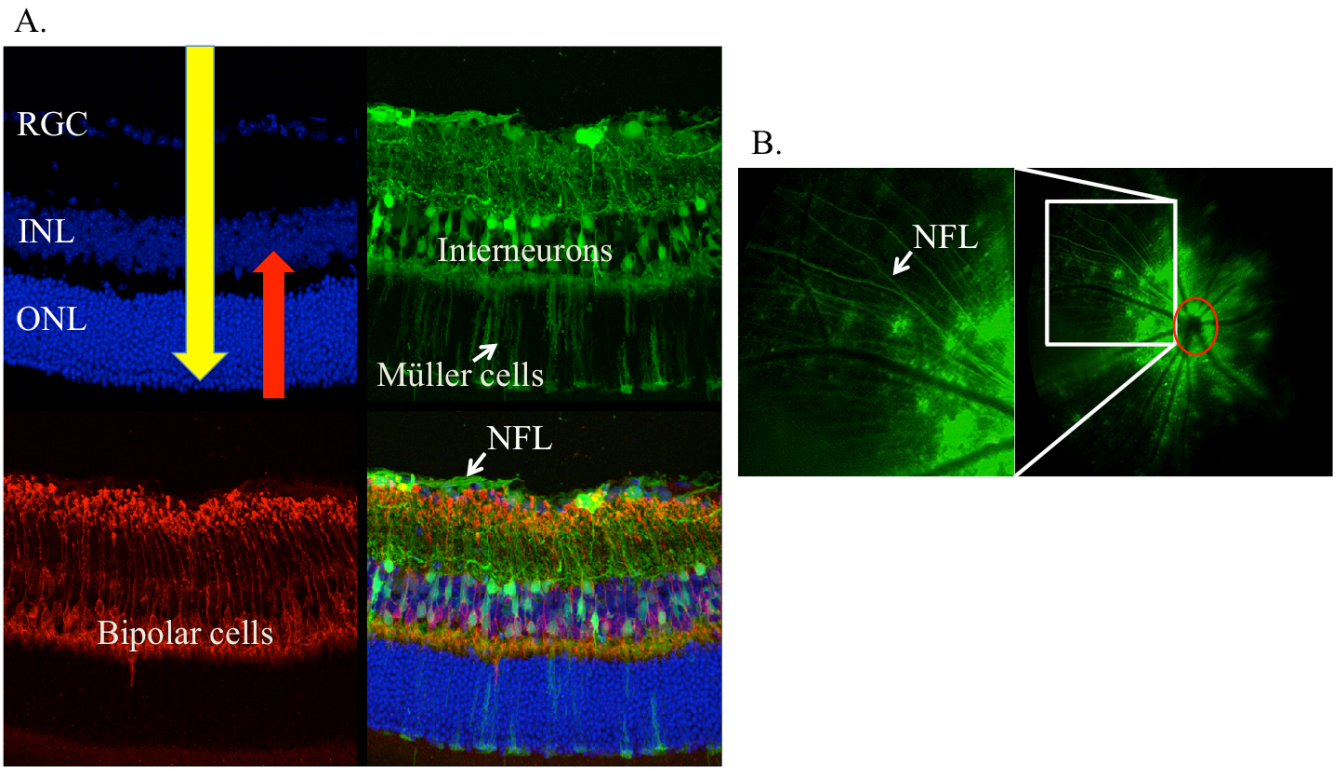

Figure 1.1. **The mammalian retina.**
Cross section (A) and fundus image (B) of the C57B6 mouse eye. Each of the four panels in (A) are the same section, imaged with various filters to show the different cell types in the retina. The light (yellow arrow) is converted into electrical energy by photoreceptors (red arrow), specifically rods and cones located in the outer nuclear layer (ONL). The impulse is then transmitted through the inner nuclear layer (INL), which is composed of interneurons, such as bipolar cells, to the retinal ganglion cells (RGC), whose axons make the nerve fiber layer (NFL). The NFL converges on the optic nerve (red circle in B) and transports the signal to the brain. The support cells of the retina are the Müller cells.

phototransduction), immune regulation and the blood retina barrier (Strauss, 2005). At the anterior margin of the neural retina is a ring-shaped structure called the ciliary body (CB). The CB controls the shape of the lens and produces aqueous humor to control intraocular pressure (Zhao et al., 2002). The CB is divided into two parts: pars plana and pars plicata. The pars plana is the portion closest to the neural retina whereas the pars plicata is the folded region where the zonules fibers attach to control the lens shape (Bhatia et al., 2010; Roll et al., 1975).

The Impact of Retinal Disease

Retinal degeneration, characterized by retinal cell death, affects more than 150 million people worldwide and this population is expected to double by the year 2020 (World Health Organization, 2010). Once a retinal cell undergoes cell death, the signaling to the brain is compromised and vision loss ensues (Chang et al., 1993; Remé et al., 2000).

Lost cells can be regenerated in certain species. In teleost fish, the support cells called Müller glia, and the stem cells within the ciliary marginal zone (the junction between the neural retina and the ciliary epithelium), are able to re-populate lost retinal cells (Raymond et al., 2006). In amphibians, this stem cell pool persists throughout life (Lamba et al., 2008). In response to injury, local Müller glia cells undergo dedifferentiation to produce neuronal progenitors that proliferate, migrate and differentiate into the respective retinal cell (Yurco and Cameron, 2005). Human retinal cells have little regenerative potential and are rarely able to differentiate into specific retinal cells (Nelson et al., 2013). The cells within the neural retina of the human eye are

permanently post-mitotic and do not regenerate to compensate for dead cells (Ezzeddine et al., 1997). As a result, any form of cell death in the retina disrupts the visual sensory pathway and ultimately leads to loss of vision.

Caspase Dependent Cell Death (Apoptosis)

The causes of many retinal diseases are unknown; what *is* known, however, is that cell death by apoptosis is often the final common pathway (Chang et al., 1993; Doonan and Cotter, 2004; Nickells and Zack, 1996; Travis, 1998). Apoptosis is a form of regulated programmed cell death which results in DNA destruction, little contamination of the surrounding environment, and speedy macrophage signaling for clean-up—while mounting a very limited and almost non-existent immune response (Cullen et al., 2013; Savill et al., 2002). It occurs when intrinsic or extrinsic stimuli activate the proteolytic caspase cascade. Caspases are cysteine proteases that are also proenzymes. The proenzyme (termed pro-caspase) requires proteolysis to be activated, at which point the active enzyme triggers the caspase cascade and instigates cellular execution by cleaving cellular and structural proteins, DNA repair enzymes and endonuclease inhibitors (Travis, 1998).

The intrinsic apoptotic pathway is stimulated by DNA damage, oxidative stress, mitochondrial damage and organelle malfunction (Figure 1.2). When these factors occur, the outer membrane of a mitochondrion forms pores (through a process called mitochondrial outer membrane permeabilization (MOMP) that release cytochrome C. Cytochrome C activates caspase 9 (via apoptosome formation with Apaf-1), which subsequently activates caspase 3 (Schuler et al., 2000). The Bcl-2 family of proteins is

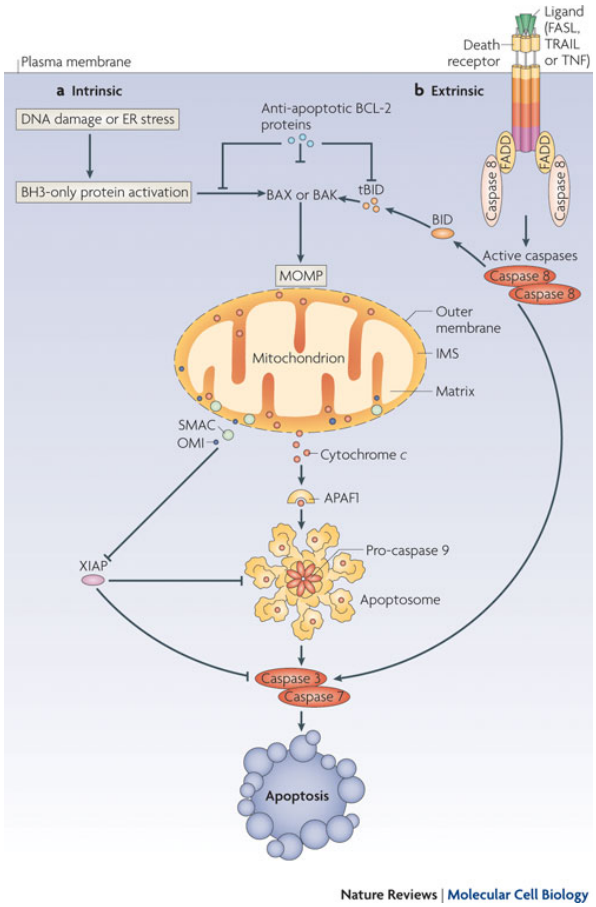

Figure 1.2. **The apoptotic pathway.**
(a) The non-receptor or mitochondrial-mediated intrinsic apoptotic pathway results in mitochondrial permeability, due to the translocation of BAX and BAK (pro-apoptotic BCL-2 family member) into the mitochondrial membrane. Consequently, there is a release of pro-apoptotic proteins into the cellular cytosol. These proteins include cyctochrome c, SMAC/DIABLO and HtrA2/Omi. They further stimulate the caspase-dependent pathway of apoptosis. As such, cyctochrome c binds to protein apoptotic protease-activating factor 1 (Apaf-1) to form the apoptosome. The apoptosome subsequently cleaves and activates pro-caspase-9, which will in turn activate the effector caspases 3 and 7 (from inactive pro-caspases). Meanwhile, Smac/DIABLO and HtrA2/Omi inhibit the IAP family. Together, this leads to cell death as the caspases fragment nuclear and cellular structural proteins, repair enzymes and endonuclease inhibitors (Vucic et al., 2011).
(b) The extrinsic pathway for apoptosis is receptor mediated, such as Fas (CD95), TNF-α or TRAIL ligands binding to their respective death receptor. This pathways works to directly activate the effector caspases (bypassing the apoptotosme and capase-9) to initiate cell death. Specifically, ligand-receptor binding initiates the formation of receptor-associated death-inducing signaling complex (DISC). Once this occurs, FADD (Fas associated death domain protein) and pro-caspase8 are recruited, this binding results in dimerization and activation or caspase 8 which will cleave and activate caspase 3 and 7. Image taken with permission from (Tait et al., 2013).

involved in the intrinsic pathway. This family is composed of an anti-apoptotic subgroup, a pro-apoptotic subgroup and a BH3 subgroup (Taylor et al., 2008). Within these three subgroups, multiple members such as Bim, Bid, Bax, Bak and Bok exist. All members of the pro-apoptotic group have the ability to directly or indirectly (through inhibition of anti-apoptotic factors) cause the release of cytochrome C from mitochondria leading to apoptosis (Adams and Cory, 2001; Zamzami and Kroemer, 2001).

The extrinsic pathway of apoptosis is stimulated by the binding of a ligand to a death receptor on the surface of the cell (Figure 1.2). For example, the binding of a tumor necrosis factor (TNF) family ligand to its appropriate receptor (eg. Fas with Apo-1, TRAIL with TRAIL receptor) triggers the stimulation of death signal adaptor proteins (eg. FADD; Cheung et al., 2006, 2008; Nuñez et al., 1998). The death signal adaptor proteins form a death inducing signaling complex, which activate the caspase cascade (Tran et al., 2001). It is important to note that the two pathways are not mutually exclusive and that extrinsic factors can also promote mitochondrial disturbances and apoptosis via cytochrome C (Nuñez et al., 1998).

In this thesis, TNF-α is used to stimulate cellular death *in vitro* (Figure 1.3). Upon binding of TNF-α to its receptor, TNF receptor associated death domain (TRADD) and receptor-interacting protein kinase 1(RIPK1) are recruited to form TRADD-RIPK1 dependent complex, which also attracts cellular inhibitor of apoptosis 1 and 2 (cIAP1/2; more on the IAPs to follow), and TNF receptor-associated factor 2 and 5 (TRAF2/5). Consequently, cIAP1/2 ubiquitinate RIPK1, which activates the Iκκ complex. The activated Iκκ complex phosphorylates Inhibitor of KB (IκB), and causes it to degrade thereby allowing p50/RelA to move into the nucleus where it will work to activate target

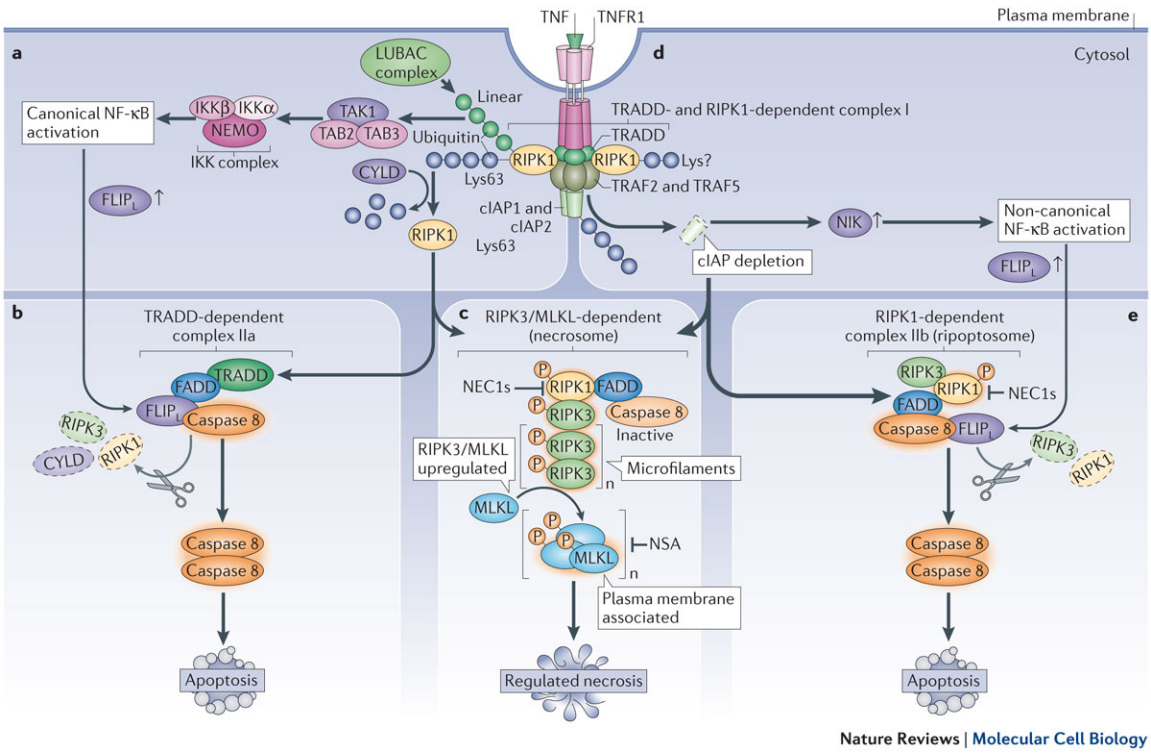

Figure 1.3. **TNF-α mediated cell death.**
If cIAPs are present and the canonical NF-κB pathway is activated (a), the long isoform of FLIP ($FLIP_L$) is expressed and along with pro-caspase 8 will form a heterodimeric complex (TRADD-dependent complex IIa), that will inactivated RIPK1, RIPK3 and cylindromatosis (CYLD), thereby negating necroptotic cell death (b), and leading to apoptosis upon the simultaneous activation of caspase 8. However, in the presense of caspase or RIP inhibitors, a RIPK1 and RIPK3 scaffold-like complex is formed called the "necrosome", which mediates regulated necrosis (c). On the other hand, in the absence of cIAPs and activation of the NF-κB pathway in a non-canonical fashion (d), a TRADD independent complex is formed and similar to panel (b), $FLIP_L$ and pro-caspase 8 will form a heterodimeric caspase (along with RIPK1 and RIPK3, called the "ripoptosome") to carry out the apoptotic pathway. However, this can also lead to necroptosis in the absence of caspase 8. Image taken with permission from (Berghe et al., 2014).

genes (pro- and anti-apoptotic genes, cytokines, chemokines and anti-microbial peptides) (Liu et al., 2004; Silke et al., 2004; Sun, 2011). This is the canonical or classical NF-κB pathway. Alternatively, cIAP1/2 ubiquitinate NIK in the non-canonical pathway, which represses its activity. However, the recruitment of cIAPs to several TNF family receptors ultimately leads to its own degradation (or the presence of cIAP antagonists) and consequently the liberation of NIK (Fulda and Vucic, 2012). NIK is required for phosphorylation of p100, which becomes p52 and comprises the p52/RelB complex. This complex travels to the nucleus and promotes transcriptional activation of NF-κB target genes (Hunter et al., 2007; Varfolomeev et al., 2007). In summation, the E3 ligase domain of either cIAP1/2 is required for ubiquitination of RIP1 in order for TNFα to activate the NF-κB classical pathway. Furthermore, degradation of cIAP1/2 is needed for activation of the alternative NF-κB pathway (Gentle et al., 2011; Vince et al., 2007; Zarnegar et al., 2008).

Through the classical pathway, FLICE-like inhibitory protein long ($FLIP_L$) is up-regulated and along with pro-caspase-8 forms a heterodimer that cleaves and inactivates RIPK1, RIPK3 and CYLD to inhibit necroptosis (Berghe et al., 2010; Bertrand and Vandenabeele, 2011). However, through this inactivation, pro-caspases 8 is quickly autoproteolysed and activated. Caspase 8 is now able to cleave the effector caspases 3 and 7 to initiate apoptosis. If caspase 8 is inhibited, it is thought that RIPK1 and RIPK3 will form the 'necrosome', ultimately leading to regulated necrosis (Berghe et al., 2014).

Finally, in the non-classical pathway and in the absence of cIAPs, a large TRADD-independent cytosolic complex is formed between RIPK1, RIPK3, FADD and $FLIP_L$/caspase 8 heterodimer, which is called the 'ripoptosome'. Similarly to what was

described above, caspase 8/$FLIP_L$ heterodimer inactivates RIPK1 and RIPK3, which in turn activates caspase 8, thereby leading to apoptosis (Berghe et al., 2014), (Figure 1.3).

Taken together, depending on the context, TNF-α ligand and receptor binding can mediate apoptosis and regulated necrosis. The X-linked inhibitor of Apoptosis (XIAP) has been shown to directly inhibit the ripoptosome (Tenev et al., 2011), the necroptosome (Yabal and Jost, 2015; Yabal et al., 2014) and apoptosis (Schile et al., 2008).

The X-linked Inhibitor of Apoptosis (XIAP)

In addition to the members of the Bcl-2 family, there are other genes that tightly regulate the apoptotic pathway within the cell. XIAP is a member of the inhibitor of apoptosis (IAP) family of proteins, which includes other members such as cellular IAP 1 (cIAP1) and cellular IAP 2 (cIAP2), as presented above. IAPs suppress programmed cell death by interacting with and inhibiting the catalytic activity of caspases. These genes contain Baculovirus IAP Repeat (BIR) domains, a Ubiquitin Binding Domain (UBA) and ubiquitin E3 ligase activity on the Really Interesting New Gene (RING) domain (Cheung et al., 2008). The BIR domains directly bind and inhibit caspase proteins. The UBA and RING domains enable the IAPs to autoubiquitinate (when apoptosis must ensue), ubiquitinate other proteins (such as caspases) and play a role in signal transduction pathways (Galbán and Duckett, 2010). XIAP is the most potent inhibitor of cell death. It binds caspases-3, -7 and -9, thus impeding proteolytic activity and subsequent cell death (Cheung et al., 2006) (Figure 1. 4).

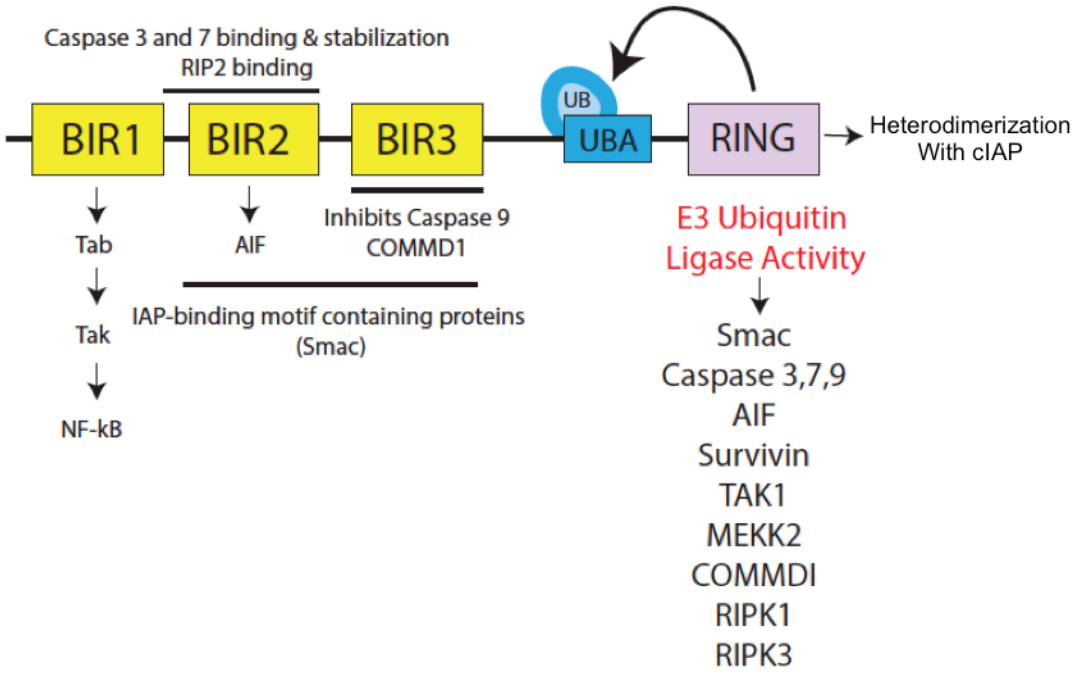

Figure 1.4. **XIAP's functional domains.**
XIAP is a 497 amino acid protein with potent E3 ubiquitin protein ligase activity imparted by its RING (really interesting new gene) domain. It is also composed of three BIR (baculovirus IAP repeat) motifs and one UBA (ubiquitin-associated) domain, which is characteristic to the IAP family. XIAP's E3 ubiquitin ligase activity can mark various proteins for proteasome degradation, such as its own inhibitor, Smac, caspase enzymes, and apoptosis inducing factor (AIF). Together with XIAP-associated factor (XAF1), XIAP mediates Survivin down-regulation by canonical ubiquitination. Furthermore, XIAP physically interacts with TGF-β activated kinase 1 (TAK1) and also ubiquitinates it to mediate formation of TAB/IκB kinase to activate p65/RelA and induce pro-survival gene expression via NF-κB pathway. Furthermore, XIAP ubiquitinates MEK kinase 2 (MEKK2) to evoke a second wave of NF-κB activation. Moreover, XIAP regulates intracellular copper levels by ubiquitinating copper metabolism domain containing 1 (COMMD1). XIAP in addition to the cIAPs controls inflammation and the RIP kinase apoptosome by ubiquitination of RIPK1 and RIPK3 to propagate pro survival signals through NF-κB signaling. XIAP can also use its own RING domain to autoubiquitinate, or be ubiquitinated by other proteins due to its UBA domain.
Adapted from: (Galbán and Duckett, 2010; Gyrd-Hansen et al., 2008; Holcik and Korneluk, 2001; Lawlor et al., 2015; Lenhausen et al., 2016; Nielsen and LaCasse, 2016; Plati et al., 2011, 2011; Rajalingam and Dikic, 2009; Wilkinson et al., 2008; Yabal et al., 2014).

Under conditions of irreparable damage, the cell must undergo apoptosis. In order for this to happen, second-mitochondria derived activator of caspases (Smac), a cellular IAP antagonist, is released from the mitochondria into the cytoplasm. It inhibits XIAP ubiquitin ligase to allow the cell to undergo apoptosis (Creagh et al., 2004). However, depending on the degree of damage to the cell, Smac can inhibit XIAP or XIAP can inhibit Smac. Recent studies have shown that, in response to intrinsic apoptotic signaling by BH3 proteins, XIAP can translocate to the mitochondria. Contradicting opinions of XIAP's role in the mitochondria have been presented. Owens *et al*. (Owens et al., 2010) suggest that XIAP may induce MOMP in an E3 ligase-dependent manner and subsequently acts as a pro-apoptotic factor. However, Hamacher-Brady *et al*. report that while inside the mitochondria, XIAP acts in an anti-apoptotic manner to recruit endolysosomes and degrade Smac, thereby reinforcing the potent effects XIAP can have over controlling apoptosis in the cytoplasm (to inhibit the caspases) and within the mitochondria (Hamacher-Brady et al., 2014). Furthermore, the most recent work by Hamacher-Brady shows that XIAP translocates to the mitochondria when apoptosis is induced by TNF or staurosporine (a broad kinase inhibitor), and that XIAP over-expression slows the onset of mitochondrial permeabilization, and it works within the mitochondria to degrade Smac, independent from cytochrome C release (Hamacher-Brady and Brady, 2015). These studies show that XIAP tightly regulates cell death in both the cell's cytoplasm and within the mitochondrial organelle, ultimately reducing the contribution of the mitochondria to apoptosis within the intrinsic pathway. In summation, the mediation of MOMP by BH3-members of the Bcl-2 family of proteins is ultimately suppressed by XIAP.

In addition to Smac, there are other proteins that allow a cell to inhibit or degrade XIAP in order to allow apoptosis. Many of these proteins (including Smac) possess a tetrapeptide domain termed an IAP binding motif (IBM). Notable examples of IBM containing proteins are Omi/HrtA2, CLPX, LRPPR, GdH and Nsp4. For example, Omi/HrtA2 regulates levels and functions of IAPs by irreversibly binding to BIR2 and BIR3 domains to inhibit anti-apoptotic function (van Loo et al., 2002; Yang et al., 2003). Like Smac, Omi is present in the mitochondria and, upon apoptotic stress, translocates to the cytoplasm with the aid of pro-apoptotic Bcl2-family members (Suzuki et al., 2001). In contrast, AIF and ARTS are proposed to antagonize XIAP through IBM independent means.

Proteasome inhibition experiments confirm XIAP and cIAP autoubiquitination by the RING domain (Galbán and Duckett, 2010). Under severe cellular stress, XIAP will autoubiquitinate and target itself for degradation to allow the cell unhampered caspase activation and destruction (Liston et al., 2003). Yang *et al* showed that proteasome inhibitors stabilized RING-containing IAPs to rescue thymocytes treated with death stimuli (Yang et al., 2000). The exact mechanism behind initiation and regulation of XIAP autoubiquitination remains unanswered. For example, does XIAP autoubiquitinate because the cell is dying or does the cell die because XIAP autoubiquitinates? There is also controversy with regards to XIAP-interacting proteins and their ability to initiate XIAP autoubiquitination (Galbán and Duckett, 2010). It has been shown that under specific conditions, this interaction can initiate the RING-dependent autoubiquitination of XIAP (Bertrand et al., 2008; Silke et al., 2004). However, some studies suggest that the

E3 ligase activity responsible for XIAP's ubiquitination may be caused by another protein's RING E3 ligase activity, such as cIAP1 (Galbán and Duckett, 2010).

Non-Caspase Roles for XIAP

XIAP mediated neuroprotection is more robust than caspase inhibitors alone because XIAP also plays multiple roles in caspase-independent pathways to inhibit cell death. Studies have suggested that XIAP can regulate the NF-κB pathway, TRAIL-mediated apoptosis and necroptosis. Each of these is briefly discussed below.

It is postulated that XIAP has a role in augmenting NF-κB activation during innate immunity (Bauler et al., 2008). XIAP may do this by mediating synergy between Toll-like and Nod-like receptors via activation of JNK and NF-κB pathways (Zarnegar et al., 2008). In addition, the BIR and RING domains of XIAP may have the ability to interact with TGFB receptor and promote TAK-1 activation of the classical NF-κB pathway and the JNK pathway, which ultimately activate transcription of NF-κB target genes (Hunter et al., 2007). Furthermore, activation of NF-κB increases expression of survival genes such as XIAP (Vince et al., 2007). Interestingly, retinal degeneration is characterized by NF-κB activation, which should therefore promote XIAP expression and cell survival (Bauler et al., 2008). It is also intriguing that oxidative stress activates NF-κB (anti-apoptotic agent) while it also causes cellular apoptosis (Chen et al., 2011; Krishnamoorthy et al., 1999). Furthermore, NF-κB activation results in the production of proinflammatory molecules, which induce neurotoxicity *in vivo*. Zeng *et al* showed that *rd* mice, a model of retinal degeneration, display significant NF-κB activation (Zeng et al., 2008). Despite the fact that the literature states NF-κB promotes cell survival genes, it

has been hypothesized that it may also be associated with photoreceptor cell death by regulation of pro-inflammatory molecules (Zeng et al., 2008). This simply proves that there must be a fine balance between NF-κB activation and suppression to maintain normal homeostasis. Surpassing the threshold can lead to cell death.

Among the TNF ligand members, TRAIL can mediate apoptosis in tumor cell lines (Ng et al., 2002). XIAP mediates TRAIL/Apo2L resistance to apoptosis in cancer cell lines. Consequently, XIAP down regulation by ActD allows release of cytochrome C from the mitochondria and overturns TRAIL mediated apoptosis (Ng et al., 2002; Zhang and Fang, 2004).

Necrosis is un-programmed cell death due to injuries or infection (noxious stimuli). The leakage of cellular debris is the cause of subsequent inflammation, which is amplified by the lack of signaling for macrophage clean-up. (Savill et al., 2002). The release of harmful chemicals and enzymes (stored in lysosomes) digest the dying cell and neighbouring cells thereby causing exponential damage. This is in contrast to the regulated form of necrosis, known as necroptosis which is mediated by the Receptor Interacting serine-threonine Protein (RIP) kinases 1 and 3, as described above (Berghe et al., 2010). As previously explained, RIP kinase activity is required for the assembly of the ripoptosome, which is composed of RIPK1, FADD and caspase-8, and can stimulate both apoptosis and caspase-independent necrosis (Silke and Meier, 2013; Vince et al., 2012). XIAP and the cIAPs are negative regulators of ripoptosome-mediated caspase-8 apoptosis and necrosis (Bertrand and Vandenabeele, 2011; Bertrand et al., 2008; Feoktistova et al., 2011; Tenev et al., 2011). It has been suggested that XIAP and the cIAPs function as inhibitors of ripoptosome assembly by direct ubiquitination of the

components of the ripoptosome (Imre et al., 2011). Necrostatin 1 (nec1) is also a potent inhibitor of RIP1 and consequently the necroptosis pathway (Feoktistova et al., 2011).

Autophagy is the highly conserved process of cellular recycling by lysosomes (Towers and Thorburn, 2016). The self-degradation of proteins, organelles and pathogens occurs under metabolic and physiological stress (He and Klionsky, 2009). Consequently, autophagy prevents the accumulation of toxic elements to maintain homeostasis (Nair and Klionsky, 2011). Specifically, the autophagosome, a double membrane vesicle, is formed to ingest damaged cellular components and foreign bodies, which then fuses with the membrane of a lysosome for degradation. This vesicle is termed the autolysosome, and its contents are recycled back into the cytosol to provide the basic material for cellular functions (Nair and Klionsky, 2011; Yorimitsu and Klionsky, 2005). This process is mediated by autophagy-associated genes (atg) such as Beclin1 (atg6) and atg5, which are required for formation and extension of the phagophore membrane (Igci et al., 2016). Changes in these proteins cause a dysregulation in autophagy. For example, inhibition of atg5 quickly leads to apoptosis (Chinskey et al., 2014; Yorimitsu and Klionsky, 2005).

Autophagy is essential for the physiological and metabolic activity of photoreceptor cells, as it is involved in degradation of phototransduction proteins, which ultimately prevents retinal degeneration (Yao et al., 2016). Dysregulation of autophagy contributes to visual diseases such as Leber's congenital amaurosis, retinitis pigmentosa, age-related macular degeneration and retinal detachment (Bo et al., 2015). Autophagy, in addition to necroptosis and apoptosis is initiated in a model of retinal detachment (Dong et al., 2014). Autophagy acts as a protective measure in photoreceptor cells upon

detachment, to delay apoptosis, thus increasing the window for cellular recovery (Chinskey et al., 2014). Furthermore, XIAP and cIAP1 work to increase Beclin1 levels via NF-κB pathway (by use of E3 ubiquitin ligase) to stimulate autophagy (Lin et al., 2015), and therefore reduce apoptosis.

Most retinal diseases have some element of apoptosis, necroptosis or autophagy in their disease pathology. Consequently, gene therapy with XIAP should be effective in halting or preventing vision loss in the diseased retina. This hypothesis will be tested in this thesis using two different types of retinal degeneration: retinal detachment and Leber's hereditary optic neuropathy (LHON).

Retinal Detachment

Retinal cells undergo apoptosis after a retinal detachment (RD), which occurs when there is trauma to the eye, accumulation of fluid in the subretinal space or tractional pulling of vitreous bands, which induce a separation between the RPE and sensory neural retina. The outermost layer of the retina, namely the photoreceptors, depend on the underlying RPE and choroid vasculature for maintenance of homeostasis (Jalali, 2003). Erickson *et al* showed histological evidence that retinal degeneration ensues as early as one hour post retinal detachment in cats, due to loss of trophic support from the underlying RPE and choroidal blood vessels (Erickson et al., 1983). Despite the fact that retinal reattachment surgery is anatomically effective, visual acuity is often compromised and depends on the nature and duration of the detachment. This loss of vision is augmented if the macula (area of the central retina which provides acute resolution) is involved in the detachment (Erickson et al., 1983).

The cause for vision loss following retinal detachment is photoreceptor apoptosis and necroptosis (Arroyo et al., 2005; Huckfeldt and Vavvas, 2013). In addition, there are changes in photoreceptor characteristics, such as shortening of the outer segments, retraction of rod terminals from the outer plexiform layer and protein redistribution. Furthermore, there is remodeling of the synapses of second-order neurons and proliferation of retinal glial cells (Fisher and Lewis, 2003).

Rodent models of retinal detachment show a peak of cell death between 1 and three days post-detachment, depending on the method for creating the retinal detachment (Cook et al., 1995; Matsumoto et al., 2013, 2014; Yang et al., 2004; Zacks et al., 2003). The physical separation of the retina from the underlying RPE actives caspase-8 and caspase-9, and leads to an increase in transcription of TNF-α, all leading to the cell death of photoreceptors by apoptosis (Nakazawa et al., 2011; Zacks et al., 2004). However, apoptosis is not the only contributor to photoreceptor death in RD. Despite the apoptotic pathway being activated, it has been shown that the pan-caspase inhibitor, Z-VAD-FMK (benzyloxycarbonyl-Val-Ala-DL-Asp-[Ome] fluoromethylketone) fails to prevent photoreceptor cell death. Receptor Interacting Protein (RIP) kinase 1 and 3-mediated necroptosis is a significant contributor to photoreceptor cell death. Consequently, when caspases are inhibited, cell death results via necroptosis. As a result, when necroptotic inhibitor, necrostatin-1 and Z-VAD-FMK are both present, cell death and oxidative stress are reduced. This shows that simultaneous inhibition of RIP kinase and caspases is necessary to prevent cell death in retinal detachment (Trichonas et al., 2010). Fortunately, XIAP works to prevent both caspase and RIPK dependent cell death, and structural evidence is shown by neuroprotection in a rodent model of RD which was rescued with

AAV-XIAP (Zadro-Lamoureux et al., 2009). Furthermore, cell death due to retinal detachment in the Bax knock out mice, was lowered compared to controls, indicating the involvement of cellular apoptosis in retinal detachment-mediated photoreceptor cell death (Yang et al., 2004).

Leber's Hereditary Optic Neuropathy

Leber's Hereditary Optic Neuropathy (LHON) is a maternally inherited mitochondrial disease that preferentially affects young males and leads to degenerative loss of the retinal ganglion cells (RGCs) and their axons (Farrar et al., 2013). The disease is caused by a single mutation in mitochondrial DNA which encodes one subunit of the NADH dehydrogenase (ND1, ND4, or ND6). A total of 7 ND subunits and approximately 34 other polypeptides make up Complex 1 of the electron transport chain, involved in oxidative phosphorylation (Kirches, 2011). LHON pathology is generally limited to the eye, but in rare cases, additional symptoms can occur, including a multiple-sclerosis-type syndrome associated with brain lesions (Kovács et al., 2005). LHON severity can be influenced by smoking and alcohol consumption (Kirkman et al., 2009). Not all LHON patients will go blind; approximately half of male patients and 10% of female patients will experience vision loss (Yu-Wai-Man et al., 2014). One hypothesis for the striking male bias of the disease is hormonal; RGCs have high amounts of estrogen beta-receptors and treatment of LHON cybrids (cellular hybrids containing mutant LHON mitochondria) with estrogen compounds have reduced reactive oxygen species (ROS) (Giordano et al., 2011). Alternatively, there may be an X-linked recessive modifier gene acting in conjunction with mitochondrial DNA, which results in vision loss

(Hudson et al., 2005; Shankar et al., 2008). Another hallmark of the disease is spontaneous recovery in some patients after onset of vision loss. It has been suggested that ETC dysfunction may cause optic nerve swelling which blocks RGC function, thus causing a reduction in central vision. However, if a significant number of RGCs do not undergo apoptotic cell death (atrophic phase), the vision loss in this acute phase is reversible (cells are still alive but not functioning optimally) (Gueven, 2014; Howell, 1998).

This thesis will focus on the most common LHON mutation; G to A point mutation within the mitochondrial DNA of the ND4 subunit, at nucleotide 11778. This mutation substitutes the highly conserved arginine to a histidine at codon 340. Mutant R340H (mND4) is the most common point mutation in LHON patients, accounting for approximately 70% of all cases. Specifically, mutations in the ND4 subunit have been restricted to the ubiquinone binding site on Complex I (Degli Esposti et al., 1994). Esponsti et al., suggest that the amino acid substitution produces resistance of Complex I to its inhibitor rotenone, which should have the same binding site as ubiquinone (coenzyme Q10). As a result, the mutation causes a change in the affinity of Complex I to bind ubiquinone substrate (Degli Esposti et al., 1994). Consequently, there is a reduction of redox energy developed by the reaction of ubiquinone with complex I, resulting in a highly unstable form of ubiquinone (ubisemiquinone), which may contribute to the radical formation and the mitochondrial damage presented in LHON patients (Degli Esposti et al., 1994). Typically, ubisemiquinone anions are stabilized by positively charged amino acids, such as arginine. However, in the mutant form, the arginine is substituted to a less basic histidine which may reduce its stability. This causes a decrease

in potential redox difference for bound ubisemiquinone and NADH (its electron donor), which further reduces the energy available for proton pumping and ultimately ATP synthesis. Although this is only affecting one small part of the ETC, the results may become compounded with aging and in addition to factors such as smoking and alcohol intake (which are known to trigger the disease). With this in mind, a potential therapy would be to provide appropriate quinones since it is most likely the ND4 mutation alters the interface between complex I and its substrate, ubiquinone. Consequently, in the midst of a number of proposed treatments such as near-infrared light therapy, hyperbaric oxygen therapy, brimonidine (lowers intraocular pressure), steroids and immunosuppressants (Yu-Wai-Man et al., 2014), the only treatment that has resulted in any gain in visual acuity for patients is idebenone, a synthetic analog of ubiquinone. Results with idebenone therapy in humans are variable, with some patients benefiting more than others, depending on their causative mutation, the degree of disease progression and the difference in visual acuity between their two eyes. However, long term studies do show trends of visual improvement in patients taking an idebenone regime (Carelli et al., 2011; Klopstock et al., 2011; Sabet-Peyman et al., 2012; Sadun et al., 2011).

As previously mentioned, when there are mutations in the NADH dehydrogenase, the complex dysfunctions and therefore perturbs its energy preserving function (Kirches, 2011). It is predicted that reactive oxygen species (ROS) and altered ATP production sensitize the retinal ganglion cells (RGCs) to apoptotic cell death, thereby causing vision loss in LHON (Baracca et al., 2005; Wong and Cortopassi, 1997; Wong et al., 2002). A recent report by Cruz-Bermudez and colleagues (2015) clearly showed LHON ‘cybrids’

(fusion of platelets from LHON donors with immortalized 143B cell line depleted of mtDNA) have a defective oxidative phosphorylation system (Complex I function) with increased ROS and reduced enzymatic function. It is important to note that calcium homeostasis (measure of mitochondrial membrane potential and function) and assembly was not altered compared to control cybrids (healthy donor platelets) (Cruz-Bermúdez et al., 2016). It appears that Complex I assembly is only altered when there is a complete loss of a subunit, such as ND4, resulting in loss of NADH-quinone oxidoreductase activity (Torres-Bacete et al., 2011).

The explicit reason for why specifically RGCs are targeted when this mutation is present throughout the body (especially when photoreceptors require more energy), is still unknown. What is known is that the central nervous system utilizes a great amount of energy and the retina is the highest consumer. One hypothesis is the nature in which RGCs are myelinated. The RGC cell body resides within the inner retina and its axon spans from the retina through a porous membrane made of collagen plates called the lamina cribrosa (LC) to join with the other RGC axons and form the optic nerve. The axons are not myelinated until they pass through the LC. As a result, there is a higher concentration of mitochondria around the cell body because excessive amounts of energy are required to propagate the action potential to the LC (Abu-Amero, 2011; Carelli et al., 2004a, 2004b; Gueven, 2014).

Pre-clinical work in LHON was limited by the challenges in generating an animal model due to the difficulty of targeting mitochondrial DNA. However, work by John Guy and colleagues (Miami, USA) showed that *allotopic* transcription of the ND4 subunit in the nucleus results in a protein that is efficiently targeted to the mitochondria

using an N-terminal targeting sequence (MTS) for mitochondrial import (Guy et al., 2009). They used this system to express mutant ND4 (AAV-mND4-MTS) in retinal ganglion cells (RGCs) using an intravitreal injection of AAV serotype 2 (which efficiently targets nerve fiber layer and RGCs). The AAV-mND4-MTS induces an LHON phenotype, characterized by optic nerve head swelling, followed by a progressive loss of RGCs and their axons which make up the optic nerve (Qi et al., 2007). LHON mice also had visual dysfunction according to pattern electroretinography (which provides a function assessment of RGCs). Moreover, the mice had disturbed mitochondrial architecture and increased reactive oxygen species (Qi et al., 2007). Subsequently, the Guy group showed that a mitochondrial targeting sequence (MTS) can be added directly to the VP2 capsid protein within AAV, leading to import (and transcription) of the AAV payload in the mitochondria. For these latter studies, a 23 amino acid cytochrome oxidase subunit 8 (COX8) was fused to the N-terminus of GFP and was inserted in-frame into the VP2 gene (Yu et al., 2012a). They then used this MTS-AAV carrying a wild type ND4 transgene to rescue the visual dysfunction found in their LHON model.

Tools Available for Retinal Degeneration Studies

Mouse Retinal Cell Lines

With the current advances in gene therapies used to prevent photoreceptor degeneration (Dalkara and Sahel, 2014), there is a growing importance placed on preliminary *in vitro* work which ultimately predict viable therapies to advance *in vivo*.

Unfortunately, when working with retinal cells, there are limited options for cell or tissue culture experiments.

With this in mind, primary cultures remain most representative of the native retina. Although the neonatal mouse retina explant survives in culture for more than a month (Caffé et al., 2001), this is not always representative of the adult retina. Adult explants and primary cultures can be cultured up to 7 days, which is not suitable for long term studies (Bull et al., 2011; Grozdanov et al., 2010). For this reason, cell lines are desirable because they have an unlimited lifespan, can be grown in large quantities, survive long-term storage and are affordable. They are quick and easy to use to perform simple cell death and growth assays. However, immortalization influences gene expression and morphology. The level of heterogeneity is unknown and may depend on culture conditions. Although, it may also closely simulate the retina which contains different cells types with different precursors, homogeneous cell lines are desired to reduce confounding factors due to varied response to stimuli.

The cone-derived photoreceptor cell line, 661W, was originally derived from retinal tumors of post-natal day 8 mouse, transformed by use of SV40 large T-antigen (Gómez-Vicente et al., 2005; Tan et al., 2004a). This expression is under the control of the human interphotoreceptor retinol binding protein promoter, for photoreceptor specificity (Tan et al., 2004a; Yokoyama et al., 1992). Interestingly, when comparing total mouse retina extracts on a 2D gel to 661W cells, there were 17 proteins identified that were unique to the cell line and not present in the whole retina lysate (Al-Ubaidi et al., 2008; Fitzgerald et al., 2008). This goes to show that despite the cone photoreceptor origin, cultured cell lines are not perfect representatives of the *in vivo* retina. However,

these cells do express cone markers such as opsins (blue and green), transducin and cone-arrestin (Tan et al., 2004a).

Tuohy *et al*., in 2002 (even before the first characterization of the cell line in 2002 by Tan *et al*.,) showed that 661W cells treated with natural (p53 over-expression) or synthetic (Z-VAD-FMK) inhibitors of apoptosis can undego neuroprotection in response to caspase dependent apoptotic cell death. This established 661W as a good tool for *in vivo* testing of photoreceptor therapeutic agents (Tuohy et al., 2002).

In addition to 661W cells, RGC-5 cells have been used extensively in vision research (Krishnamoorthy et al., 2001). This cell line was believed to be a rat-derived immortalized retinal ganglion cell line, but recent work suggests that RGC-5 cells may actually be 661W cells (Krishnamoorthy et al., 2013) since they express photoreceptor markers similar to 661W cells. It is thought that RGC-5 cells were contaminated with 661W cells early in the culture process. Even though RGC-5 cells have slightly different responses to light and expression of tyrosine sulfate receptors when compared to 661W cells (Al-Ubaidi, 2014; Krishnamoorthy et al., 2013), the controversy surrounding these cells has resulting in their dis-use in the vision research community.

In vivo Retinal Electrophysiology

Retinal electroretinography, or ERG, is a powerful non-invasive technique used to measure the function of the retina *in vivo*. This system has been adapted from human patients to a number of animal models, such as rat, mouse and feline. Distinct ERG protocols can be used to assess function in different parts of the retina. The experiments

described in his thesis employed two different types of ERG; full-field flash ERG and pattern ERG (PERG) (Figure 1.5).

The full-field ERG provides information about the retina as a whole. This is in contrast to a multifocal ERG which uses topographical mapping of the retina to identify specific areas of retinal function (Yap et al., 2015). Both the flash and multifocal ERGs utilize the same principals; stimulating the retina with a Ganzfeld stimulator which projects different intensities of light onto the eye (Vincent et al., 2013). Electrodes are placed on the cornea, with a grounding and reference electrode in the tail and head, respectively. The information from the electrodes is translated into a waveform. The characteristics of the waveform are indicative of the health of different cells within the retina. The negative a-wave is generated by the hyperpolarization of the photoreceptors, whereas the positive b-wave arises from the depolarization of ON-bipolar cells (mostly from rods), thereby acting as both a rod and bipolar cell functional modality (Stockton and Slaughter, 1989; Vincent et al., 2013). The small waves seen on the ascending b-wave are indicative of amacrine cell health, and are termed oscillatory potentials. The parameters of the flash ERG can be manipulated to isolate a specific cell type. For example, using 30 Hz flickering light (flicker ERG) under light adaptation, provides information about cone-specific function and can be an early indicator of retinal disease (Larsson et al., 2000). The 30Hz flicker ERG is generated primarily by cone OFF-bipolar cells and is the most sensitive read-out of cone photoreceptor health (Vincent et al., 2013). It was traditionally thought that the ERG could only predict bipolar, photoreceptor and amacrine cell health and did not provide any information about RGCs.

A.

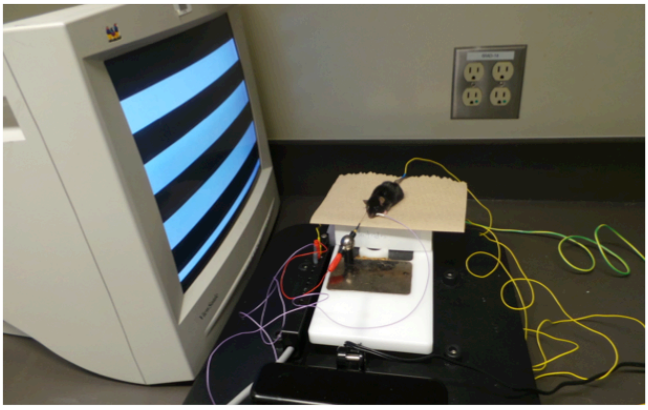

B.

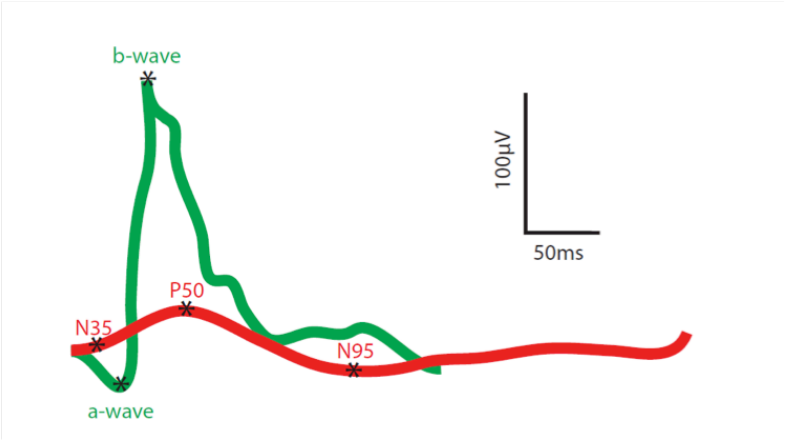

Figure 1.5. **Electroretinography.**
An image of a mouse pattern ERG set-up (A). Representative mouse waveforms (to scale) of a photopic response (green) and pattern ERG response (red) (B). Pattern ERG values to generate figure adopted from (Mohan et al., 2012) (n=37 healthy male adult C57BL/6).

However, in the early 1980's, it was discovered that recording a flash ERG while having a cat look at a screen with contrast reversing patterns (black/white rectangles), resulted in output waves which were abolished upon optic nerve and RGC axon cell death (Mafei and Fiorentini, 1981). After a great deal of optimization, the pattern ERG was born—perhaps the most sensitive measure of RGC function to date (Porciatti, 2015). The basis for this technique is that the neurons within the inner retina (mainly RGCs) are organized into receptive fields with antagonistic regions which respond to the contrast pattern (Porciatti, 2015). The ultimate output from this test is a waveform with a weak negative trough (N35), followed by a positive peak (P50) and another negative trough (N95) (Miura et al., 2009; Mohan et al., 2012). The peak to peak amplitude of P50 (N35-P50) and N95 (P50-N95) infer RGC function; however P50 may also denote other cell types which are not yet fully elucidated (Holder, 2001; Uva et al., 2013). It is important to note the low amplitude readings from mice generated by pattern ERG (Mohan et al., 2012). This may cause problems for researchers if their system is sensitive to surrounding noise interference (Figure 1.5).

Since the electroretinogram in general is such a highly sensitive read-out of retinal health in mammals, it has been extensively used, both in the clinic and in research (especially the full field ERG in mice), to distinguish between normal retinal health and retinopathy or optic neuropathy (Yap et al., 2015). Consequently, this robust tool has been used throughout the thesis to assess the state of retinal health and the efficacy of our interventional therapy.

Gene Therapy and Clinical Trials

The easily accessible, fairly immune privileged and post-mitotic nature of the retina makes it an ideally suited target for gene therapy. The anatomical structure of the eye (and in particular the clear cornea) allows controlled localized delivery of the vector to the retina. The existence of a blood-retina barrier creates a somewhat immune privileged site for gene delivery, reducing the immune response to the vectors. Furthermore, the cells of the retina are post-mitotic (non-dividing), preventing the therapy from interfering with growth and functional development of the retina. In addition, extensive non-invasive imaging and functional tools are available to allow testing of the adverse effects or efficacy of the therapy. Finally, the multitude of inherited retinal diseases, many of which are monogenic in nature, allows the eye to be a prime candidate for retinal gene therapy (Buch et al., 2008; Carvalho and Vandenberghe, 2015).

There have been numerous animal studies, and now clinical trials, involving AAV therapy to target retinal diseases (Boye et al., 2013; Carvalho and Vandenberghe, 2015). The first pre-clinical studies that paved the way for clinical trials utilized AAV2 carrying wild-type RPE65 to restore vision in a canine model of Leber's congenital amaurosis (LCA), a form of childhood blindness (Acland et al., 2001, 2005). Based on the success of these animal studies, in 2008, three independent groups initiated gene therapy clinical trials for LCA patients with the RPE65 mutation (Bainbridge et al., 2008a; Hauswirth et al., 2008a; Maguire et al., 2008). After eight years, there have been many lessons and limitations elucidated from these human intervention studies. To broadly state the results from all trials is very difficult due to the differences in vector design (promoters), area of injection in the retina (foveal or extra-foveal), dosage and volume injected, vector

purification, and even outcome measure. However, overall, gene therapy intervention improves retinal sensitivity and navigation through mobility mazes in low light (Bennett et al., 2016; Maguire et al., 2009). Importantly, these studies also showed that AAVs are well tolerated with low evidence of complications or deleterious effects (Bainbridge et al., 2008b; Cideciyan et al., 2008, 2009a).

One group recently reported long-term results (up to 6 years) for 3 out of 15 patients treated with AAV2 gene therapy (Jacobson et al., 2015). They reported improvements in visual sensitivity at 6 months post intervention, which was proceeded by a slow increase in the area of functional retina (likely due to the spread of the gene therapy vector from the initial injection site). This was followed by a contraction in the area of improved retinal sensitivity (Jacobson et al., 2015). A second group also reported a decline in vision after 3 years in 6 out of 12 patients (Bainbridge et al., 2015). Even though visual sensitivity was increased, the steady underlying natural degeneration of the photoreceptor cells continued to occur. It was furthermore suggested by Cideciyan *et al*., 2013 that this degeneration may have caused a toxic environment for the photoreceptor cells, resulting in a reduction in trophic support and continued vision loss (Cideciyan et al., 2013a). With this in mind, Testa *et al*., showed a sustained improvement at 3 years post intervention (Testa et al., 2013).

In order to better understand the results obtained in patients, Cideciyan *et al*. (2013a) reexamined the results obtained in the canine model. In the dog model of LCA, there are distinct stages of disease. For the first 4-5 years of life, RPE65 mutant dogs have retinal dysfunction (the retinal cells do not function and the animals are essentially blind), but there is no evidence of retinal degeneration. Degeneration begins after this

time. Initially, most of the LCA pre-clinical studies were performed on the RPE65-mutant canine during the dysfunctional stage of the disease. This resulted in long-term robust protection of the ONL (photoreceptor layer) and restoration of sight (Acland et al., 2001; Bennicelli et al., 2008). However, when the dogs were treated during the degenerative phase, there was restoration of functional vision, but the ONL thickness continued to decline, similar to the human clinical trials. Cideciyan *et al*., (2013) showed that the transition from dysfunction to degeneration occurs much later in dogs and mice than in humans; in fact, they could not identify a dysfunction-only stage with the human form of the disease (Cideciyan et al., 2013b). Even younger patients that were treated with the RPE65 gene therapy (patients as young as 6-11 years old) were already in the degenerative stage of the disease, and thus continued to undergo degeneration of their retina. Consequently, in diseases such as LCA that may not have a dysfunction stage, multiple strategies may be required to prevent the inevitable degeneration of the photoreceptors. These diseases may require combination therapies involving both gene replacement and a neuroprotective or anti-apoptotic agent (such as XIAP) to protect the structure of the cells.

Despite the underlying retinal degeneration, it is important to note that patients had improved visual fields 6 months after the injection and despite the decline, it did not fall below baseline after 5-6 years (Bennett et al., 2016; Jacobson et al., 2015). Furthermore, some studies have shown a correlation between age and visual improvement (Maguire et al., 2009; Weleber et al., 2016). Treatment of the younger, more robust retina (perhaps at the beginning of the degenerative phase) even showed improvement in the electroretinogram, which is typically not sensitive enough to show

differences, further emphasizing the need to intervene as early as possible to delay the degeneration (Maguire et al., 2009; Weleber et al., 2016). It is important to note that Bainbridge *et al*., (2015) and Jacobson *et al*., (2012) did not see a correlation between age and visual improvement (Bainbridge et al., 2015; Jacobson et al., 2012). Differences in these studies may be accounted for by different sources of vector, different promoters, different injection sites and a variable patient cohort.

Despite the variability in the results obtained, the overall success of the clinical trials in improving visual sensitivity has led to expanded trials in patients. In July 2016, Dr. Jean Bennett published the first results from the University of Pennsylvania clinical trials that injected their highest dose ($1.5x10^{11}$ viral genomes/patient) into the contralateral eye of patients already treated with gene therapy in the weaker eye. They showed prolonged improvement in the originally injected eye, (Bennett et al., 2016) as well as a significant difference in full field light sensitivity and mobility testing in the second injected eye up to three years. These results lead the way for subretinally injected gene therapy approaches and open the door for Phase III clinical trials.

In terms of the intravitreally injected gene therapy, the Guy group (University of Miami, Florida) has shown promising results in non-human primates (Koilkonda et al., 2014; Koilkonda RD et al., 2014), and based on this work has initiated clinical trials in human patients with LHON. The clinical trial administered AAV2-wild type ND4 into the vitreous of patients with the G11778A mutation in order to compensate for their mutant dysfunctional ND4. Results in 5 legally blind LHON patients who received the gene therapy revealed no serious safety concerns with the treatment, although patients did experience increased intraocular pressure, keratitis, subconjunctival hemorrhage, a sore

throat and an increase in neutralizing antibodies to AAV2 (Feuer et al., 2015). Two of the patients had an improvement in visual acuity equivalent to three lines, whereas the other three patients did not show any difference from baseline (Feuer et al., 2015). However, it is important to note that the amelioration is not significant beyond the "spontaneous improvement range" (Lam et al., 2014). Secondly, the doses used are low ($5x10^9$ and $2.46x10^{10}$ viral genomes/patient), thereby bringing efficacy into question. Finally, the baseline neutralizing AAV antibody titers of one patient were extremely high and typically out of range of an ideal candidate for gene therapy intervention (based on the RPE65 clinical trial for Leber's congenital amaurosis; clinicaltrials.gov, NCT00481546). These observations together cast doubt on the efficacy of the initial findings. However, since the main focus of a phase I clinical trial is safety, it is promising for the gene therapy field that one of the first intravitreal injections of AAV is handled relatively well in the eye. A second LHON gene therapy clinical trial is currently underway in France by Gensight (clinicaltrials.gov, NCT02064569). This trial, led by Dr. Catherine Vignal, is utilizing higher doses of AAV2-ND4. To date, no results have been released from this trial.

Taken together, the future for gene therapy is extremely positive and the possibilities are endless. The specific parameters to ensure sustained and prolonged improvements are still being delineated, however, for these patients that are going completely blind, the ability to navigate through mazes and go about daily activities is life-changing. Future trials that combine gene augmentation therapy with neuroprotective agents will likely be the most effective route for vision preservation.

RATIONALE

Retinal degeneration is a significant clinical problem that is the result of over two hundred different genetic mutations (not all genes have been identified) (Veleri et al., 2015). As a result, a general neuroprotective agent, such as XIAP, employed in the context of gene therapy to the retina is an effective strategy to target the final common pathway of all retinal diseases.

HYPOTHESIS

XIAP can protect retinal cell structure and function in various models of retinal degeneration. XIAP will be effective in multiple types of retinal degeneration paradigms because it targets the final common pathway shared by all of these diseases, namely the death of the retinal cells by apoptosis.

OBJECTIVES

Objective 1: Test the hypothesis in a model of Leber's Hereditary Optic Neuropathy.

Objective 2: Test the hypothesis in a large animal model of retinal detachment.

Objective 3: Explore alternatives to gene therapy since the transgene onset of expression is not fast enough to treat acute diseases, such as retinal detachment.

CHAPTER 2: XIAP PROTECTS OPTIC NERVE STRUCTURE IN THE MUTANT ND4 MOUSE MODEL OF LEBER'S HEREDITARY OPTIC NEUROPATHY

XIAP protects optic nerve structure in the mutant ND4 mouse model of Leber's Hereditary Optic Neuropathy

Sarah J. Wassmer,[1,2*] Yves De Repentigny,[2] Derek Sheppard,[3] Lijun Fang,[2] Stuart G. Coupland,[1,2,4] Rashmi Kothary,[1,2] William W. Hauswirth,[5] Catherine Tsilfidis[1,2,4]

[1]Department of Cellular and Molecular Medicine, University of Ottawa, Ottawa, ON, Canada

[2]Ottawa Hospital Research Institute, Regenerative Medicine Program, Ottawa, ON, Canada

[3]Department of Biology, Carleton University, Ottawa, ON, Canada

[4]Department of Ophthalmology, University of Ottawa, Ottawa, ON, Canada

[5]Department of Ophthalmology, University of Florida College of Medicine, Gainesville, Florida

[*]Current Address: 20 Staniford Street, Boston, MA 02114

Grant support: This work was supported by Canadian Institutes of Health Research (CIHR) and Foundation Fighting Blindness (FFB) grants to CT, and NIH grant P30-EY021721, MVRF and RPB Inc funding to WWH. CT is supported by the Don and Joy Maclaren Chair for Vision Research. SW was supported by the David S. Shillito Scholarship in Ophthalmology and by an Ontario Graduate Scholarship.

Author Contributions:

Sarah Wassmer designed and carried out all of the experiments, wrote the manuscript and made figures.

Yves De Repentigny performed downstream processing of optic nerves for toluidine blue imagining and TEM.

Derek Sheppard assisted with fundus imaging and hematoxylin and eosin staining.

Lijun Fang assisted with PERG analysis.

Stuart G Coupland set-up PERG functional testing protocols.

Rashmi Kothary is the project supervisor for Yves De Repentigny.

William W Hauswirth provided all adeno-associated viral vectors.

Catherine Tsilfidis funded the studies, helped to design experiments and to write the manuscript.

Manuscript prepared for submission to *Investigative Ophthalmology and Visual Science (IOVS)*, October 2016.

Abstract

Purpose. Leber's Hereditary Optic Neuropathy (LHON) is a genetic form of vision loss that occurs primarily due to mutations in the NADH dehydrogenase (ND) subunits that make up Complex I of the electron transport chain (ETC). LHON mutations result in the apoptotic death of retinal ganglion cells (RGCs). We tested the hypothesis that gene therapy with the X-linked Inhibitor of Apoptosis (XIAP) would prevent RGC apoptosis and reduce disease progression in a mouse model of LHON that carries the ND4 mutation.

Methods. Adeno-associated virus (AAV) encoding full length hemagglutinin-tagged XIAP (AAV2.HA-XIAP) or green fluorescent protein (AAV2.GFP) was injected into the vitreous of DBA/1J mice. Two weeks later, the LHON phenotype was induced by AAV delivery of mutant ND subunit 4 (AAV2.mND4FLAG) to the vitreous. Retinas and optic nerves were harvested at 4 months, and the effects of XIAP therapy on nerve fiber layer (NFL) and optic nerve integrity were evaluated.

Results. During LHON disease progression, RGC axons become demyelinated. Apoptotic bodies are seen in the nuclei of astrocytes or oligodendrocytes in the optic nerve, and there is thinning of the optic nerve and the NFL of the retina. XIAP gene therapy protects the RGC nerve fiber layer and optic nerve architecture by preserving axon cross-sectional area and reducing demyelination. XIAP also reduces nuclear

fragmentation in resident astrocytes or oligodendrocytes, decreases glial cell infiltration and provides evidence of functional protection.

Conclusions. XIAP therapy appears to improve optic nerve health and delay disease progression in Leber's Hereditary Optic Neuropathy, when applied before the insult.

Introduction

Greater than 95% of cases of LHON are caused by mutations within the mitochondrial ND4 (G11778A), ND1 (G3460A) and ND6 (T14484) genes which affect approximately 1: 45,000 people in Europe (Al-Enezi et al., 2008; Man et al., 2003; Mascialino et al., 2011). These three mutations pose a significant risk of developing vision loss due to retinal ganglion cell (RGC) death, optic disc atrophy, RGC axon demyelination (oligodendrocyte degeneration) and glial cell activation (Carelli et al., 2002).

Insights into the effects of LHON mutations have been provided by studies with cellular hybrid (cybrid) cell lines that were generated by introducing LHON mutant mitochondrial DNA (mtDNA) into mtDNA-depleted cells. Studies in these cells have shown defects in mitochondrial function, characterized by decreases in ATP levels, decreases in mitochondrial inner membrane potential (MIMP) and increases in superoxide levels (Cruz-Bermudez et al, 2016). How these defects lead to RGC degeneration is unknown; however, a number of studies have suggested that LHON mutations induce oxidative stress, which make RGCs more susceptible to apoptotic cell death. For example, cybrids carrying the ND1 and ND4 mutations are sensitized to Fas-induced apoptosis and can be rescued by incubation with the synthetic caspase inhibitor, zVAD-fmk (Danielson 2002). LHON mutation-carrying cybrids also undergo apoptotic cell death when grown in galactose rather than glucose medium (which forces the cells to use mitochondrial respiration to generate ATP). The cell death is accompanied by an increase in mitochondrial cytochrome c release into the cytosol (Ghelli et al 2003).

Studies in LHON patient peripheral blood lymphocytes (PBLs) show increased apoptosis in comparison to healthy controls upon treatment with an oxidizing agent, and this result is attributed to the involvement of the mitochondria in the activation of the apoptotic cascade (Battisti *et al*., 2004).

The X-linked Inhibitor of Apoptosis (XIAP) is the most potent inhibitor of apoptosis within the Inhibitor of Apoptosis (IAP) family of proteins. It binds to and inhibits caspases 3,7, and 9 and further mediates caspase degradation via the E3 ligase activity of its C-terminal RING domain (Berthelet and Dubrez, 2013; Silke and Vucic, 2014; Takahashi et al., 1998). Furthermore, it has been shown that XIAP can enter the mitochondria to compete with Bax/Bak-mediated mitochondrial outer membrane permeabilization to suppress mitochondrial-mediated cell death (Chaudhary et al., 2015; Hamacher-Brady and Brady, 2015). Thus, XIAP is able to block both the mitochondrial (intrinsic) and death receptor-mediated (extrinsic) apoptotic cascades. Moreover, XIAP has additional functions that are unrelated to its role in caspase inhibition. XIAP and related family members cIAP1 and cIAP2 can inhibit the "ripoptosome" which is involved in necroptosis (Vince et al., 2012; Yabal and Jost, 2015; Yabal et al., 2014). In addition, XIAP has been shown to regulate the NF-κB and JNK pathways (Hofer-Warbinek et al., 2000; Kaur et al., 2005; Lu et al., 2007) to suppress TNF-alpha and TGF-β1-induced apoptosis (Kaur et al., 2005). More recent studies point to a critical role for XIAP in reducing inflammation and a role in innate immunity (Lawlor et al., 2015).

Recently, the LHON phenotype has been successfully replicated in DBA/1J mice by adeno-associated viral delivery of mutant ND4 (mND4) to the mitochondria of RGCs (Guy et al., 2009; Koilkonda et al., 2014; Qi et al., 2007; Yu et al., 2012a, 2012b, 2012c).

Studies in these mice have confirmed that RGC loss is due to apoptosis (Qi et al, 2007). Since many visual disorders involve the ultimate death of retinal cells by apoptosis, anti-apoptotic therapy holds tremendous promise as a general treatment for multiple types of retinal disease. To date, adeno-associated virus (AAV)-mediated XIAP gene therapy has been used to effectively protect retinal ganglion cells (RGCs) in rat models of retinal ischemia (Renwick et al., 2005), and glaucoma (McKinnon et al., 2002). XIAP has also been shown to protect photoreceptor structure and function in chemically-induced retinal degeneration (Petrin et al., 2003) and in retinitis pigmentosa (Leonard et al., 2007). In a model of retinal detachment, XIAP preserved photoreceptor structure for up to 2 months of continuous detachment (Zadro-Lamoureux et al., 2009). XIAP also increased the survival of transplanted retinal progenitor cells (Yao et al., 2011), and prolonged the treatment window in a mouse model of retinal degeneration treated with gene replacement therapy (Yao et al., 2012).

Given the success of XIAP gene therapy in multiple forms of retinal degeneration and the fact that RGC loss in LHON is apoptotic in nature, we evaluated the efficacy of XIAP gene therapy in protecting RGCs in the mouse model of LHON. We show that XIAP reduces glial cell infiltration, nuclear fragmentation and demyelination in the optic nerve and preserves RGC axon thickness.

Materials and Methods

Adeno-Associated Viral Vectors

AAV2/2 (referred to as AAV2) vectors were generated for these studies. All constructs were under the control of the cytomegalovirus (CMV) enhancer and chicken beta-actin (CBA) promoter. The AAV2.HA-XIAP vector contained the human XIAP open reading frame with an N-terminal hemagglutinin (HA) tag. Gene expression was enhanced by the presence of a woodchuck postregulatory element (WPRE) in the viral construct. AAV2.GFP virus was similarly generated for use as an injection and viral control. Details of vector construction are found in Renwick et al. (2006). Construction of the mutant human R340H ND4 (mND4) construct has been described elsewhere (Qi et al., 2007). The mND4 construct contained the ATP1 mitochondrial targeting sequence (MTS) to allow the allotopically-expressed protein to be shuttled to the mitochondria, and a C-terminal FLAG tag for immuno-detection. Furthermore, the capsid harboured three tyrosine to phenylalanine mutations for increased expression (Y444,500,730F). Gene expression was enhanced by the presence of a WPRE in the construct. AAV vectors were generated and titered as previously described (Hauswirth et al., 2000; Zolotukhin et al., 2002).

Animals and Injection Procedures

Adult male DBA1/J mice were purchased from The Jackson Laboratory and kept under standard 12h light/12h dark laboratory conditions. All procedures were approved by the University of Ottawa Animal Care and Veterinary Service, and adhered to the ARVO

statement for the Use of Animals in Ophthalmic and Vision Research. Two cohorts of male mice, between the ages of 10-12 weeks of age, were used for these studies. The first cohort of 27 animals were used to monitor disease progression and to determine the injection parameters for the subsequent cohort. This first set of animals was injected intravitreally in the left eye with 1 μl of $1x10^{11}$ VG/mL of AAV2.mND4FLAG and an equal dose of AAV2.GFP in the right eye. Eyes and optic nerves were sampled between 2 weeks and 3 months post-injection to monitor progression of the disease. The second cohort of 27 animals were injected with AAV2.GFP in the right eye and AAV2.HA-XIAP in the left, both eyes receiving a dose of 1μl at $1x10^{11}$ VG/mL. Two weeks after the initial injection (to allow the onset of gene expression), one third of the animals received 1μl of AAV2.mND4FLAG in the left, XIAP-treated eye, one third received AAV2.mND4FLAG in the right, GFP-treated eye, and one third received AAV2.mND4FLAG in both eyes. AAV2.mND4FLAG was delivered at a dose of $2x10^{12}$ VG/mL. Eyes and optic nerves from this second cohort of animals were sampled at 4 months.

Immunohistochemistry

Enucleated eyes were processed for sectioning or flatmounts. Tissue sampling for cryosections were conducted as previously described (Renwick et al, 2006). For flatmounts, retinas were carefully dissected and flattened onto nitrocellulose membranes with the RGC layer facing upwards. Retinas were fixed for 30 min with 4% paraformaldehyde at RT and then transferred to PBS at 4°C (for up to 3 days). The retinas were then carefully teased off the membranes and treated with ascending

concentrations of sucrose (10, 20, 30%) each for 10 minutes, followed by 3 freeze/thaw cycles on dry ice and room temperature, respectively. The retina flatmounts were mounted onto Fisherfrost ™ Superfrost ™ slides (Fisher Scientific) in 30% sucrose, and placed at -80°C until staining. Hematoxylin and eosin staining was performed according to standard protocols. Immunostaining was performed with anti-FLAG M2-cy3 (1:100, Sigma), anti-HA high affinity (1:100, Sigma), RBPMS (1:100, Phosphosolutions) and anti-GFP (1:200, Invitrogen). All primary antibodies were incubated for 2 days. Secondary antibodies Alexa 488 (Invitrogen) and Cy3 (Jackson ImmunoResearch) were used at 1:500 and incubated at room temperature for 1 hour.

Preparation of Optic Nerves for Transmission Electron Microscopy (TEM)

DBA/1J mice were anesthesized by intraperitoneal injection of tribromoethanol (Avertin) and perfused transcardially with 5 ml of phosphate-buffered saline (PBS) followed by 10mL of Karnovsky's fixative (4% paraformaldehyde, 2% glutaraldehyde and 0.1 M sodium cacodylate in phosphate-buffered saline, pH 7.4). Left and right optic nerves were carefully extracted and fixed individually overnight (or until processed) at 4ºC in the same fixative. Under a stereomicroscope, each nerve was cut with a surgical blade in the central region of the cranial portion of the nerve into a straight segment of 1 mm of length. All central segments were subsequently washed twice in 0.1M sodium cacodylate buffer for 1 hour and once for overnight. Segments were post-fixed with 1% osmium tetroxide in 0.1 M sodium cacodylate buffer for 1 hour and were washed in distilled water two times for 5 min. Specimens were dehydrated in an ascending concentration of alcohol and infiltrated in 30 % spurr resin/acetone for 20 min and for 15 hours, then

transferred into 50% spurr resin/acetone for 6 hours and into fresh 100% spurr resin for overnight. Spurr resin was changed twice a day for three days and all infiltration steps were performed on a rotor at low speed. Segments were embedded in fresh liquid spurr resin and oriented inside the molds and then polymerized overnight at 70ºC. Ultrathin sections (80 nm) from the central segment of the left and right optic nerves were collected onto 200-mesh copper grids and stained with 2% aqueous uranyl acetate and with Reynold's lead citrate. Stained sections on grids were observed under a transmission electron microscope (Hitachi 7100) at 2,000x, 4,000x, 10,000x and 20,000x magnifications. Ultrastructural analysis was conducted on approximately 300 electron micrographs of left and right optic nerves at the central region of the optic nerve.

Toluidine Blue Staining and Microscopy of Semi-thin Sections

Semi-thin cross sections of 0.5 μm from resin embedded central segment of optic nerves were mounted on glass slides and stained with 1% Toluidine blue and 2% borate in distilled water. Sections were scanned with a MIRAX MIDI (Zeiss) and observed at 60x and 400x magnifications on a computer screen using Zeiss MIRAX Viewer software. Stained sections were also examined by light microscopy using a Zeiss Axioplan microscope equipped with a digital camera for a quantitative analysis of myelinated axons.

Axons counts

Toluidine blue images containing scale bars were imported into ImageJ, and processed using the Enhance Local Contrast (CLAHE) Plugin. After the scale bar was set, two

grids of 1300 μm^2 were overlaid on the image and axons were counted using the Cell Counter Plugin at 150% zoom. An average of 5 images (10 grids) was counted for each optic nerve and the numbers averaged to get a mean count per grid for each optic nerve. In order to determine cross-sectional areas of axons, images imported into ImageJ were scaled and processed using CLAHE. Using the Threshold Colour Plugin, 'threshold' and 'invert' were selected and the brightness was adjusted to allow visualization of the axons. The image was converted to 8-bit and the threshold colour was adjusted to red. Axonal cross-sectional areas were determined using the Analyze Particles Plugin with size set to "0-infinity" and circularity set to "0.3-1". The number and proportion of axons less than 1 μm^2 were recorded.

Pattern ERG

Pattern ERGs were recorded on the Espion E^2 system (Diagnosys, Inc.). The mice were anesthetized with ketamine (50mg/kg) and medetomidine (1mg/kg), and placed on an elevated heating (37°C) platform 20 cm from a computer monitor. The monitor displayed 200 mm inter-spaced black and white bars at 50cd/m^2, 0.05 cycles/deg, 100% contrast and 2 Hz temporal frequency. A 2mm diameter gold loop electrode was placed on the undilated pupil facing the screen. A total of 1800 traces were generated (two consecutive sequences of 900 traces, sample frequency 1000 Hz, 10ms sweeps pre-trigger and 400ms sweeps post-trigger). Retinal signals were amplified (10,000 fold) and a band-pass filter of 0.3-300 Hz was used. The reference stainless steel needle electrode was placed in the scalp and the ground electrode was placed in the tail. Final waveforms were scored by deleting all traces above +30uV and below -30uV.

MRI

A 7T GE/Agilent MR 901 Magnetic Resonance Imaging (MRI) machine was used to generate cross-sectional images of 8 orbits (3 mice with right eye injected with AAV2.HAXIAP and AAV2.mND4FLAG, and left eye injected with AAV2.GFP and AAV2.mND4FLAG). Animals were anesthetized for the MRI procedure with isoflurane. Each orbit was imaged with a fast spin echo pulse sequence, with echo time 25 ms, repetition time 1075 ms, slice thickness 350 μm, and in-plane spatial resolution 78 μm. The slices were prescribed in an oblique fashion so that the entire length of the optic nerve would lie completely within the plane of one of the slices. Images were imported into ImageJ (Schneider et al., 2012) and optic nerve diameters were measured at the same distance from the optic disc in each image. Measurements were taken by 3 independent observers who were blind to the experimental groups.

Viability Assays

The transformed cone photoreceptor cell line, 661W was kindly provided by Dr. M. Al-Ubaiddi (Tan et al., 2004). 661W cells were transfected with pCI-neo containing the full-length coding sequence of human XIAP which was generated from pCM-SPORT6-XIAP (Origene, Rockville, MD), digested with SalI and NotI to isolate XIAP coding sequence, and ligated into the pCI-neo vector (Promega). Transfections were conducted using Lipofectamine 2000 (ThermoFisher Scientific), according to the manufacturer's instructions. Control cell lines were transfected in a similar manner with the pCI-neo empty vector (EV). Stably-expressing cells were grown under G418 selection. All cells

were used below passage 15, and XIAP expression was monitored in each assay by western blot or RT-qPCR.

For the death assays, cells were plated onto 96-well plates at 60% confluency and incubated with 1mM hydrogen peroxide (Sigma Aldrich) for 32 hours or 15μM menadione (Sigma Aldrich) for four hours. Cell viability was measured using AlamarBlue ® Cell Viablity Reagent (Invitrogen) and Synergy BioTek plate reader (BioTek Instruments, Inc.) as per manufacturer's directions. Read-out measurements of treated cells were divided by vehicle control treated cells to determine final viability. Three individual plates with five replicates each were averaged for final viability analysis.

Results

XIAP Over-expression protects against oxidative stress-induced photoreceptor cell death *in vitro*

Oxidative stress is a major factor in the ultimate death of retinal ganglion cells in LHON. The ability of XIAP to protect against oxidative stress-induced apoptosis in retinal cells was tested *in vitro* prior to testing XIAP therapy in an animal model of LHON. Full-length human XIAP was cloned into the pCI vector and the construct was transfected into the 661W cone photoreceptor cell line (the empty pCI vector was transfected as a control). Pooled G418-resistant cell lines were established. XIAP over-expression significantly protected the cells from hydrogen peroxide and menadione, two potent inducers of oxidative stress and apoptosis (See Supplementary Fig. 2.1).

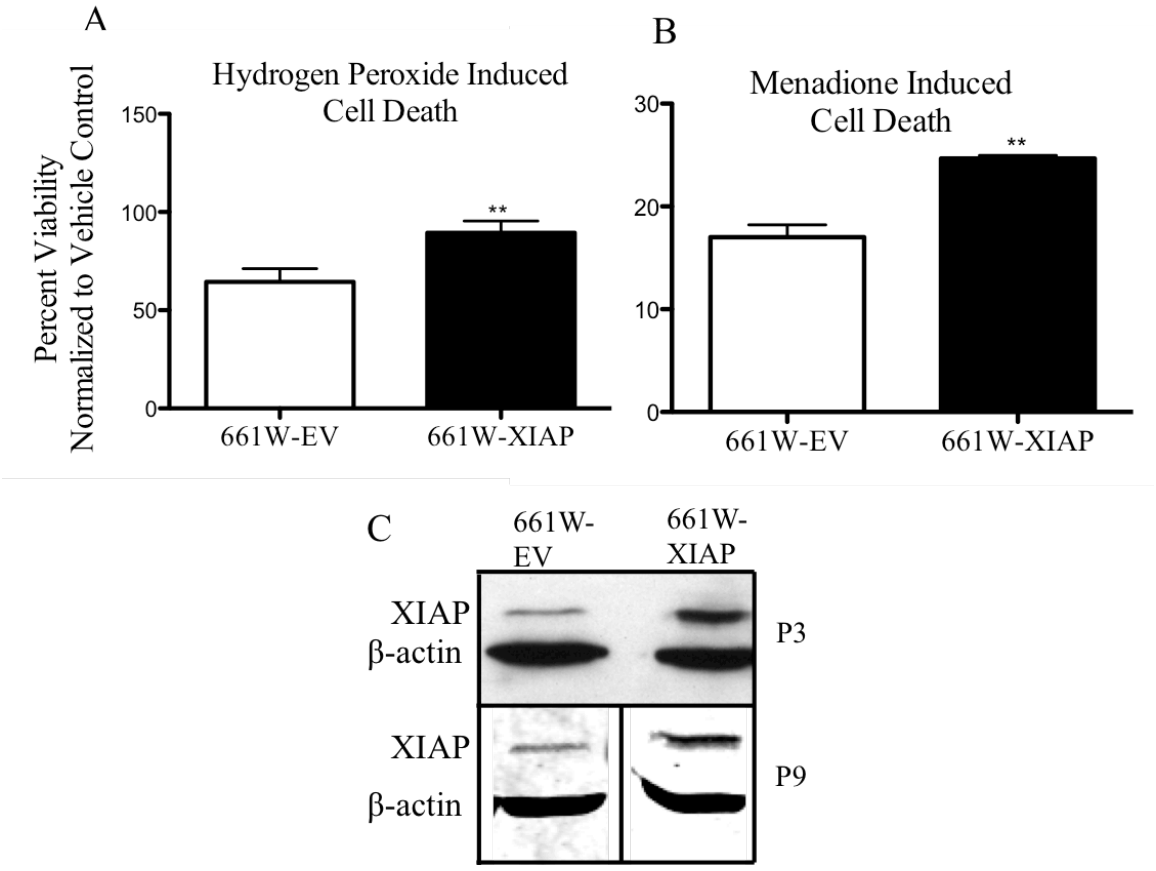

Supplemental Figure 2.1. XIAP protects 661W cells from oxidative stress. pCI.XIAP or pCI (empty vector; EV) backbone were transfected into 661W cone photoreceptors. Cells were incubated with 1mM hydrogen peroxide for 32 hours (A) or 15μM menadione for 4 hours (B). Using the AlamarBlue cell viability assay, the percentage viability was calculated by comparing hydrogen peroxide or menadione-treated cells with vehicle treated control cells (equal volume of either PBS or ethanol). C) Western blot shows XIAP expression levels, along with β-actin loading control in pCI.XIAP transfected and control cells at an early and late passage.** $p<0.005$, *$P=0.05$, using a Student's t-test.

Allotopically expressed mND4 induces RGC axon thinning, indicative of retinal degeneration onset

The first series of *in vivo* studies examined the ability of mutant ND4 to initiate disease and assessed the timeline for disease onset. These studies informed the gene therapy studies that followed. AAV2 vectors carrying mutant ND4 (mND4) with an N-terminal mitochondrial targeting sequence and a C-terminal FLAG tag (AAV2.mND4FLAG) were delivered into the vitreous of the mouse eye. AAV2.GFP was injected in the contralateral eye as a control. Since ND4 is a gene that is normally transcribed in the mitochondria, the mitochondrial targeting sequence ensured that the allotopically expressed protein product would be directed to the mitochondria. Three months after the injection, retinal flat-mounts (n=10) were used to assess the presence of the virally-expressed proteins in RGCs (Figure 2.1). These studies showed strong mND4 expression throughout the inner retina. This staining was mostly restricted to the retinal ganglion cell layer and showed a widespread perinuclear pattern within RGCs (that were co-labelled with the RGC marker RNA Binding Protein With Multiple Splicing, RBPMS) (Figure 2.1A-B). Contralateral GFP-injected retinas showed good coverage by the viral injection (Figure 2.1C).

Three months after the mND4 injection, eyes and optic nerves were analyzed using transmission electron microscopy (TEM, n=2), optic nerve axon counts (n=3) and hematoxylin and eosin staining (n=7). TEM analysis of optic nerves showed extensive demyelination, axon swelling, axon loss, and glial cell infiltration (Figure 2.2, Supplemental Figure 2.2). These degenerative changes were further confirmed in toluidine blue (TB) stained optic nerves (Figure 2.3), which also showed glial cell

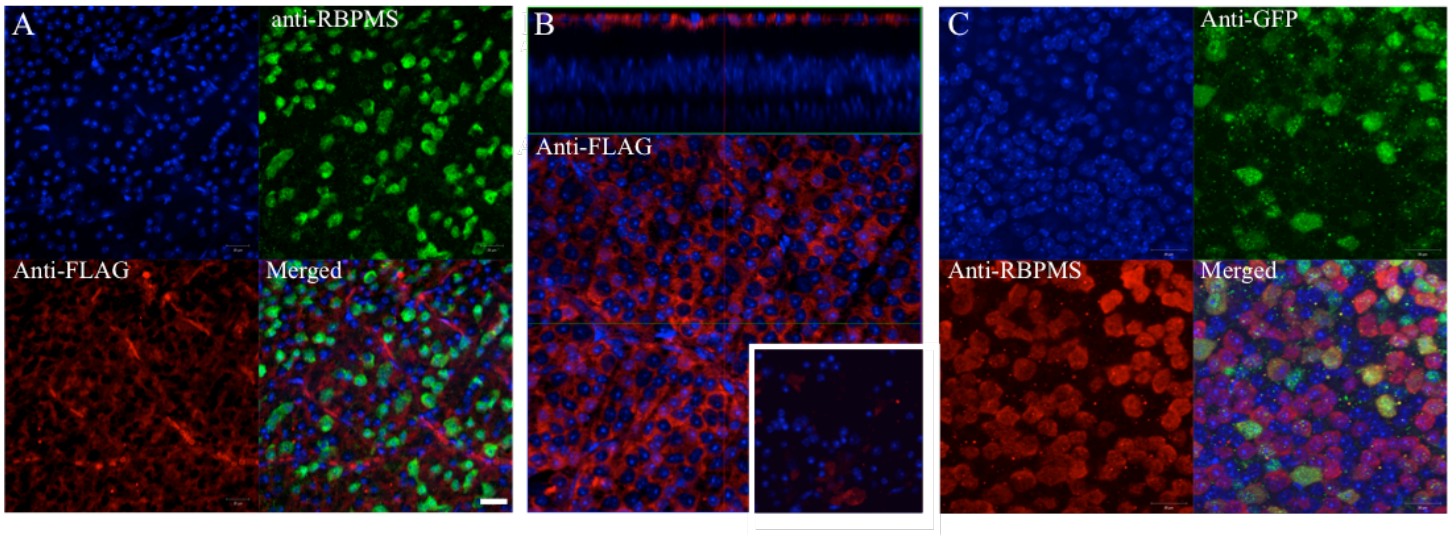

Figure 2.1. mND4 and GFP expression in the retina after intravitreal injection. A) Immunofluorescent images of a retinal flatmount of an eye injected with AAV2.mND4FLAG and stained with the nuclear marker DAPI (blue), anti-RBPMS antibody to identify RGCs (green) and an antibody to the FLAG tag to show the localization of the mND4 protein. There is robust perinuclear mND4 expression. B) Perinuclear staining for mND4 is confirmed in a second retinal flatmount. Z-stack confocal microscopy shows that the mND4 (FLAG-tag) is present in the RGC layer of the retina. Small insert on bottom right shows negative control (uninjected eye) treated with Cy3 conjugated FLAG antibody in the same manner, using the highest gain parameters. C) Immunofluorescent images of an AAV2.GFP-injected retina shows co-localization of GFP (green) and RGC marker RBPMS (red). Scale bar represents 20µm.

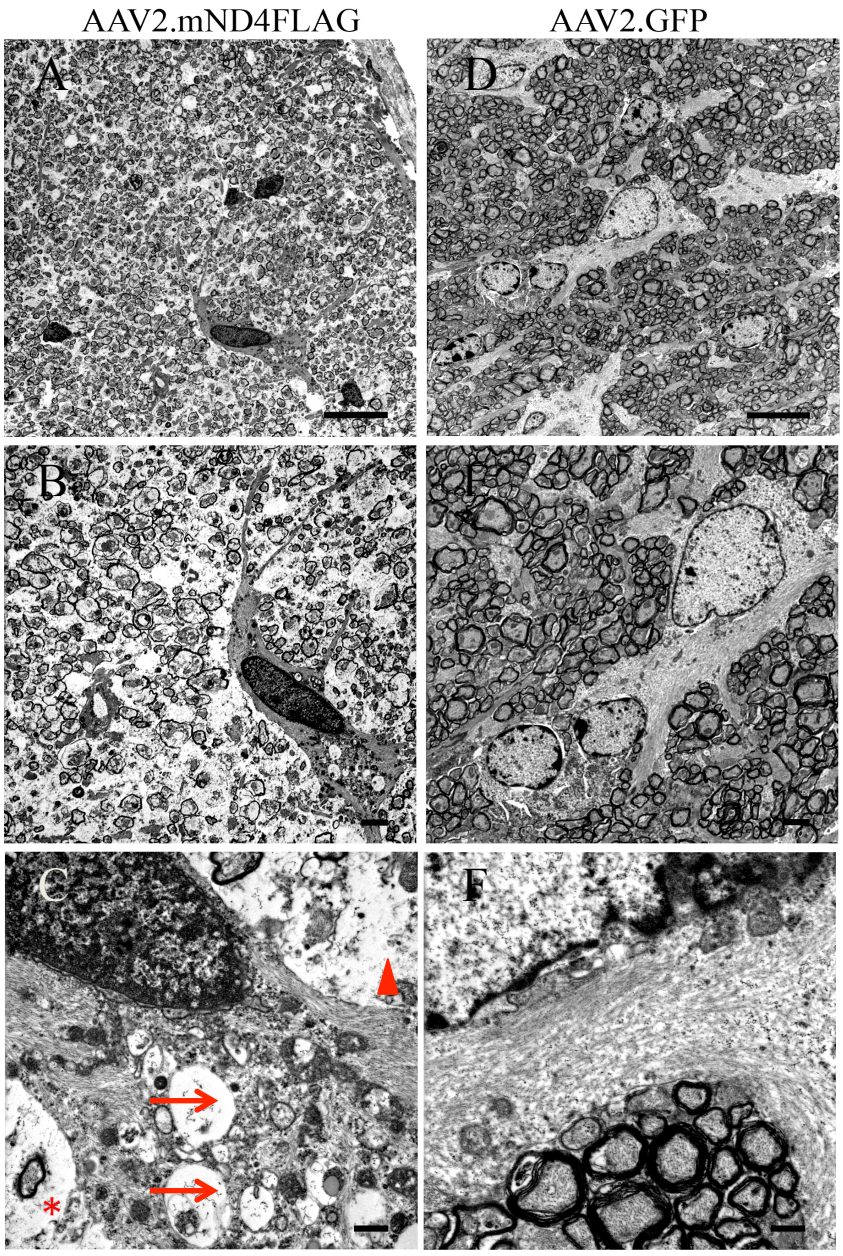

Figure 2.2. mND4 over-expression induces optic nerve degeneration.
A) Transmission Electron Microscopy (TEM) comparing an mND4 injected optic nerve with a GFP-injected optic nerve at 3 months post-injection. (A-C) Increasing magnification images of an mND4-injected retina show axon swelling (arrows), empty spaces resulting from degenerated axons (arrow head) and evidence of autophagy (asterisk). (D-F) The GFP-injected (control) eye has a normal optic nerve with healthy glial cells and robust myelination of axons. Scale bars represent 10µm (A,D) and 2µm (C-F).

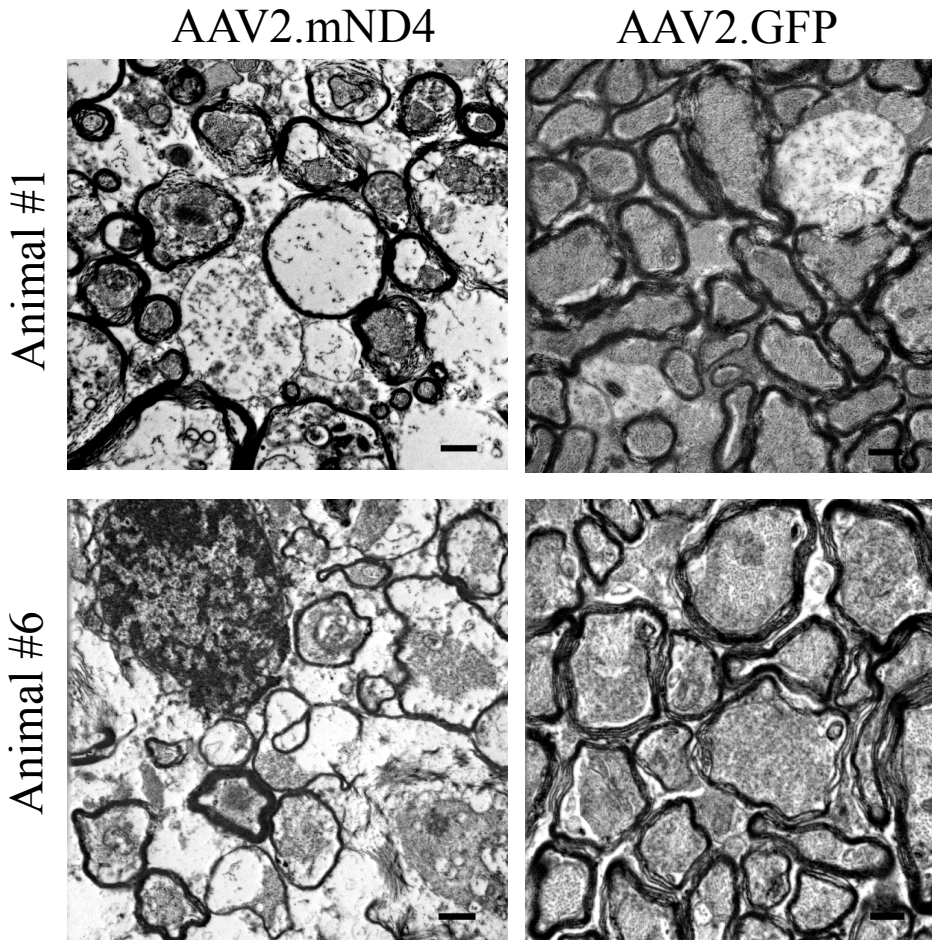

Supplemental Figure 2.2. mND4 induces optic nerve degeneration. TEM images of mND4 or GFP-injected retinas show that mND4 induces demyelination and axon degeneration in the optic nerve. The GFP-injected eye shows normal myelination of the axons, and closely packed axons with very few spaces between them. Scale bar represents 500nm.

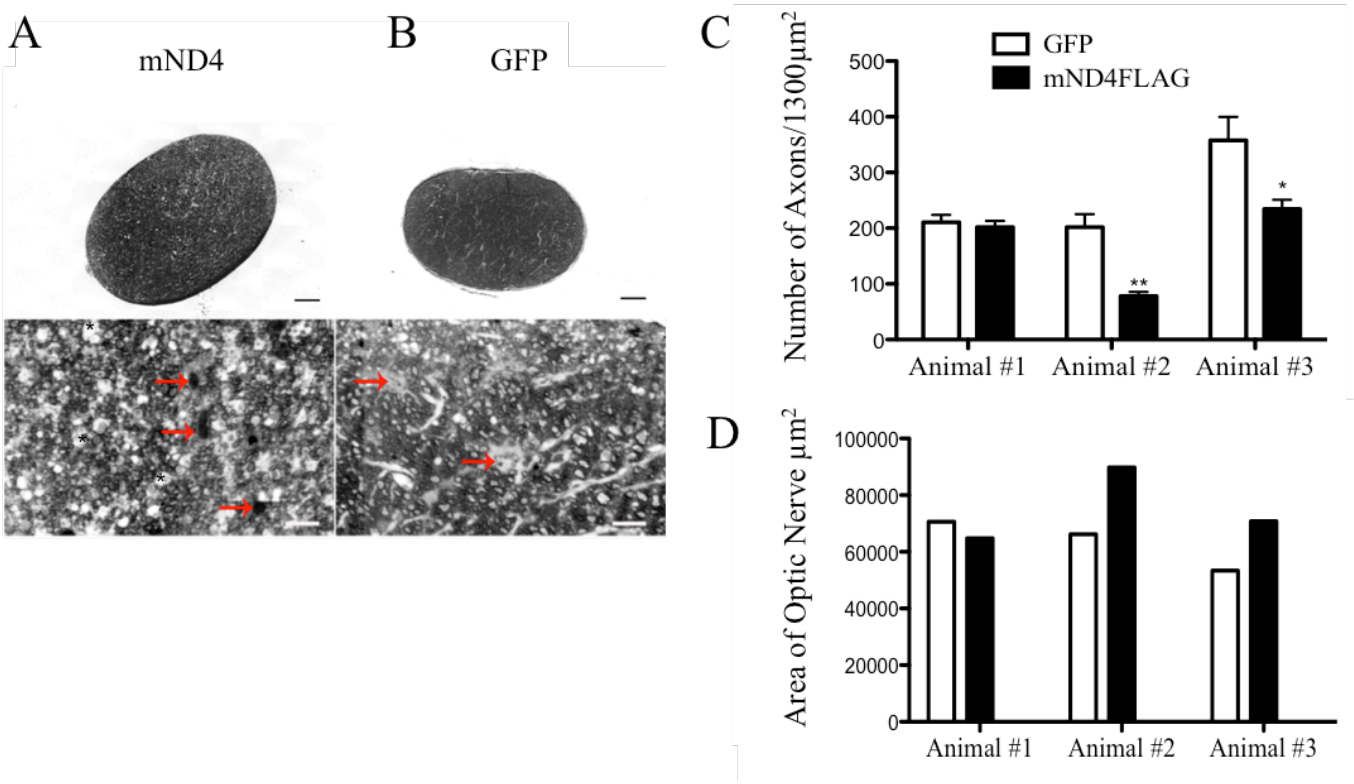

Figure 2.3. mND4 induces degeneration and axon loss.
Toluidine blue staining of optic nerve cross-sections show enlarged optic nerve, axon swelling (asterisks), glial cell infiltration and apoptotic bodies which have taken up the TB stain (red arrows) in mND4-injected animals (A), whereas the control optic nerves are normal, with healthy glia (red arrow) (B). C) Axon counts in 3 animals show variability in disease progression with 2 of the 3 showing significant reductions in axon counts. ** $p<0.00005$, *$P=0.007$, using a Student's t-test. D) The animals with reduced axon numbers show increased optic nerve cross-sectional areas, possibly due to axon swelling and glial cell infiltration in the early stages of the disease. Scale bars represent 50µm (low magnification) and 10µm (high magnification).

infiltration, glial cell apoptosis and axon swelling, although not to the extent of the optic nerves analyzed by TEM. Detailed analysis of the toluidine blue-stained optic nerves showed a range of effects in AAV2.mND4FLAG-injected animals with some optic nerves affected more than others. For example, axon counts revealed significant reductions in 2 of the 3 AAV2.mND4FLAG-injected eyes (34.5% and 57.8% reductions) in comparison to the contralateral control eye, whereas one animal did not appear to be affected (4.4% axon loss) (Figure 2.3C). Interestingly, when cross-sectional areas of the optic nerves were measured, the optic nerves with axon losses actually had larger areas, potentially due to axon swelling and glial infiltration, which is a hallmark of early stages of the LHON disease (Figure 2.3D). Haematoxylin and eosin stained cross-sections of the retinas of mND4-injected animals showed nerve fibre layer (NFL) thinning and destruction (Figure 2.4), also supporting the LHON phenotype of RGC degeneration.

Overall, the disease characteristics seen at three months after mND4 delivery to the retina were highly variable, with some animals clearly showing significant signs of axon demyelination and axon loss, and others showing few changes. This indicates that the 3-month timepoint represents an early stage of the disease when pathological changes are emerging but not fully established in all animals.

XIAP gene therapy in the mouse model of LHON

The above studies clearly showed that disease was initiated in some animals at 3 months after mND4 injection. However, since the pathological changes were extremely variable between animals, we conducted a more extended (4-month) disease time course for the subsequent study, which examined the ability of XIAP to protect RGCs from

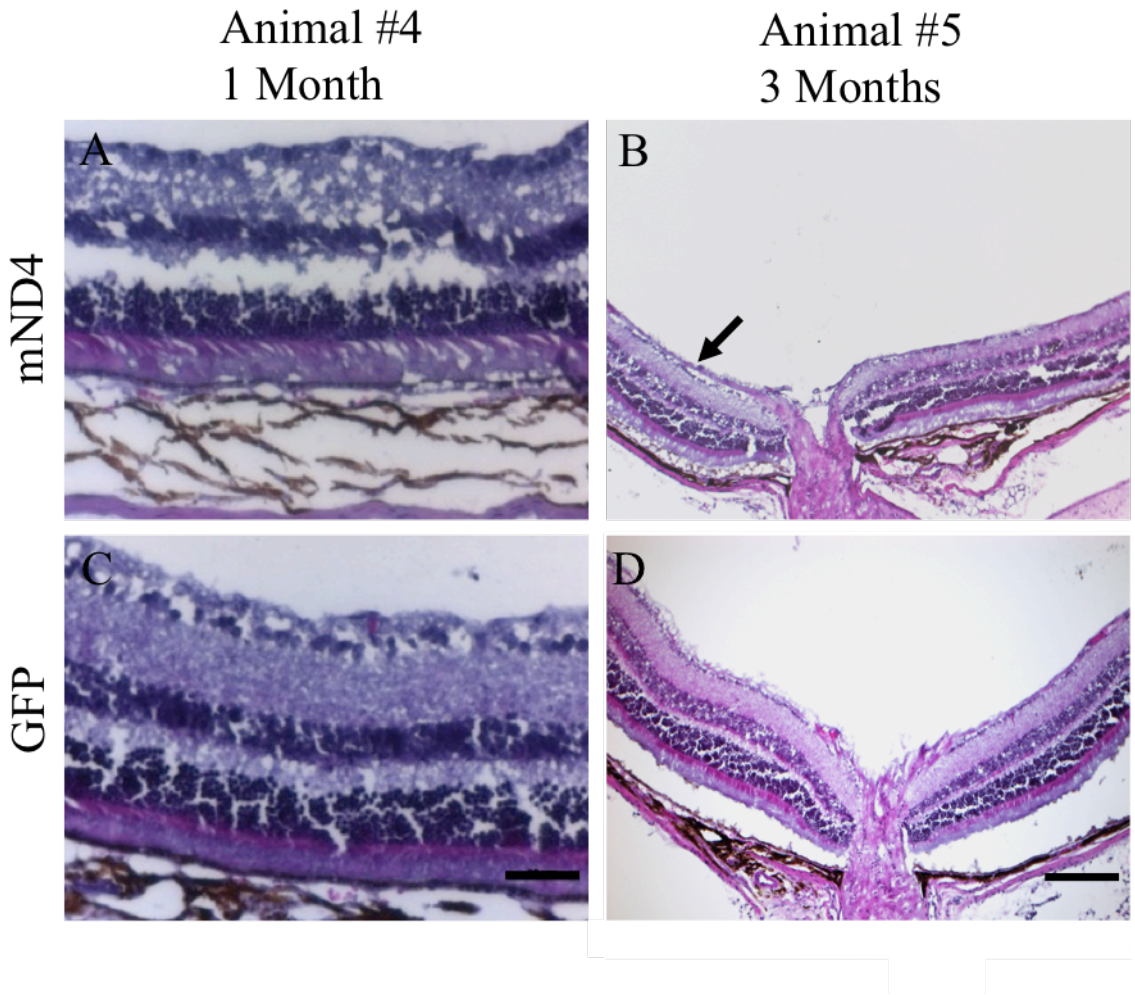

Figure 2.4. H&E sections show reduced nerve fiber layer (NFL) thickness in mND4-injected eyes. The NFL (arrow) is very thin in the mND4-injected mouse 1 and 3 months after the injection. A) High and B) low magnification of two different mND4-injected retinas. C) High and D) low magnification of two different GFP-injected contralateral retinas showing a thick NFL covering the RGC layer. Scale bar represents 50µm (high magnification) and 200µm (low magnification).

LHON disease progression. For these studies, animals received an intravitreal injection of AAV2.HA-XIAP in one eye and AAV2.GFP in the contralateral eye. Two weeks later, the animals received AAV2.mND4FLAG in the XIAP-treated eye, in the GFP-treated eye or in both eyes. *In vivo* fundus imaging 2 weeks after the injection showed GFP fluorescence in an AAV2.GFP/ AAV2.mND4FLAG double-injected retina, confirming that the viral transgene was expressed soon after viral delivery (Figure 2.5A). Immunolabelling with HA and FLAG antibodies (representing XIAP and mND4, respectively) showed the continued presence of the proteins in the retinal ganglion cell layer 4 months after AAV2.mND4FLAG injection (Figure 2.5B,C).

XIAP over-expression protects axon structure in early onset LHON disease

The effects of XIAP gene therapy on RGC axon health were analyzed using several parameters. Transmission electron microscopy (TEM) was conducted in two randomly selected mice that were injected with GFP/mND4 in the right eye and XIAP/mND4 in the left eye. In both animals, the XIAP-treated mND4 eyes showed reduced pathology compared to the GFP-treated mND4 eyes. In one of these animals, the GFP-treated eye showed demyelination, axon swelling, advanced nuclear fragmentation in resident astrocytes or oligodendrocytes, areas of axon loss and axon compaction. In contrast, the contralateral XIAP/mND4 treated optic nerves showed thick myelinated axons, no swelling, less advance nuclear fragmentation and less axon loss (Figure 2.6). Although the second animal also showed improved optic nerve integrity in the XIAP-treated eye, the differences between XIAP and GFP-treatment in this animal were not as pronounced. In this animal, there was evidence of optic nerve damage in both eyes

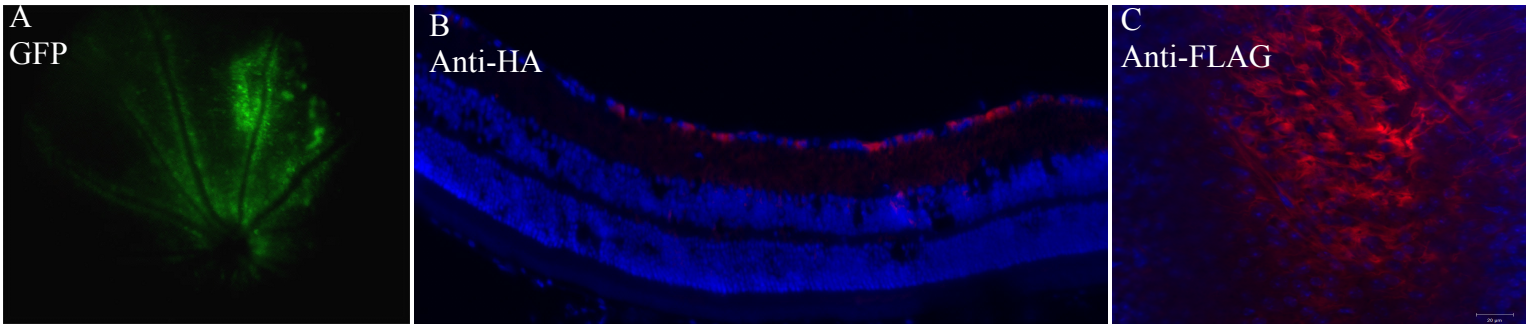

Figure 2.5. Imaging in double-injected retinas confirms expression from all viruses injected.
A) Fluorescent fundus image of an eye that received both AAV2.GFP and AAV2.mND4-FLAG shows robust GFP expression at two weeks following the second injection, indicating good coverage from the viral injection. B) Immunofluorescent image of a retinal section through an eye that received AAV2.HA-XIAP and AAV2.mND4-FLAG. The HA tag shows robust XIAP expression in the RGC layer. C) Retinal flat mount of an eye that received AAV2.HA-XIAP and AAV2.mND4-FLAG shows mND4 expression in the RGC layer.

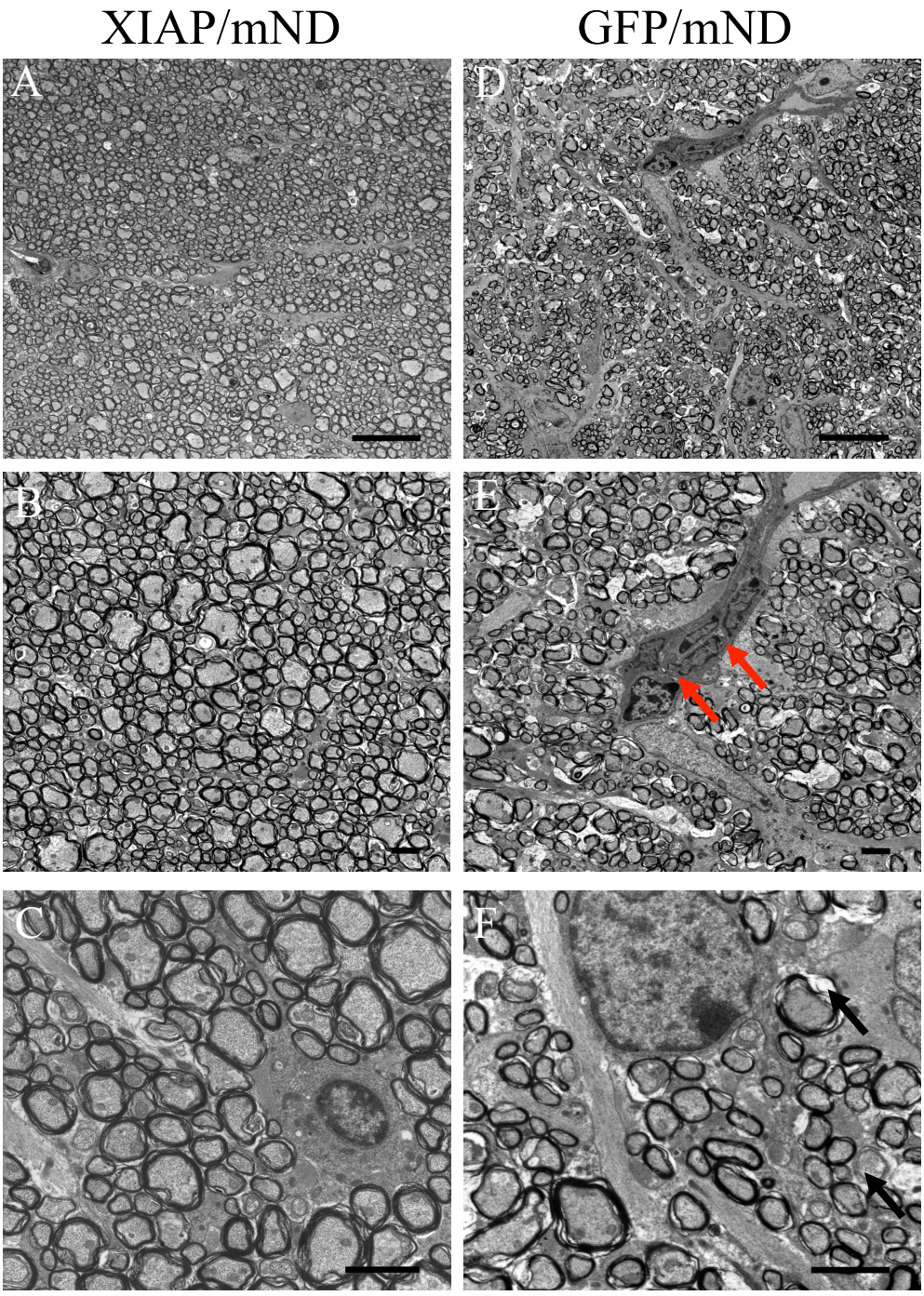

Figure 2.6. TEM analysis shows improved optic nerve morphology in XIAP-treated retinas.
GFP/mND4 treated eyes (D-F) show axonal compaction and thinner cross-sectional areas (D) as well as increased nuclear fragmentation of resident glial cells (red arrows, E) and reduction in myelin (black arrow, F). By comparison, XIAP/mND4 injected retinas have thicker axons, less glial cell infiltration and healthier nuclei. Scale bars represent 10µm (A,D) and 2µm (B-F).

(Supplemental Figure 2.3), but the XIAP-treated eye showed reduced damage. Axon counts from toluidine blue stained sections of the optic nerves in these two animals revealed a two-fold higher number of axons in the XIAP-treated optic nerve in the first animal and a 1.4-fold higher number of axons in the second animal in comparison to the GFP-treated eye (see Supplemental Figure 2.4).

In vivo magnetic resonance imagining (MRI) showed a significant difference in optic nerve diameter between XIAP-treated and GFP-treated mND4 eyes. Optic nerve diameter measurements showed XIAP optic nerves were 12.5% thicker than their GFP-treated counterparts (Figure 2.7A, B). Axon counts were conducted on cross-sectioned, toluidine blue-stained optic nerves. Despite the increased timeline (4 months of disease projection rather than the 3 months of the first cohort of animals), there was still considerable inter-animal variation in axon counts, with some animals showing considerable axon losses, while others did not show any reductions in axon counts. Even though GFP/mND4-treated eyes showed a 28.5% trend towards a reduction in axon numbers in comparison to the XIAP/mND4 group (Figure 2.7C), this number did not reach significance ($p=0.06$) based on the high degree of variability between animals. Although there were no significant losses in the number of axons, cross-sections of optic nerves clearly demonstrated that the mND4 mutation caused significant axon thinning, indicating that axons are in the process of dying. Measurements of axonal cross-sectional areas revealed that GFP/mND4 animals had significantly higher numbers of thinner axons (51.9% more) in comparison to the XIAP/mND4 animals ($p=0.05$) (Figure 2.7D, and Supplemental Figure 2.5). In support of this data, hematoxylin and eosin staining of retinal cross-sections showed thinning of the nerve fibre layer (NFL) in GFP/mND4

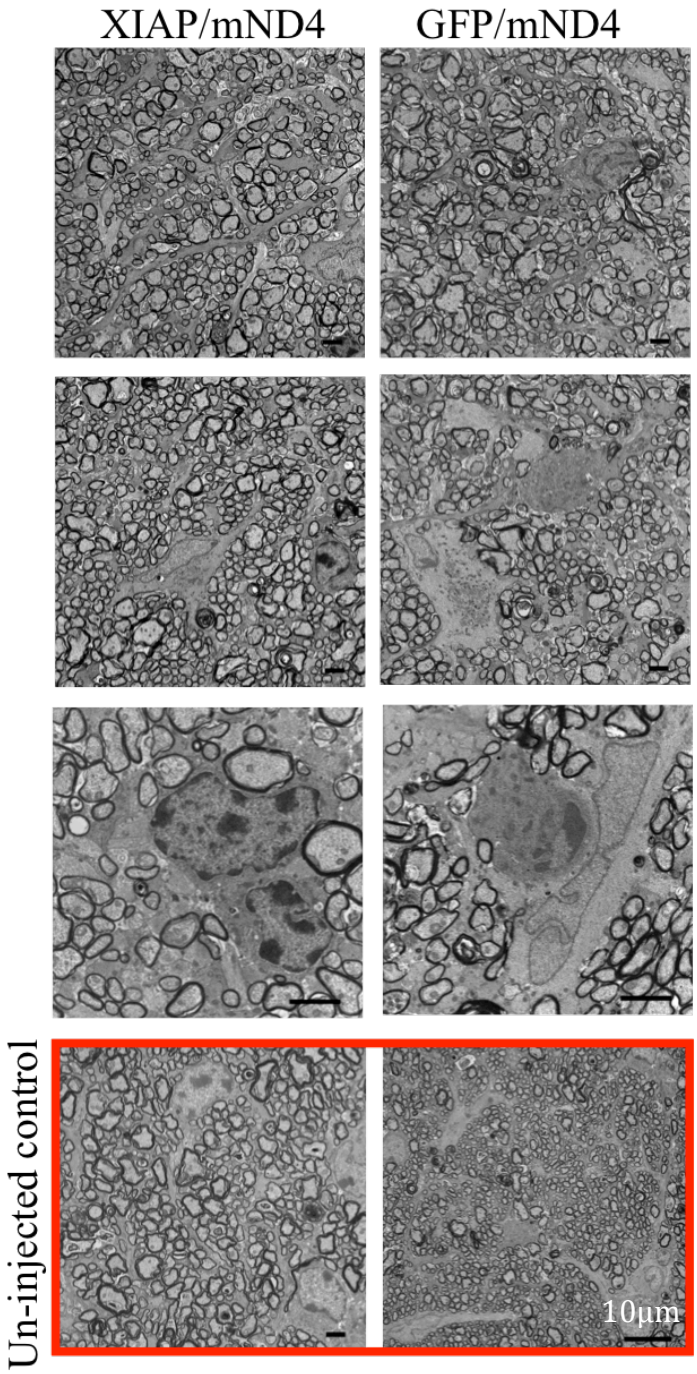

Supplemental Figure 2.3. XIAP-treated mND4 eye has reduced optic nerve pathology. The variability in the efficacy of XIAP therapy is seen in this animal which shows pathology in both eyes (nuclear fragmentation), showing that XIAP is not always entirely effective in protecting the optic nerve. However, the damage in the XIAP/mND4-treated eye is not as severe as in the contralateral GFP/mND4-treated eye. Axon counts showed that the XIAP/mND4 optic nerve had 1.4X the number of axons found in the contralateral GFP/mND4-treated eye. Two uninjected control optic nerves are shown for comparison. Even in these eyes, there are pyknotic vessels, and evidence of autophagy indicating that some degree of axon loss is associated with normal aging. Scale bar represents 2µm, unless indicated.

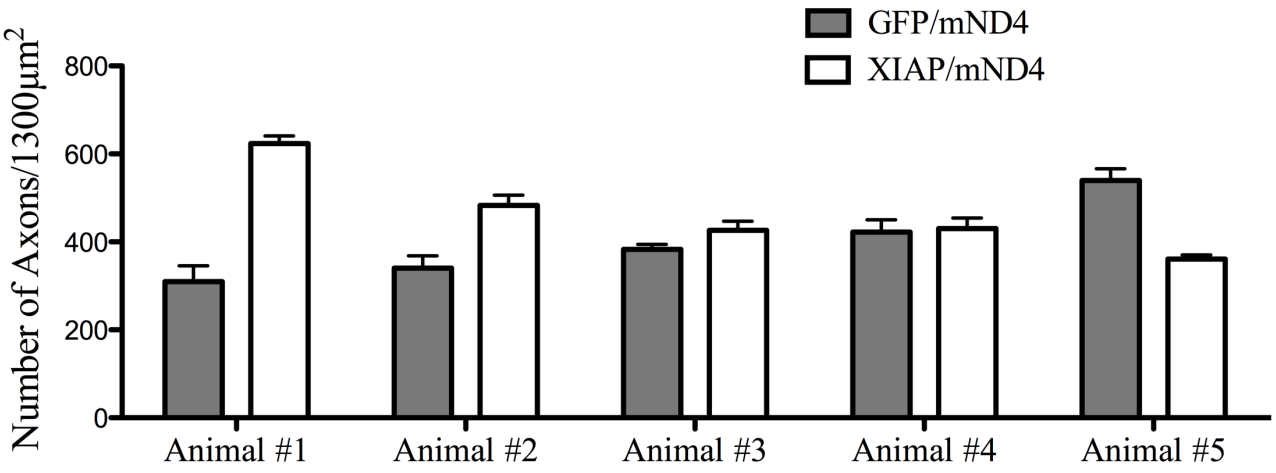

Supplemental Figure 2.4. **Variation in axon number between animals.**
Axon counts in 5 animals that received GFP/mND4 in one eye and XIAP/mND4 in the contralateral eye. The axon counts were conducted at 4 months after the double injection. In three of the 5 animals, there was no significant loss in axon numbers, indicating that the disease had not progressed to the point where axon loss was evident. Animals 1 and 2 were used for TEM analysis.

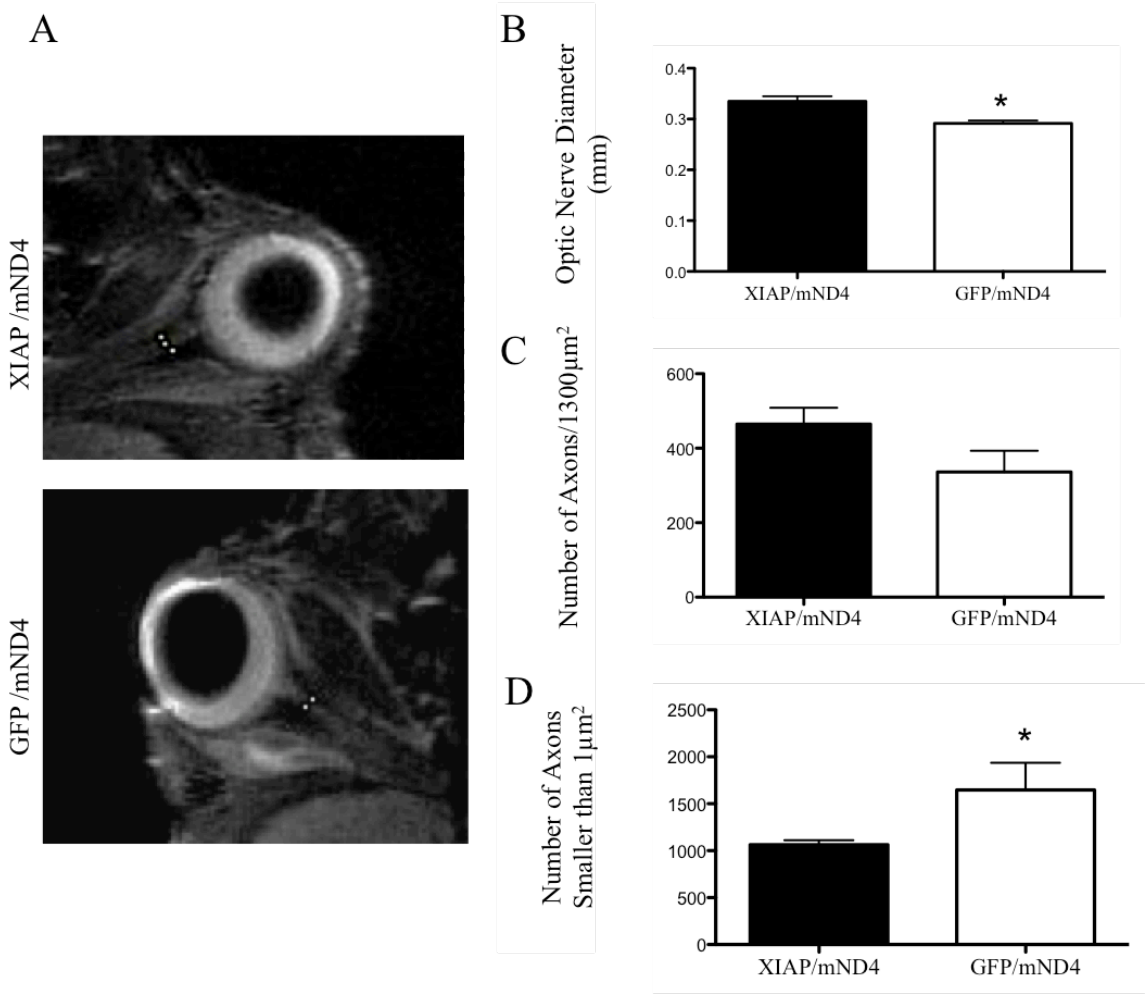

Figure 2.7. Optic nerve measurements show efficacy of XIAP therapy in preserving axonal integrity. A) Magnetic resonance imaging of the orbit allows measurements of the diameter (white dots) of the optic nerve. Measurements were taken at the same distance from the optic cup in all the animals. B) Optic nerve diameters of GFP/mND4-treated retinas are significantly smaller than XIAP/mND4-treated retinas. $P<0.05$, n=3 eyes. C) GFP/mND4-treated eyes show a 28.5% trend towards reduction in axon numbers in comparison to the XIAP/mND4 group, but this number does not reach significance ($p=0.06$) based on the high degree of variability between animals. D) Although there are no significant losses in the number of axons, cross-sections of optic nerves show that the mND4 mutation causes significant axon thinning ($p=0.05$) in comparison to the XIAP/mND4 animals. For (C) and (D), n=5 XIAP and n=7 GFP treated mND4 eyes.

animals and the preservation of the NFL in the majority of XIAP/mND4 animals (Supplemental Figure 2.5).

Pattern ERG (PERG) analysis was conducted to assess the effect of XIAP gene therapy on retinal function. It is important to note that the PERG traces did not show typical patterns as they were affected by background noise, although, more XIAP animals had typical waveforms. Preliminary analysis after three months showed that XIAP/mND4 animals had stronger ganglion cell response, compared to GFP/mND4 animals. This suggests that the pathology seen in the GFP/mND4 animals do impact ganglion cell function. Further studies are required to determine the veracity of these results (Supplemental Figure 2.6).

Overall, in both the initial characterization of the disease and in the subsequent gene therapy studies, mND4 led to axon thinning, glial cell infiltration, axon swelling, demyelination and nuclear fragmentation in resident astrocytes or oligodendrocytes. These degenerative changes only represented the early stages of LHON disease in most of the animals and did not result in significant losses in axon numbers, however, there was significant loss in function. Importantly, however, XIAP gene therapy reduced axon thinning, preserved axon diameters in the optic nerve, reduced NFL thinning in the retina and may have preserved function (further analysis is required).

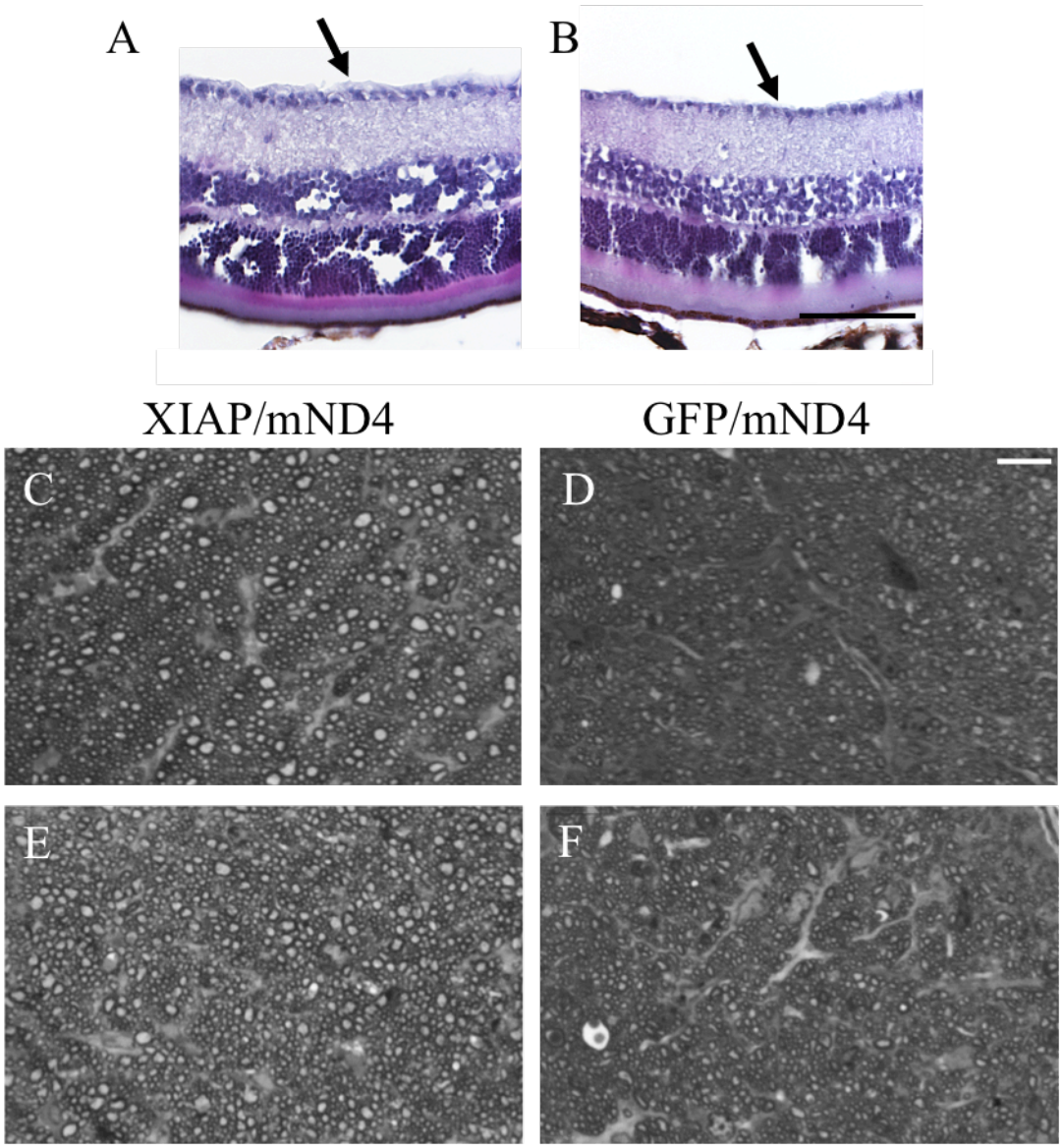

Supplemental Figure 2.5. Axon and NFL thinning in GFP/mND4-treated retinas. H&E sections (A) and Toluidine blue (B,E) confirm that the XIAP/mND4-treated retinas have thicker NFL layer and thicker axons, when compared to GFP/mND4-treated retinas (B,D,F). Scale bar represents 100µm (A,B) and 10µm (C-F).

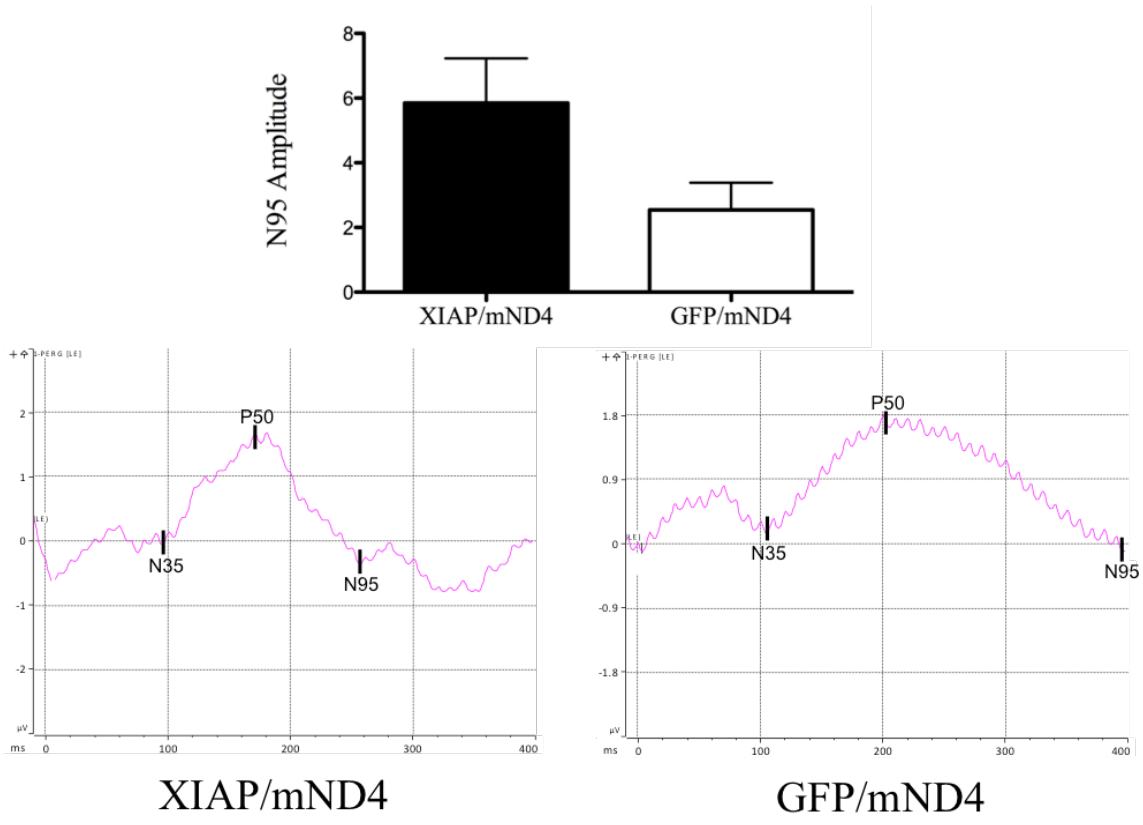

Supplemental Figure 2.6. Evidence of functional protection with XIAP gene therapy.
At three months post injection, PERG traces were confounded by background noise and variability. However, XIAP/mND4 eyes had stronger N95 values than GFP/mND4 treated animals (n=5 eyes/group). It is important to note that further analysis with more controls must be performed.

Discussion

LHON symptoms typically present in patients during early adulthood, although the age of onset can vary from childhood to late adulthood. LHON manifests as a bilateral loss of central vision, but often vision loss occurs initially in one eye followed within weeks to months by the contralateral eye. In some cases, the central vision loss may spontaneously improve, but most patients experience gradual deterioration, leading to permanent vision loss. Overall, the human form of the disease presents as a spectrum with differences even between affected individuals carrying the same mutation. We, too, saw variation in disease progression in the mutant ND4 mouse model of LHON. Some animals presented with severe degeneration of the optic nerve, characterized by nearly complete axon loss, glial cell infiltration, the absence of myelin and large sections of empty spaces in the optic nerve, which was detected as early as three months post-injection. Conversely, other animals showed modest axon loss and myelin thinning at the later time point of 4 months, when AAV-mND4 was administered after a first AAV injection. Other studies using this animal model have examined disease progression at 6 months and 1 year, clearly showing the progressive nature of the disease and the reduced variability in symptoms with an advanced disease timeline (Koilkonda et al., 2014; Qi et al., 2007; Yu et al., 2012b).

The variation in human and mouse disease cannot be attributed to similar mechanisms. Whereas the human disease has potential genetic modifiers and clear environmental agonists (such as alcohol and tobacco), the same cannot be said of an inbred, environmentally controlled mouse colony. In the mouse model, the likely sources

of variation between animals were the variability of the injection procedure (which may target different numbers of retinal ganglion cells every time) and the difficulty in targeting the potentially hundreds or thousands of mitochondria within a cell with the mutant ND4 protein. In addition, we cannot discount the possibility that circulating neutralizing antibodies following the first AAV-XIAP or AAV-GFP injection may have reduced the efficacy of the AAV-mND4 injection delivered two weeks later, also adding to the variability in the model and reduced phenotype as compared to the first study with one injection. Transgenic models of LHON, which are currently under development (Yu et al., 2015), may help to reduce some of this variability in future studies.

In this study, XIAP efficacy in preventing retinal cell death was examined both *in vitro* and *in vivo*. In the *in vitro* studies in 661W cells, XIAP over-expression prevented oxidative stress-induced apoptotic cell death. *In vivo*, XIAP had a significant effect on optic nerve diameter and it significantly reduced the number of thinned axons, maintaining axonal cross-sections at control values. XIAP-treated retinas also had a preserved nerve fiber layer, and optic nerves showed reduced glial cell infiltration and preserved myelination. Furthermore, despite variable pattern ERGs waveforms, taken together, XIAP treated animals had the strongest functional response as indicated by N95 amplitude.

We delivered XIAP prior to inducing LHON in order to ensure that there would be adequate levels of XIAP expressed in the retina before LHON-associated damage had begun. These studies provide proof-of-principle for XIAP efficacy in the prevention of RGC damage, but would not be directly applicable to human disease. It would be interesting to evaluate XIAP neuroprotection at later and, therefore, more severe stages of

the disease (6 months to 1 year), and to determine if XIAP can protect RGCs from dying after the onset of disease has begun. These studies should, ideally, be conducted in LHON transgenic animals so that only a single therapeutic injection of AAV2 would be required. With the current model, the two AAV injections required (one to induce the disease and the second therapeutic injection many months later) may allow sufficient time in between injections for neutralizing antibodies to be generated that would limit the therapeutic outcome (Kotterman et al., 2015).

Recently, work by Guy and colleagues (University of Miami, Florida) has shown significant rescue in mouse and non-human primate models of LHON treated with AAV2 carrying wild-type ND4 (Koilkonda et al., 2013, 2014). The success of these studies has resulted in a human clinical trial that is currently underway (Feuer et al., 2015). It remains to be seen whether this therapy will have long-term effects in protecting retinal ganglion cells, or if the retina will continue to degenerate, similar to the clinical trials in Leber's congenital amaurosis (LCA), which showed functional improvements following gene replacement therapy, but continuing retinal degeneration (Cideciyan et al., 2013a; Jacobson et al., 2015). Based on the promising results obtained in this study, XIAP therapy presents an alternative strategy for the treatment of LHON. Moreover, if degeneration continues in the LHON patients in the ongoing clinical trial despite gene replacement, then combination therapy with wildtype ND4 and XIAP may provide a better outcome than either therapy alone. Dual therapy is supported by a study that used XIAP as an adjunct to AAV-mediated PDEβ gene replacement therapy in the rd10 mouse and showed that it decreased rates of retinal degeneration compared to AAV-PDEβ alone (Yao et al, 2012).

Acknowledgements

The authors thank Dr. John Guy for providing the AAV constructs used to generate viruses for this study, and Dr. Gregory Cron and his team for performing magnetic resonance imaging. Special thanks are extended to Adam Baker for technical assistance with intravitreal injections and John Hamilton for assistance with pattern electroretinography.

This work was supported by Canadian Institutes of Health Research (CIHR) and Foundation Fighting Blindness (FFB) grants to CT, and NIH grant P30-EY021721, MVRF and RPB Inc funding to WWH. CT is supported by the Don and Joy Maclaren Chair for Vision Research. SW was supported by the David S. Shillito Scholarship in Ophthalmology and by an Ontario Graduate Scholarship.

CHAPTER 3: THE DEVELOPMENT OF A CAT MODEL OF RETINAL DETACHMENT AND RE-ATTACHMENT

The development of a cat model of retinal detachment and re-attachment

Sarah Wassmer[1,2*], Brian C. Leonard[1,3*], Stuart G. Coupland[1,2,3], Adam Baker[1], John Hamilton[1], Renée Torlone[4], David N. Zacks[5], and Catherine Tsilfidis[1,2,3]

*These authors contributed equally to this work

[1]Ottawa Hospital Research Institute, Regenerative Medicine, K1H 8L6, Ottawa, Canada

Departments of [2]Cellular and Molecular Medicine, [3]Ophthalmology, University of Ottawa, Faculty of Medicine, K1H 8M5, Ottawa, Canada

[4]Ottawa Hospital General Division, Eye Institute, K1H 8L6, Ottawa, Canada

[5]Department of Ophthalmology and Visual Sciences, Kellogg Eye Center, University of Michigan Medical School, Ann Arbor, MI.

Corresponding Author: Catherine Tsilfidis, 501 Smyth Road, CCW-W6113, Ottawa, Ontario, Canada, K1H 8L6; Phone: (613) 737-8233; E-mail: ctsilfidis@ohri.ca

Author Contributions:

Sarah Wassmer helped to design and carry out the experiments, collected and analyzed all of the data, wrote the manuscript and made the figures.

Brian C Leonard helped to design the experiments and performed the retinal detachment surgeries.

Stuart G Coupland, Adam Baker and John Hamilton set-up the ERG, fundus and OCT machinery and assisted in data collection.

Renée Torlone acted as a surgical assistant to Brain Leonard.

David N Zacks assisted with the design of the surgeries.

Cather Tsilfidis funded the studies, helped to design the experiments and write the manuscript.

Article published October 2015 in *Advances in Experimental Medicine and Biology*, Volume 854, pages 315-321.

Abstract

We present an optimized surgical technique for feline retinal detachment which allows for natural re-attachment, reduces retinal scarring and vitreal bands, and allows central placement of the detachment in close proximity to the optic nerve. This enables imaging via Optical Coherence Tomography (OCT) and multifocal electroretinography (mfERG) analysis. Ideal detachment conditions involve a lensectomy followed by a three-port pars plana vitrectomy. A 16-20% retinal detachment is induced by injecting 8% C_3F_8 gas into the subretinal space in the central retina with a 42G cannula. The retinal detachment resolves approximately 6 weeks post-surgery. Imaging is enhanced by using a 7.5 and 20 diopter lens for OCT and mfERG fundus imaging, respectively, to compensate for the removed lens.

Introduction

Retinal detachment is a common form of injury. Treatment typically involves surgical re-attachment of the retina, but recovery of vision depends on the nature and duration of the detachment. Retinal detachments often lead to changes in the retina that can have permanent effects on visual function. Loss of vision is further increased if the macula is involved in the detachment (Erickson et al., 1983).

Animal studies have shown histological and molecular evidence that retinal degeneration ensues as early as one hour post detachment (Erickson et al., 1983; Zacks et al., 2003). A major cause for vision loss is photoreceptor apoptosis (Zacks et al., 2003).

Oxidative stress has also been implicated in photoreceptor apoptosis and disease pathology (Cederlund et al., 2013; Huang et al., 2013).

We have shown that the X-linked Inhibitor of Apoptosis (XIAP) is effective in protecting photoreceptor structure in a rat model of retinal detachment (Zadro-Lamoureux et al., 2009). However, due to the small size of the rodent eye, surgical re-attachment is technically very challenging. Thus, while the effects of XIAP on the structure of photoreceptors can be determined, the function of the photoreceptors is difficult to assess. Consequently, for our studies, and for those of others interested in studying therapeutic strategies for retinal detachment, there is still a critical need to develop a larger animal model of detachment and re-attachment of the retina. We present here a feline model of detachment and re-attachment which allows central placement of the detachment so that structural and functional recovery of photoreceptors can be assessed using OCT and multifocal ERG.

Materials and Methods

Animals

Three wild type (domestic) cats (Liberty Research, Waverly, NY) aged 12 months were studied. Animal procedures were conducted in accordance with the University of Ottawa Animal Care Committee rules and regulations and adhered to the ARVO statement for the Use of Animals in Ophthalmic and Vision Research.

Pre- and Post-Operative Treatments

Cats were given propofol (1mL/min) intravenously or 5% isoflurane by aerosol mask before surgery and during the anesthetic regime (see below). Throughout the surgery animals were kept on 2% to 3% isoflurane. After the surgery, the eyes were treated with 5 to 10 drops of 1.0% w/v atropine sulphate (Chauvin Pharmaceuticals) and covered with Tobradex Ophthalmic Ointment (tobramycin 0.3%, dexamethasone 0.1%) (Alcon). The animals were treated 4 times daily with Tobradex for ten days.

Animal Anesthetic Regimes

Animals were treated with one of five anesthetic regimes in order to optimize the drug cocktail and concentrations. Regime 1: hydromorphone (Sandoz) 0.1mg/kg (2mg/mL), acepromazine (Boerhinger) 0.1mg/kg (10mg/mL), glycopyrrolate (American Regent) 0.01mg/mL (0.2mg/mL) and propofol (1mL/min); Regime 2: medetomidine hydrochloride (Modern Veterinary Therapeutics) 0.015mg/kg (1mg/kg) and hydromorphone 0.1mg/kg (2mg/mL) and isofluorane; Regime 3: medetomidine hydrochloride 0.04mg/kg (1mg/kg) and isoflurane; Regime 4: medetomidine hydrochloride 0.015mg/kg (1mg/mL), hydromorphone 0.1mg/kg (2mg/mL), cerenia (Pfizer) 0.5mg/kg (10mg/kg), buprenorphine (Champion Alstoe) 0.02mg/kg and isoflurane; Regime 5: medetomidine 0.015mg/kg (1mg/mL), hydromorphone 0.1mg/kg (2mg/mL), cerenia 0.5mg/kg (10mg/kg) and isoflurane. Animals were administered normosol fluids under all regimes, and given mydiacyl (Alcon) (1%), mydfrin (Alcon) (2.5%) and alcaine (Alcon) (0.5%) drop-wise to the surgical eye.

Retinal Detachment Procedure

Animals were administered one of the anesthetic regimes discussed above by intramuscular injection, in addition to pre-operative treatment and held on 2% to 3% isoflurane during the procedure. All techniques were performed under sterile operating room conditions. The head was elevated to ensure the eye was directly under the Zeiss ophthalmic operating microscope. The operative field was swabbed with 10% providone iodine (3M). Supplemental oxygen (2L/min) was administered via intubation (Engler Engineering Corporation), and vital signs (oxygen saturation, heartrate, blood pressure) were monitored throughout the procedure (Surgivet Smith Medicals).

A generous lateral canthotomy was performed to enhance surgical exposure. A fornix-based conjunctival and Tenon's capsule flap was dissected temporally. A Barraquer wire eye speculum was placed incorporating the eyelid margins, the nictitating membrane and the conjunctival and Tenon's capsule flap. Bipolar cautery of the scleral surface with a 25 gauge (G) straight disposable bipolar pencil (Kirwan Surgical Products) minimized bleeding from the rich ciliary vascular complex. Three sclerotomies were then fashioned 4 mm from the limbus within this tight temporal area of exposure. One 20G equatorial incision was placed centrally with a 20 G 1.3mm V-lance knife (Alcon) to accommodate a 20 G Alcon Accurus Fragmatome handpiece, flanked by two 25G cannula ports used interchangeably for a 25G Accurus vitrectomy handpiece, an intraocular infusion cannula and an endoilluminator probe. Placement of all three sclerotomies into the lateral temporal quadrant was necessary due to the limited exposure imposed by the large feline eye, deeply set within a small tight socket.

A pars plana lensectomy was performed with linear phacofragmentation using a 20G Accurus Fragmatome handpiece. A vitrectomy was performed with a 25G Accurus vitrectomy handpiece with visualization from an Oculus BIOM posterior segment panoramic imaging system with image inverter. A 16-20% retinal detachment was placed in the posterior central pole by subretinal injection of 8% C_3F_8 gas via an angled 42G subretinal cannula using a disposable vitrectomy flat lens (Dutch Ophthalmic). Coaxial illumination from the microscope through the contact lens system, without an endoilluminator probe, provided a sufficient magnified view of the posterior segment to allow precise two-handed placement of the subretinal cannnula.

At the completion of the surgery, the posterior chamber was filled with automated air-fluid exchange to promote internal sclerotomy wound integrity. The sclerotomies, conjunctiva and Tenon's capsule were closed with 7-0 Vicryl suture (Ethicon).

Functional Testing

Multifocal electroretinograms (mfERGs) were recorded with the VERIS^{TM} Multifocal System (Electro-Diagnostic Imaging, Inc), using an unscaled stimulus containing 7 hexagonal elements projected on the central 45 degrees of retina through a dilated pupil. Multifocal ERGs were recorded with OcuScience ERG-jet contact lens electrodes and ERG signals were amplified 50,000 times using Grass P511J amplifiers (Grass Technologies) with a 10-100Hz bandpass. The first order kernel of the M-13 sequence was extracted and displayed. Spectral-domain Optical Coherence Tomography (sd-OCT) (OPKO SLO/OCT) was used to image the area of the retinal detachment. Accessory lenses (Eschenbach Optik GmbH) were used for mfERGs and sd-OCT imaging to

compensate for the aphakia and provide focused conditions. Line scans, raster scanning and 3-D retinal topographic scanning modes were used.

Results

In order to optimize the retinal detachment model, three parameters were evaluated: type of surgery required (lens/vitreous removal or sparing), method of detachment (percentage of the C_3F_8 gas), and the optimal anesthetic regime to be administered.

A total of three cats were studied to determine the proper parameters for a retinal detachment and re-attachment. The detachment surgery for the first animals was a "direct" approach in which the lens and vitreous were spared. We used a 42G cannula to inject C_3F_8 gas into the subretinal space. In an attempt to place the detachment as centrally as possible, the lens was slightly nicked, and this later presented as a mild, stable cataract. The detachment surgery caused a small retro-vitreal hemorrhage (which later resolved) and the appearance of vitreal bands that extended from the pars plana sclerotomy sites to the posterior retinotomy. However, the fiber tracts did not progress to full tractional bands, as one would expect in a non-vitrectomised eye. Overall, we found that the large size of the feline lens discouraged lens and vitrectomy-sparing procedures because it made it virtually impossible to place the detachment site in the central retina. Consequently, imaging of the detached retina via sd-OCT and functional assessment with mfERG was impossible since the instruments can only monitor the central 29 and 45 degrees, respectively, of the retina. As a result, removal of the lens and vitreous was

necessary to allow central placement of the detachment and to remove hemorrhages or vitreal bands from the posterior chamber.

In the second cat, a mechanical suction cutter (cutter speed of 800 and vacuum up to 175) was used to remove the lens. However, the size and viscosity of the lens posed challenges that interfered with the timely and complete removal of the lens, and created post-operative complications in the eye. Therefore, the ideal technique for rapid and efficient removal of the lens involved phakofragmentation of the lens, with 100% power, 2500 cut rate and 600mmHg with an Alcon Accuris Vitrector & Fragmatome. This was followed by a vitrectomy to clean the vitreous cavity and to prevent retinal scarring and vitreal bands.

A 42G needle was used to deliver C_3F_8 gas into the subretinal space to induce the retinal detachment. We tested several different concentrations of the C_3F_8 gas (100%, 16% and 8%) and monitored the detachment over time for spread and speed of reabsorption. The 100% and 16% C_3F_8 gas expanded in the subretinal space, allowing less control over the size of the detachment. The 8% gas did not expand. In all cases, the gas was slowly reabsorbed (within 6 weeks), allowing the retina to re-attach on its own without surgical intervention. A 6-week detachment is ideal for neuroprotection studies as it creates a significant amount of permanent damage, allowing the testing of therapeutic interventions to prevent photoreceptor death.

Notably, we found that the anesthetic protocol can drastically affect the multifocal ERG waveform. Animals administered drug regimen 3, 4 or 5 (see Materials and Methods) displayed flat-lined mfERGs. These results were not due to a malfunction of the equipment, as a similar set up yielded healthy waveforms in rats (under 2% isoflurane

administration) and human volunteers. Using the same equipment, and anesthetic regimens 1 and 2 in the cats (ie. no cerenia and a low dose of medetomidine [0.015mg/mL]), the mfERG waveforms obtained were typical of a healthy cat (Figure 3.1).

Discussion

In this study, we determined the ideal experimental conditions for the creation of a cat model of retinal detachment and re-attachment. We found that a 3-port pars plana phacofragmentation lensectomy followed by a full vitrectomy allows unfettered access to the central retina where a controlled retinal detachment can be induced by the injection of 8% C_3F_8 gas into the subretinal space through a 42G cannula. The detachment slowly resolves over 6 weeks, allowing the retina to re-attach without surgical intervention. We also determined that an anesthetic regimen that contains low dose medetomidine and no Cerenia is critical for obtaining mfERGs. The effects of the anesthetic on the amplitude of the ERG may not be surprising since it has been shown that mild to moderate sedation in dogs using medetomidine significantly lowers flash electroretinogram a- and b-wave values (Lin et al., 2009; Norman et al., 2008). Furthermore, the antiemetic, Cerenia, is a substance-P inhibitor. Substance-P is an important signaling neuropeptide in two subpopulations of amacrine cells in the feline (Pourcho and Goebel, 1988). Inhibiting this neuropeptide may have contributed to the flat-line mfERG responses.

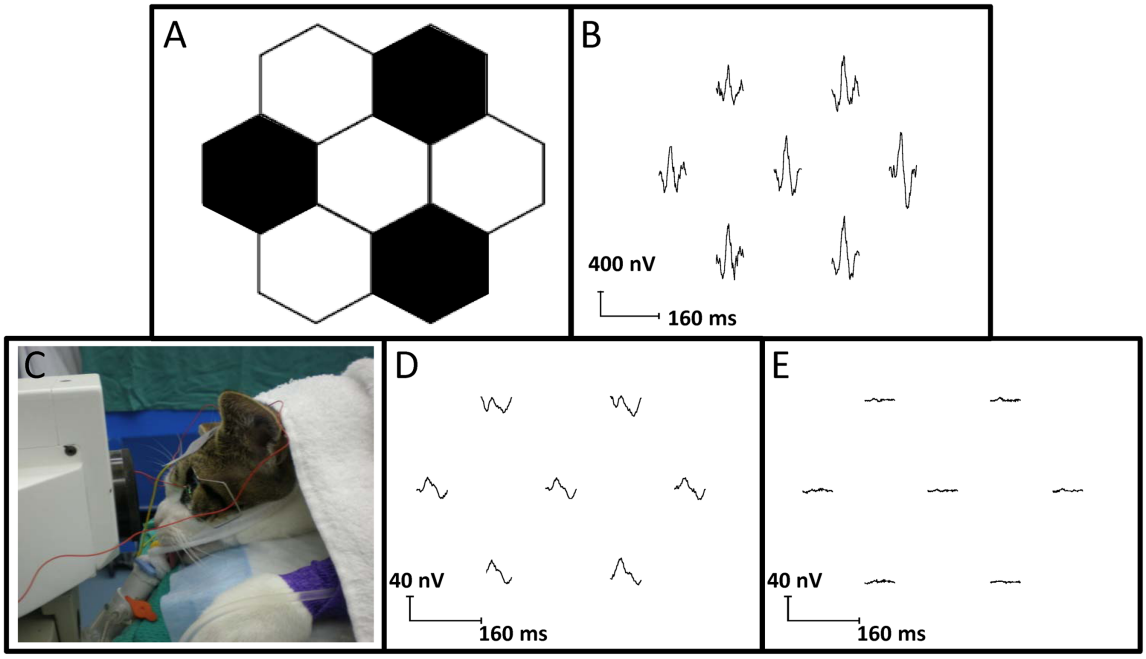

Figure 3.1. **Multifocal ERG set-up and results.**
A 7 hexagon array (A) was projected onto the central 45º of the retina. B) Control image of a human subject. C) Experimental cat set-up with contact lens electrode on the cornea, and reference and ground electrodes in the forehead and ear, respectively. D) Healthy mfERG in a cat. E) Flat-lined ERG with the same experimental setup as D, but with the anesthetic cocktail containing cerenia and a higher dose of medetomidine hydrochloride.

It has previously been reported that vitreous or sclerotomy hemorrhage is quite prevalent in cat models of stem cell or allograft transplantation (Bragadóttir and Narfström, 2003). This is due to the large vascular plexus in the pars plana region. Cauterization of the episcleral venous plexus and the use of topical vasoconstriction drugs to reduce intraocular hemorrhage have been proposed as a solution. In our hands, intraoperative hemorrhage did not present a significant problem. Small haemorrhages, when they presented, were treated by cauterizing the vessels.

The feline model that we have developed offers advantages over small rodent models of retinal detachment for testing therapeutic compounds. In rodent models, retinal detachment is most often induced by injection of hyaluronic acid into the subretinal space. The viscosity of the hyaluronic acid, and the small size of the rodent eye makes surgical reattachment and functional assessment of photoreceptors technically challenging. The size of the cat eye allows re- attachment of the retina and subsequent analysis of retinal structure and function by OCT and mfERG. Moreover, a number of studies have previously been conducted on retinal detachment in cats (Lewis and Fisher, 2000; Sakai et al., 2014), although as far as we are aware, none of these studies have subsequently re-attached the retina after long-term detachment. Thus, a good body of literature exists on the structural alterations (remodeling) in the retina following retinal detachment, and this information is very useful for assessing the therapeutic efficacy of experimental compounds.

Acknowledgments

We would like to thank the members of the University of Ottawa Animal Care and Veterinary Services for their help with animals and surgeries.

CHAPTER 4: XIAP OVER-EXPRESSION PROTECTS AGAINST RETINAL DEGENERATION IN A FELINE MODEL OF RETINAL DETACHMENT

XIAP over-expression protects against retinal degeneration in a feline model of retinal detachment

Sarah Wassmer[1*], Brian C. Leonard[2-4], Stuart G. Coupland[1-4], Adam N. Baker[3], John Hamilton[4], Renée Torlone[4], William W. Hauswirth[5], Catherine Tsilfidis[1-4]

[1]Department of Cellular and Molecular Medicine, University of Ottawa, Ottawa, ON, Canada

[2]Department of Ophthalmology, University of Ottawa, Ottawa, ON, Canada

[3]Ottawa Hospital Research Institute, Regenerative Medicine Program, Ottawa, ON, Canada

[4]Ottawa Hospital, Eye Institute, Ottawa, ON, Canada

[5]Department of Ophthalmology, University of Florida College of Medicine, Gainesville, Florida

Correspondence should be addressed to C.T. (ctsilfidis@ohri.ca)

Corresponding author's address:
Catherine Tsilfidis
Ottawa Hospital Research Institute
501 Smyth Road, Box 307
Ottawa, Ontario, K1H 8L6
Canada
Tel: 613-737-8233
Fax: 613-737-8836
Email: ctsilfidis@ohri.ca

Author Contributions:

Sarah Wassmer assisted with surgeries, conducted all the data collection and analysis, wrote the manuscript and made the figures.

Brian C Leonard performed all of the surgeries on the felines.

Stuart G Coupland, Adam N Baker and John Hamilton assisted with functional testing and feline imaging. Adam N Baker also helped with figure design.

Renée Torlone acted as a surgical assistant to Brain Leonard

William W Hauswirth provided all adeno-associated viral vectors.

Catherine Tsilfidis funded the studies, helped with experimental design and to write the manuscript.

Manuscript submitted to *Human Gene Therapy*, submission number HUM-2016-161.

Short title: **XIAP gene therapy in retinal detachment**

Abstract

Retinal detachment is an acute disorder in humans that is caused by trauma or disease, and it can often lead to permanent visual deficits. Our laboratory has previously shown that delivery of the gene encoding X-linked inhibitor of apoptosis (XIAP), using an adeno-associated viral (AAV) vector, can protect photoreceptor structure in a rat model of retinal detachment. The small eye of the rat made surgical re-attachment of the retina technically challenging and prevented the assessment of retinal function. In order to test the effects of XIAP therapy on retinal structure *and* function, we employed a feline model of retinal detachment. Retinas were detached by injecting C_3F_8 gas into the subretinal space. Detached retinas were treated with AAV-XIAP or AAV-GFP (as a control). Over a period of 3-6 weeks, the retinas re-attached by slow reabsorption of the gas. Photoreceptor structure was assessed with optical coherence tomography (OCT), fundus photography and histology, and function was assessed using full-field flash electroretinography (ERG). The results confirm that XIAP robustly protects photoreceptor structure in a large animal model of retinal detachment. These studies support the potential for XIAP therapy in the treatment of human retinal detachment.

Introduction

Retinal detachment (RD) occurs when trauma to the eye, accumulation of fluid in the subretinal space, or tractional pulling of the retina by vitreous bands induces a separation between the retinal pigment epithelium (RPE) and the sensory neural retina. The outermost layer of the retina, where the rod and cone photoreceptors reside, depends on the underlying RPE and choroidal vasculature for trophic support and maintenance of homeostasis (Jalali, 2003). Consequently, retinal detachment can lead to relatively rapid degenerative changes in the outer retina, with one study suggesting that there are histologic signs of retinal degeneration as early as one hour after retinal detachment in a cat model (Erickson et al., 1983). Despite the fact that retinal reattachment surgery is anatomically effective, visual acuity is often compromised and depends on the nature and duration of the detachment. Loss of vision is accentuated if the macula, the central area of the retina which provides detailed visual acuity, is involved in the detachment (Erickson et al., 1983).

Based on animal studies, the final pathway for photoreceptor cell death in retinal detachment involves both apoptosis and necroptosis (Arroyo et al., 2005; Huckfeldt and Vavvas, 2013). The physical separation of the retina from the underlying RPE leads to an increase in transcription of TNF-α and activates caspase-8 and caspase-9, ultimately leading to cell death by apoptosis (Nakazawa et al., 2011; Zacks et al., 2004). However, apoptosis is only one contributor to cell death in RD. Necroptosis, mediated by the formation of a ripoptosome by Receptor Interacting Proteins (RIP) 1 and 3 is also involved in RD-induced photoreceptor cell death (Trichonas et al., 2010). It has been

postulated that inhibition of apoptosis promotes a shift towards necroptosis and that caspase inhibitors alone cannot prevent photoreceptor cell death following retinal detachment (Trichonas et al., 2010).

The X-linked Inhibitor of Apoptosis (XIAP) has the ability to inhibit both apoptosis and necroptosis (Bertrand and Vandenabeele, 2011; Bertrand et al., 2008; Feoktistova et al., 2011). XIAP is a direct inhibitor of caspases 3, 7 and 9 and has been previously shown to preserve retinal cells in multiple forms of retinal degeneration (Leonard et al., 2007; McKinnon et al., 2002; Petrin et al., 2003; Renwick et al., 2005; Zadro-Lamoureux et al., 2009). Additionally, XIAP has also been shown to control TNF and RIP3-dependent inflammasome formation (Yabal et al., 2014). Furthermore, it has been suggested that XIAP and other members of the Inhibitor of Apoptosis family (cIAP1 and cIAP2) function as inhibitors of the ripoptosome by direct ubiquitination of its components (Imre et al., 2011).

In light of XIAP's roles in caspase-dependent apoptosis, in inflammation and in caspase-independent necroptosis, we hypothesized that XIAP would protect photoreceptor structure and function following retinal detachment. Consistent with this hypothesis, our previous work had shown that XIAP can protect photoreceptor structure in a rat model of retinal detachment (Zadro-Lamoureux et al., 2009). However, the technical challenges of surgery in the small rat eye prevented both re-attachment of the retina and functional testing using electroretinography. As a result, we developed a cat model of retinal detachment (Wassmer et al., 2016), and we employed this model to study XIAP efficacy in protecting photoreceptors through detachment and re-attachment of the retina. We show that XIAP inhibits TNF-α induced cell death in photoreceptor

cells *in vitro,* and protects outer nuclear layer thickness *in vivo*. Histology, optical coherence tomography (OCT) and electroretinography are used to assess XIAP effects in more detail on photoreceptor structure and function.

Results

XIAP protects 661W cone photoreceptor cells in an *in vitro* model of retinal cell death

TNF-α has been shown to mediate photoreceptor cell death in a rodent model of retinal detachment (Nakazawa et al., 2011). Therefore, we examined the ability of XIAP to protect 661W cone photoreceptor cells from TNF-α-induced cell death. 661W cells were transfected with either plasmid pCI.CMV.XIAP or pCI empty vector (XIAP and EV, respectively). Three stable and pooled XIAP over-expressing cell lines were generated (XIAP1-3, Figure 4.1a, and see Supplemental Figure 4.1), and their ability to protect against TNF-α was assessed. All three lines showed increased protection of 661W photoreceptors cells, accompanied by increased levels of the anti-apoptotic protein Bcl2, and decreased levels of cleaved caspase 3 (see Supplemental Figure 4.1). The cell line that was consistently the most robust in neuroprotection assays was further characterized and used for the assays described below.

XIAP- and EV-transfected cells were treated with 5 ng/mL TNF-α in complete media for 4 days. The mean cell viability from seven independent cell death assays was 60.5% for XIAP and 8.5% for EV cells ($p=<0.001$, Figure 4.1b) using the Trypan Blue

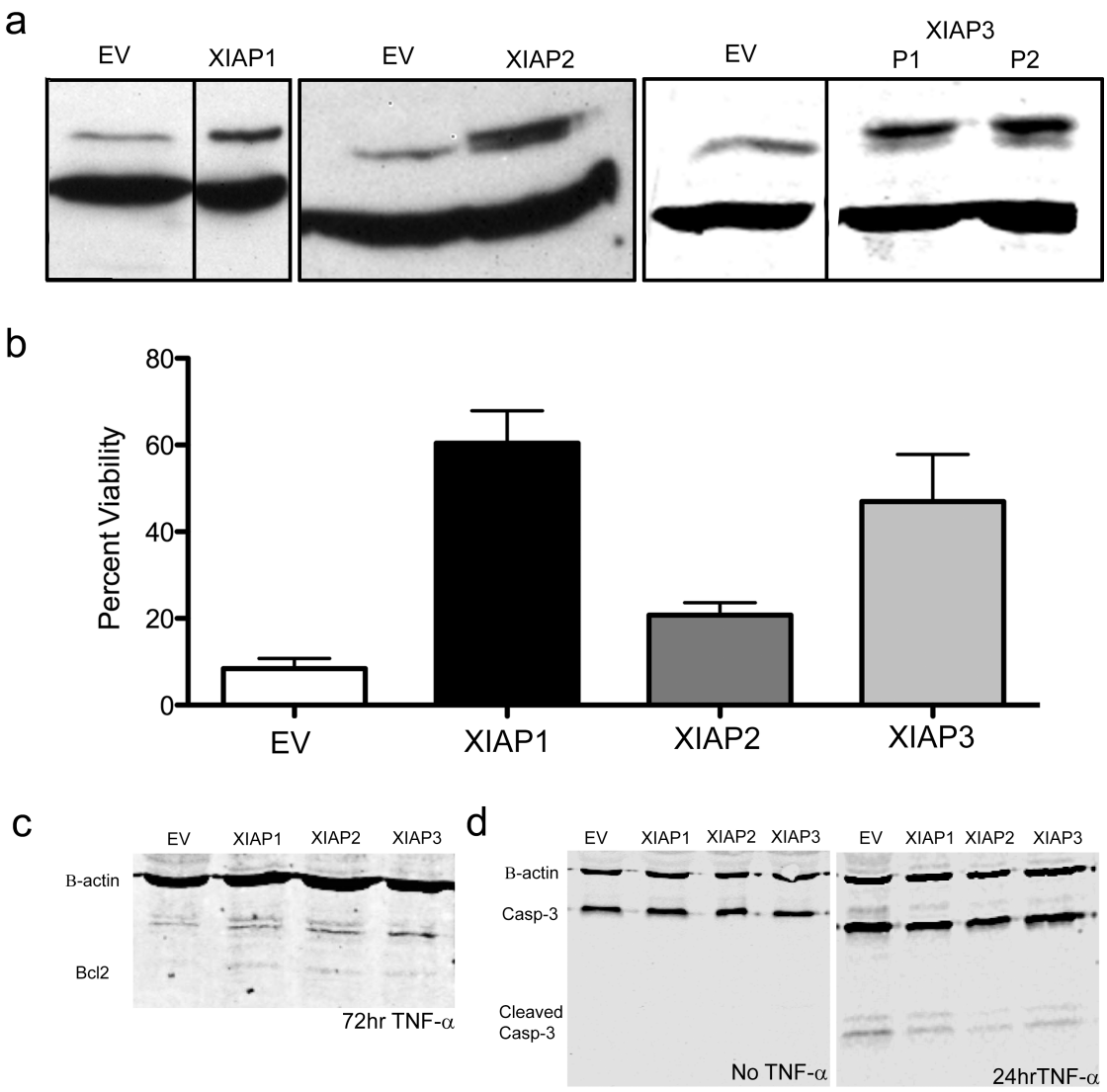

Supplemental Figure 4.1: XIAP over-expressing cells are protected from TNF-α induced cell death.

(a) Western blot showing protein over-expression in three 661W cell lines (XIAP1-3). β-actin (lower band) is used as the loading control. EV – empty vector, P1, P2 – passages 1 and 2. (b) All XIAP-transfected cell lines provide protection again a 4-day treatment with 5ng/mL TNF-α, but XIAP1 provides the best protection. (c) Following 72-hour treatment with TNF-α, XIAP over-expressing cell lines have increased levels of Bcl2. (d) Following a 24-hour treatment with TNF- α, XIAP over-expressing cell lines have reduced levels of activated caspase-3.

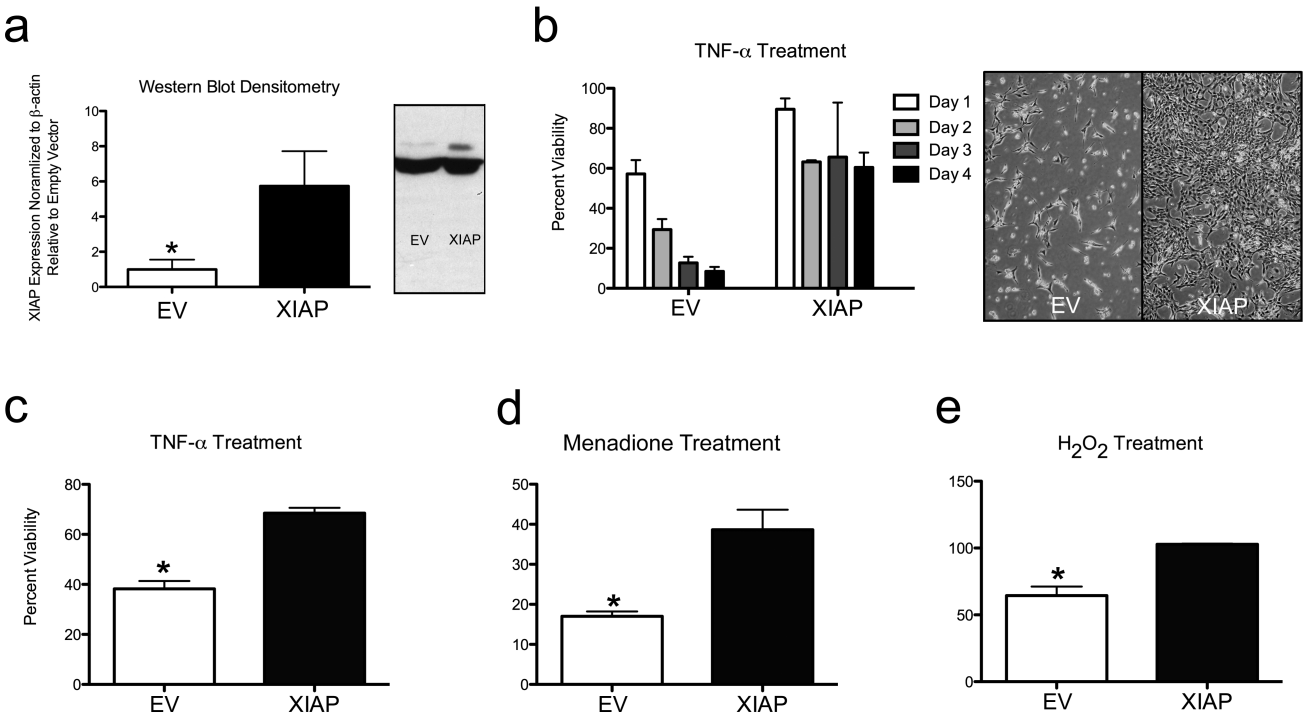

Figure 4.1. XIAP protects 661W photoreceptor cells against various cell death triggers.
(a) Densitometry analysis of 3 independent western blots showing XIAP over-expression in stably transfected 661W cells. XIAP expression was normalized to the β-actin loading control. One of the western blots is shown in the right panel. (b) XIAP protects 661W cells from 5ng/mL TNF-α over a 4 day incubation period. Bar graph shows cell survival in comparison to the vehicle control, assessed using the trypan blue exclusion assay. Representative images of 661W cells treated with 5ng/mL of TNF-α for 4 days are shown in the right panel. (c, d, e) Cell viability assessed using the AlamarBlue assay for 661W cells treated with 5ng/mL TNF-α for 4 days (c), 15 μM menadione for 4 hours (d) or 1mM hydrogen peroxide for 32 hours (e).

exclusion assay. The protective effects of XIAP against TNF-α were further confirmed using the AlamarBlue viability assay (Figure 1c). Since retinal detachment has been shown to be associated with oxidative stress in both animal models and human retinal samples (Cederlund et al., 2013; Huang et al., 2013; Roh et al., 2011), we also tested the ability of XIAP to protect against menadione and hydrogen peroxide, two potent oxidative stressors. In both assays, XIAP over-expression significantly protected the 661W photoreceptor cells (Figure 1d,e).

XIAP gene therapy in a cat model of retinal detachment

To test the effects of XIAP over-expression in an *in vivo* model of retinal detachment, six domestic cats were subretinally injected with adeno-associated virus expressing hemagglutinin-tagged XIAP driven by the rhodopsin kinase promoter (AAV-HA-XIAP). Another six animals received AAV-GFP as a control. The shallow detachments induced by these injections normally resolve within 24 hours and do not create any complications with retinal structure (confirmed by OCT analysis) or function. Three weeks after the viral injection, a retinal detachment was induced at the site of the viral delivery (or as close as possible to it) by injecting 8% C_3F_8 gas into the subretinal space. A detachment, spanning approximately 15-20% of the retina, was induced (Figure 4.2). C_3F_8 gas was used for the detachments because it is slowly resorbed, allowing a gradual reattachment of the retina over the ensuing weeks without requiring surgical

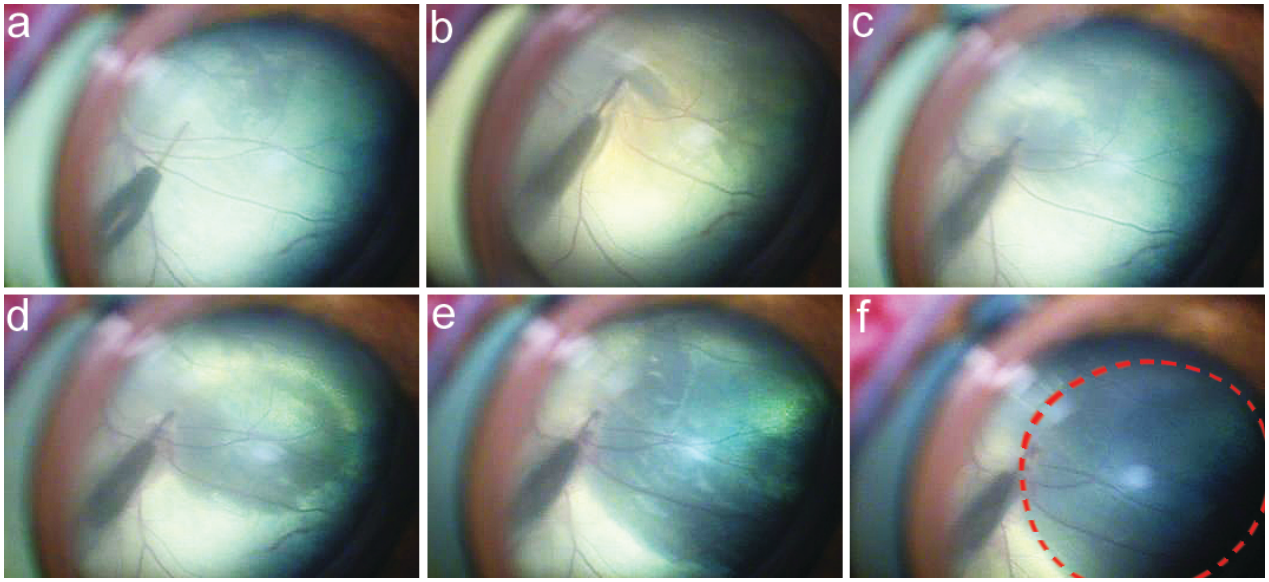

Figure 4.2. Retinal detachment induced by injection of 8% C_3F_8 gas into the sub-retinal space.
An angled 42G subretinal cannula, was connected to a syringe containing the C_3F_8 gas via flexible sterile tubing. The gas was slowly injected into the subretinal space until approximately 20% of the retina was detached. (a-f) Sequential images showing the growing retinal detachment as C3F8 gas in injected. The detachment is outlined in f.

intervention. All detachments were placed in the superior pole of the retina. Animals were examined weekly using an ophthalmoscope, and retinal function was assessed every three weeks with a full-flash electroretinogram (ERG). OCT and fundus images were also taken every three weeks, concurrent with the ERGs.

Three animals (one XIAP-treated and 2 GFP-treated) were eliminated from the study because their experimental partial detachments progressed into complete retinal detachments. Despite the precise placement of the viral vectors and the retinal detachment, for humane reasons we did not restrict the movement of the animals, and the animals' head motion allowed the displacement of the gas bubble throughout the retina in those 3 animals, resulting in a complete retinal detachment.

The two retinotomy sites created by the viral injection and the detachment were visible throughout the experiment (Figure 4.3), allowing us to accurately serially image the same retinal areas by OCT by reference to these injection sites. These OCT images confirmed that the C_3F_8 gas had been resorbed and the retina had re-attached within 3-6 weeks after the detachment (Figure 4.4). Specifically, the detachment only presented as small ripples in the retina at three weeks which were almost completely flat and re-attached by 6 weeks in most of the animals (Figure 4 and Supplemental Figure 4.2). However, three animals presented with some complications from the surgeries. XIAP1 showed retinal puckering on the OCT, indicating that the retinal detachment had not properly resolved (see Supplemental Figure 4.3). XIAP 5 (Supplemental Figure 4.3) had a vitreal hemorrhage, making fundus imaging and OCT impossible at the latest time-point. And finally, GFP1 appeared to have both a possible solid detachment which prevented the acquisition of a clear fundus image and two additional retinal irregularities

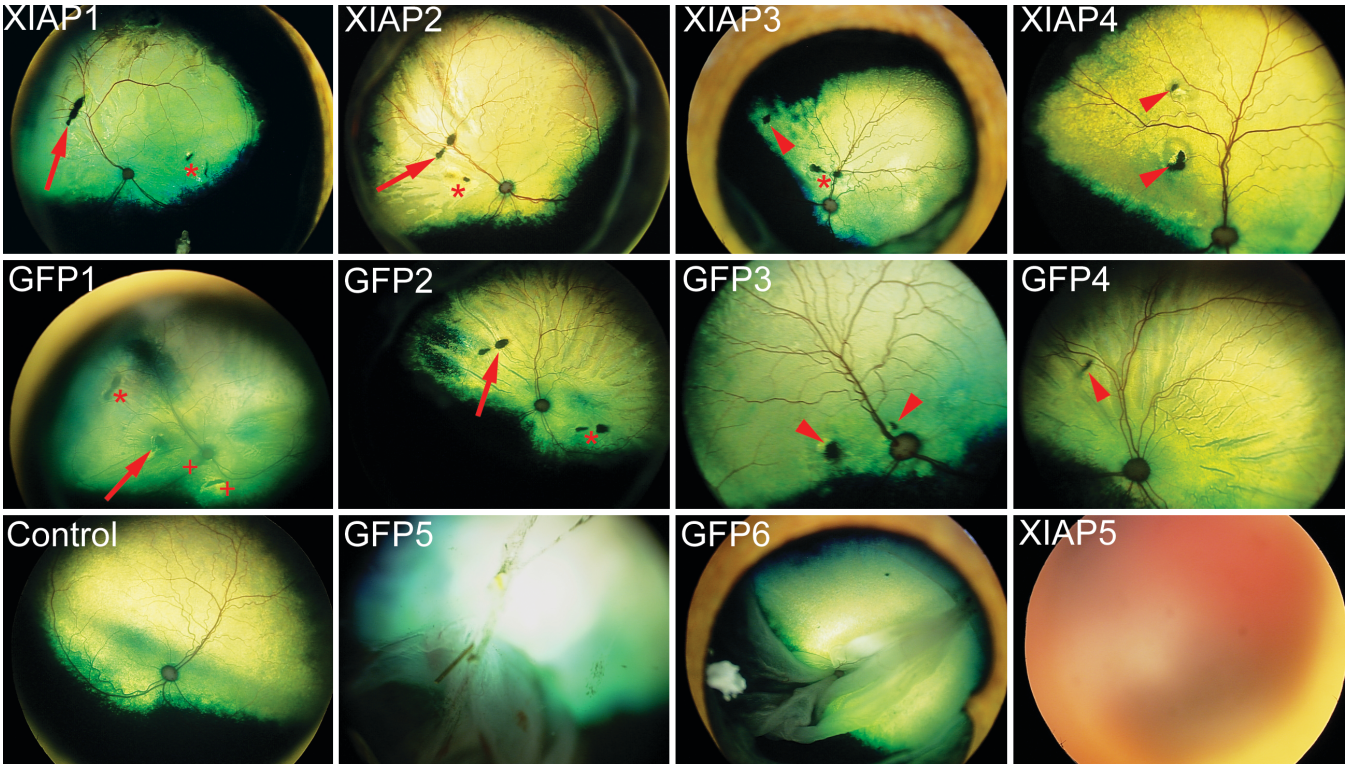

Figure 4.3. Fundus images of the animals at the endpoint of the experiment. The retinotomies created by the viral injection (asterisk) and by the detachment (arrow) are visible in most of the fundus images. Arrowheads are used to identify retinotomies that could not be specifically assigned to the viral or gas injection based on the video of the surgery or the surgical notes. In GFP1, a solid detachment prevented the acquisition of a clear fundus image, and '+' symbols identify two damaged areas of the retina that cannot be attributed to the virus or gas injection. GFP5 and GFP6 suffered complete detachments and XIAP5 shows a vitreal hemorrhage which developed at later stages in the experiment, preventing the acquisition of a fundus image.

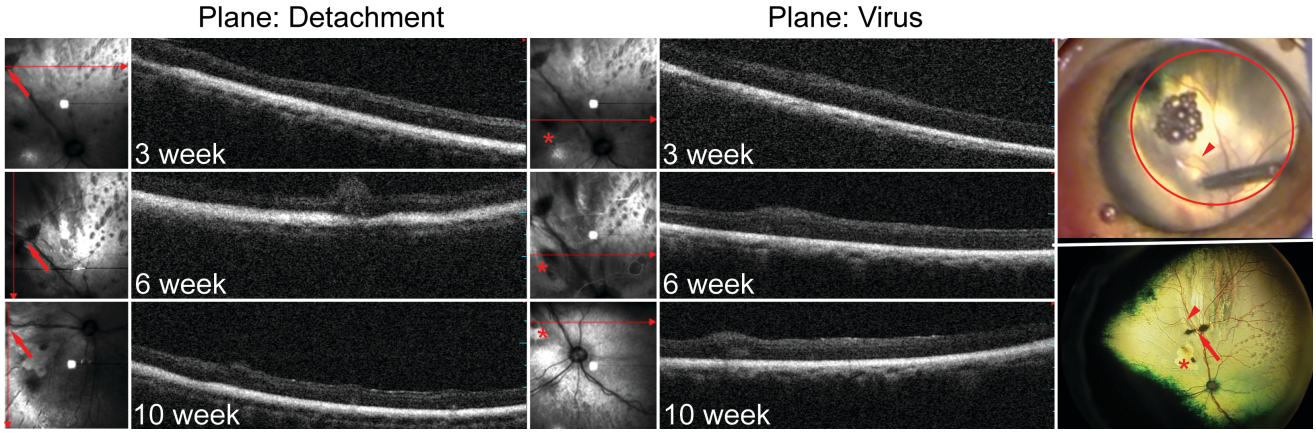

Figure 4.4. OCT images of XIAP-injected, detached retina at various timepoints after detachment.
Panels on right show an image of the cannula making the retinotomy to inject the C_3F_8 gas (top) and the fundus image of the retina at 10 weeks after the detachment (bottom). The arrowhead in both images identifies a minor arching blood vessel which can be used to identify the retinotomy for the gas injection (arrow) and for the viral injection (asterisk). OCT images on the left, through the plane of the gas injection or the virus injection, show that the retina has reattached, with no appearance of abnormal pathology due to the detachment. Small areas of elevation in the OCT may represent large blood vessels.

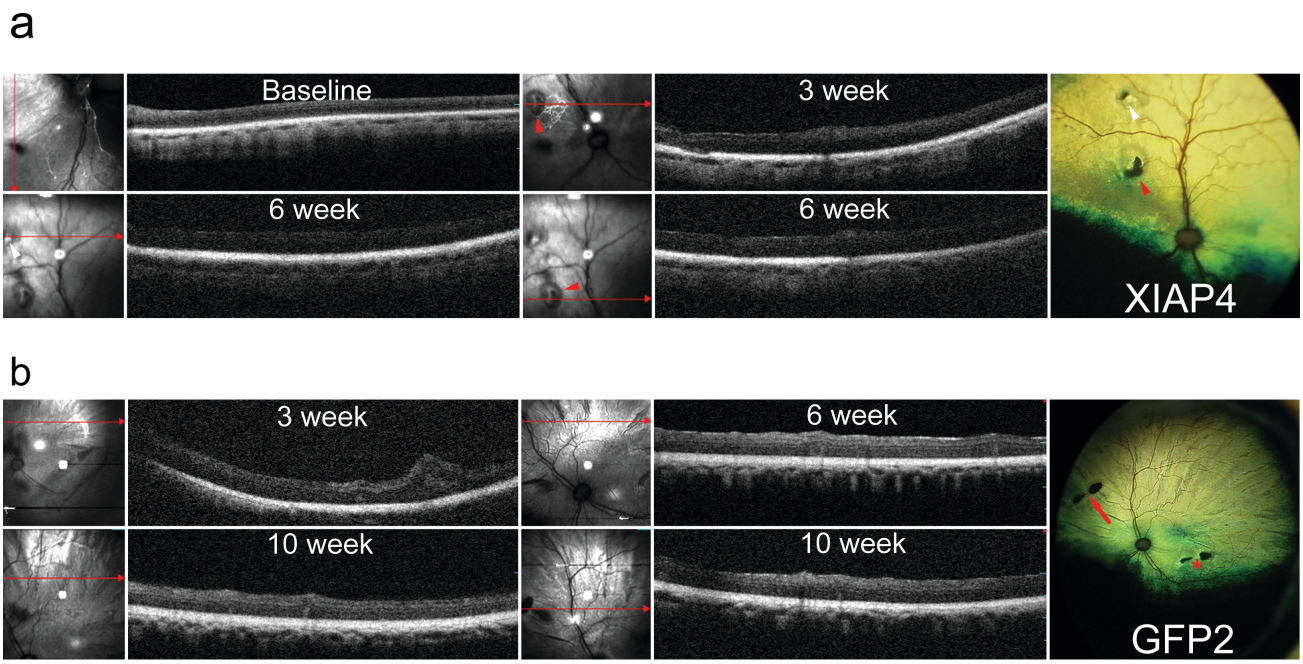

Supplemental Figure 4.2. OCT shows re-attachment of retina 3-6 weeks after retinal detachment.
(a) OCT at baseline (prior to virus or gas injection) and at 3 and 6 weeks following detachment in a XIAP-treated retina. At 6 weeks, imaging through both the plane of the viral injection and the plane of the gas injection shows a quiet normal-appearing retina that has completely reattached. (b) OCT at 3, 6 and 10 weeks in a GFP-treated retina shows some puckering at 3 weeks, suggesting that the retina has not completely re-attached yet, but this completely disappears at 6 and 10 weeks, suggesting that the detachment has completely resolved.

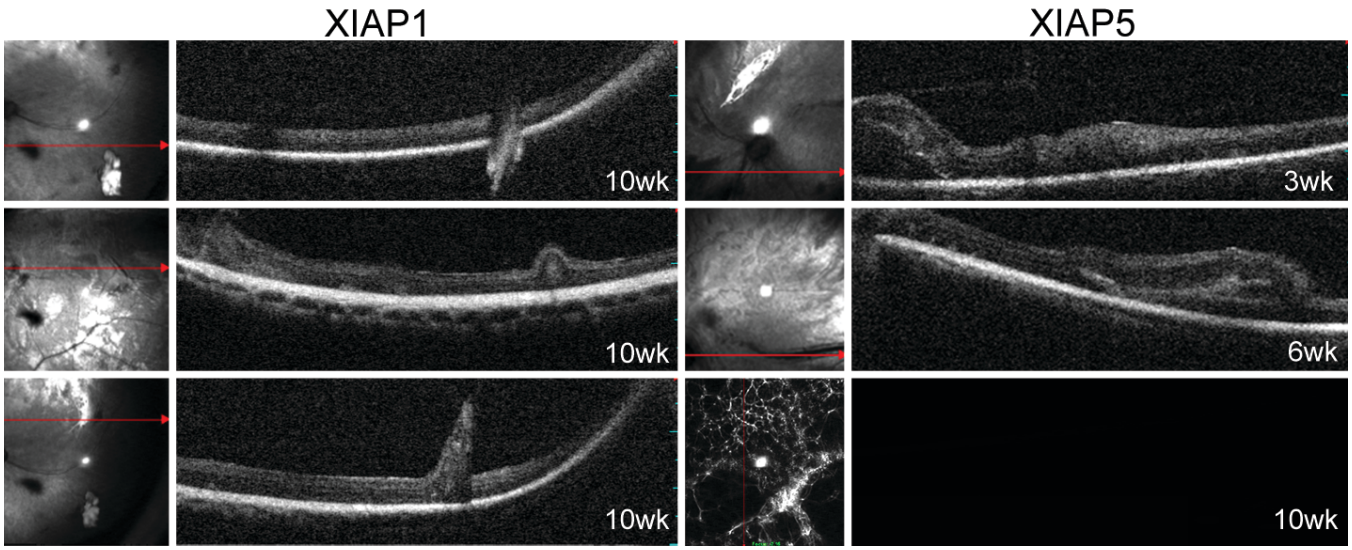

Supplemental Figure 4.3. OCT in 2 XIAP animals showing incomplete re-attachment of the retina.
XIAP1 shows retinal puckering and incomplete attachment at 10 weeks, possibly explaining the retinal damage seen in the histology, in addition to a possible mass (white). XIAP5 presents with possible subretinal hemorrhage at 3 and 6 weeks and a clear vitreal hemorrhage at 10 weeks which prevents the acquisition of an OCT image.

aside from the retinotomies associated with viral or gas injections (Figure 4.3 and Supplemental Figure 4.4). All of these animals are discussed in more detail below in the context of the histological analysis of the retinas.

XIAP over-expression protects photoreceptor structure in retinal detachment

For histological analysis, sagittal sections were taken through the eye in the plane of the optic nerve and 0.3 cm nasal to the plane of the optic nerve. One or the other of these sections would have encompassed the sites of the injection and detachment. Since the retinas had already reattached at the time that the eyes were sampled, any signs of retinal damage were assumed to be sites of the original retinal detachment.

Overall, XIAP-treated detached retinas showed greatly improved retinal structure in comparison to GFP-treated detached retinas (Table 4.1, Figure 4.5 and Supplemental Figure 4.5). Excluding the XIAP animal with the vitreal and subretinal hemorrhage (which were confirmed by fundus imaging and histology, respectively), 3 of 4 XIAP-treated retinas in the nasal plane (and 2 of 4 in the plane of the optic nerve) showed a completely intact outer nuclear layer (ONL), where the photoreceptors are found. In these animals, there was no evidence of retinal damage whatsoever. This was not seen in any of the GFP-treated animals, which had some evidence of retinal damage in every animal and in both histological planes.

Since retinal detachment leads to photoreceptor cell death, damage should be reflected in a reduction in the area occupied by the ONL. In order to further assess the ability of XIAP to protect photoreceptors, the ONL area was measured in XIAP-treated

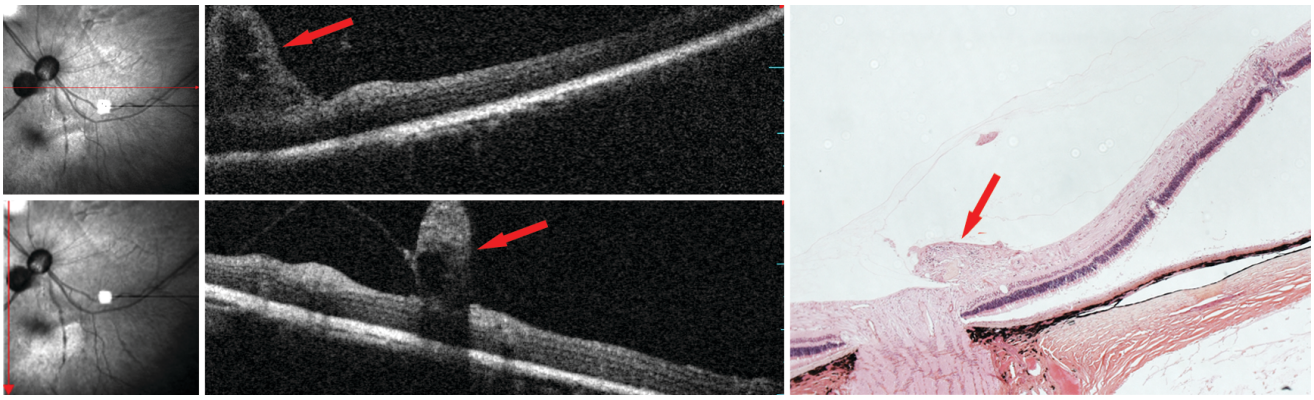

Supplemental Figure 4.4. Abnormal OCT in GFP-treated animal. GFP1, which appears to have a solid detachment based on fundus imaging, shows a clearly abnormal OCT with an unexplained protrusion (red arrow) that is also evident in the histological section (right panel).

Table 1. Experimental notes and outcomes for all animals in the study

	Structural Integrity	Proximity of Retinotomies[a]	Notes	Exclusion from Analysis
XIAP1	+++	Far apart	Incomplete re-attachment (retinal puckering)	
XIAP2	+++	Close		
XIAP3	+++++	Close		
XIAP4	+++++	Close		
XIAP5	+	ND[b]	Vitreal hemorrhage	Excluded from quantification
XIAP6	Complete RD[c]	ND	ND	Excluded from quantification
GFP1	+	Close	Solid partial detachment	Excluded from quantification
GFP2	+	Far apart		
GFP3	++	Close		
GFP4	++	Close		
GFP5	Complete RD	ND	ND	Excluded from quantification
GFP6	Complete RD	ND	ND	Excluded from quantification

[a]The retinotomies are the surgical incisions made by the virus injection and the detachment
[b]ND – not done
[c]RD – retinal detachment

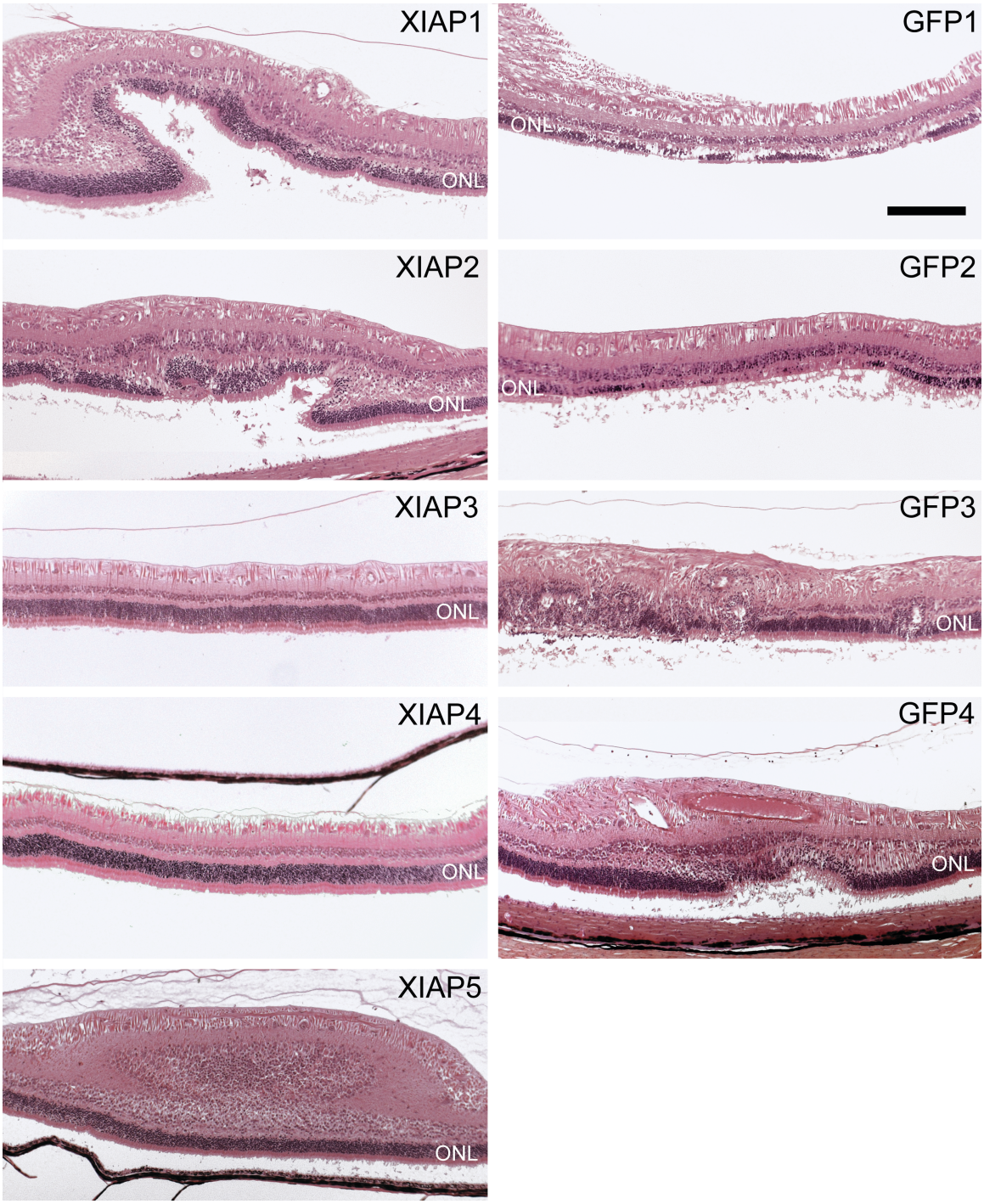

Figure 4.5. Histological sections in the plane of the optic nerve. Since the retinas had reattached at the time that the eyes were sampled, sections that showed any sign of retinal damage were imaged because it was assumed that the damaged areas were the sites of the original retinal detachment. XIAP3 and XIAP4 show perfectly intact retinas with no evidence of damage to the outer nuclear layer (ONL). All GFP animals show damage resulting from the retinal detachment.

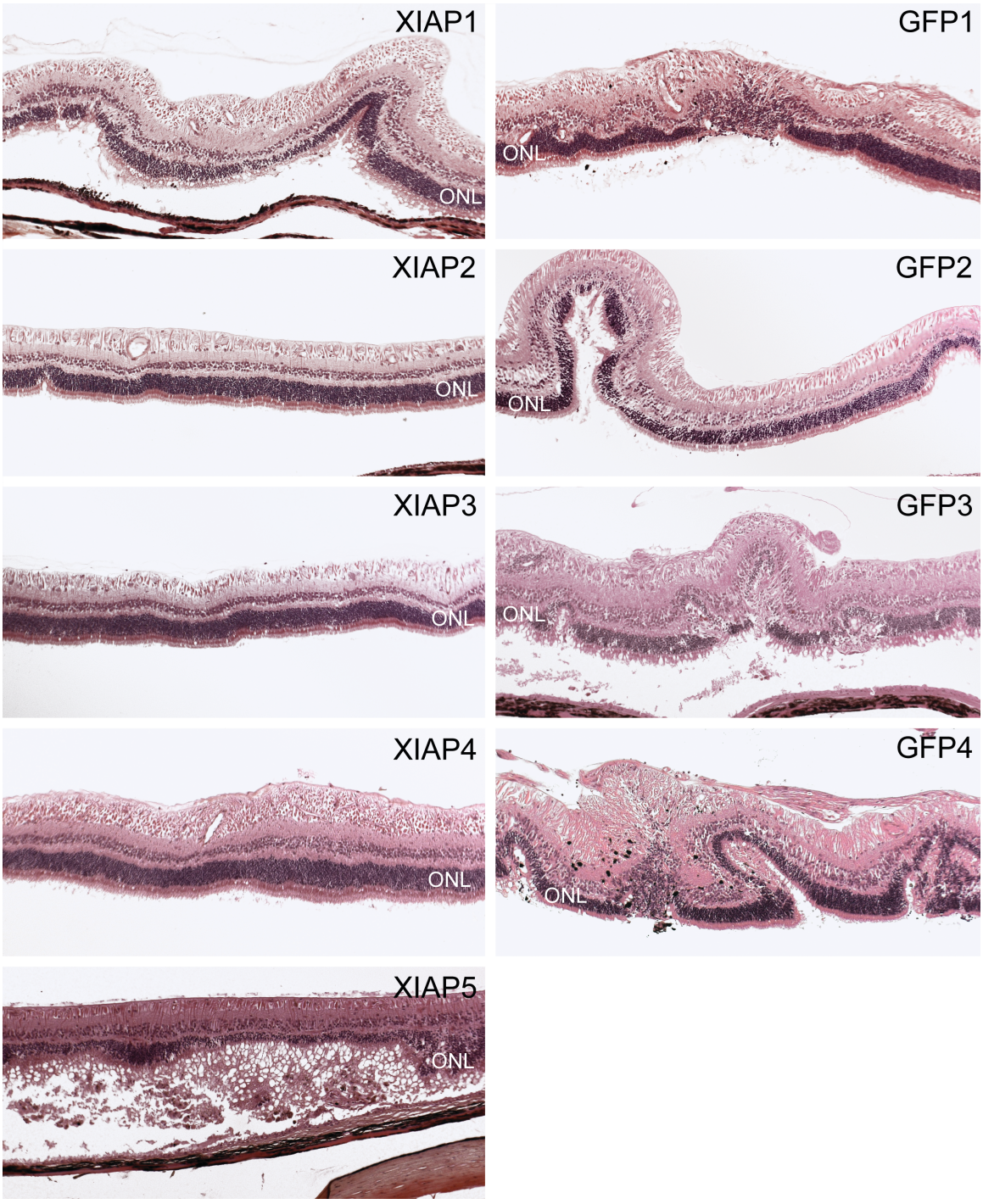

Supplemental Figure 4.5. Histological sections in the sagittal plane nasal to the optic nerve.
Three of the 5 XIAP-treated eyes (XIAP2, 3, 4) show perfect histology of the outer nuclear layer within the nasal sections, suggesting optimal protection of photoreceptors following retinal detachment. All of the GFP-treated retinas show damage resulting from the retinal detachment.

and GFP-treated eyes in the superior retina where the detachments were placed. The analysis was conducted in the plane of the optic nerve, from the optic disc to a distance of ~8800 μm towards the peripheral retina. The XIAP-treated animal with the vitreal and subretinal hemorrhage and the GFP-treated animal with the solid detachment were excluded from the analysis. ONL thickness was significantly greater in the XIAP-treated group (Figure 4.6a, $p=0.05$), indicating greater preservation of photoreceptors following retinal detachment. All final quantification values correlated with visual observations.

Importantly, the hemagglutinin (HA)-tagged XIAP was localized to the outer and inner segments of the photoreceptor cells near the site of the protected ONL (Supplemental Figure 4.6). Due to autofluorescence of the retinal sections, the GFP protein was more difficult to see and it necessitated a non-fluorescent colorimetric assay for detection (Supplemental Figure 4.6).

XIAP appears to protect photoreceptor function following retinal detachment

Full-field electroretinograms (ERGs) provide information on retinal function and can be parsed into separate waveforms each of which are indicative of the health of specific neurons in the retina. The a-wave of the ERG is a measure of photoreceptor health and function. ERGs were taken prior to sampling the eyes in order to assess the ability of XIAP gene therapy to protect photoreceptor function (Figure 4.6b). Although there is variability among animals (even in normal intact eyes), all the XIAP-treated animals have a-wave amplitudes that are equal to or higher than those of the GFP-treated animals. Importantly, one of the highest a-wave values in the XIAP-treated animals was found in an animal that also had the best outcomes according to the histology

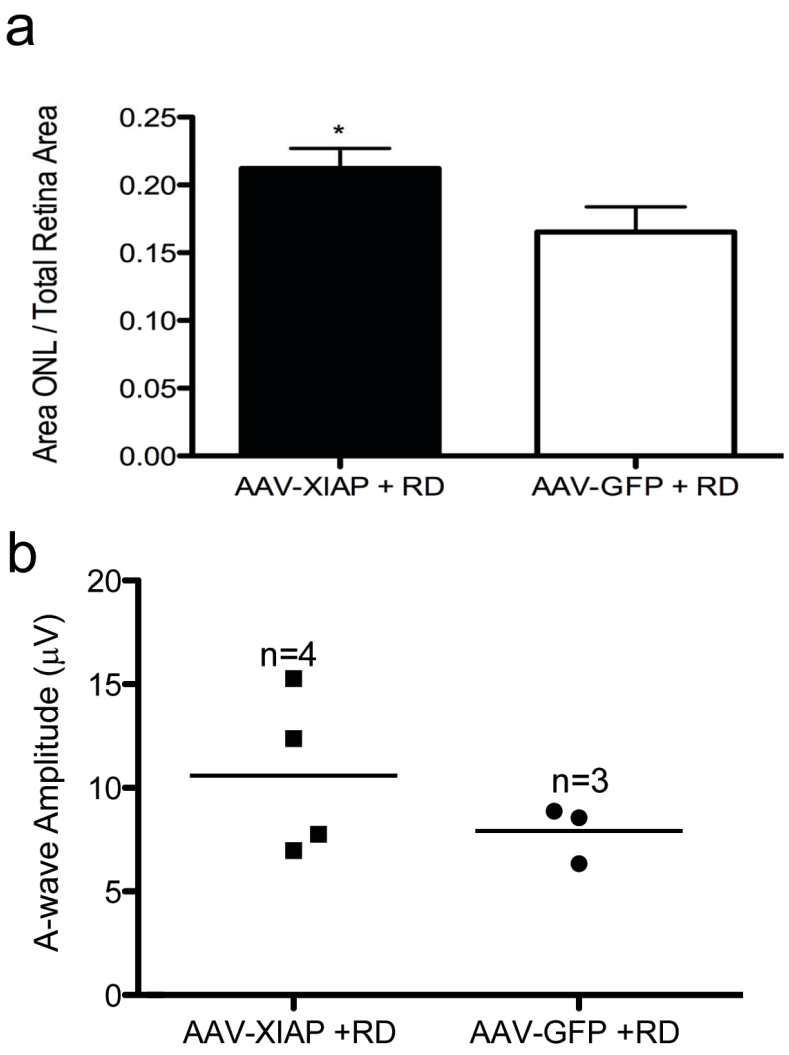

Figure 4.6. Structural and functional effects on the retina following XIAP therapy. (a) XIAP therapy significantly protects photoreceptors following retinal detachment in comparison to the control. H&E images imported into ImageJ were used to calculate the area occupied by the outer nuclear layer (photoreceptors) and this was divided by the total retinal area. Averages represent three GFP animals and four XIAP animals (see Table 1 for animals included in the analysis). * p=0.05, by Students t-test. (b) Scatter plot showing full-field ERG values at the endpoint of the experiment for animals used in the structural analysis in (a). The values did not reach significance due to the small number of animals in the analysis (p=0.16, by Students t-test).

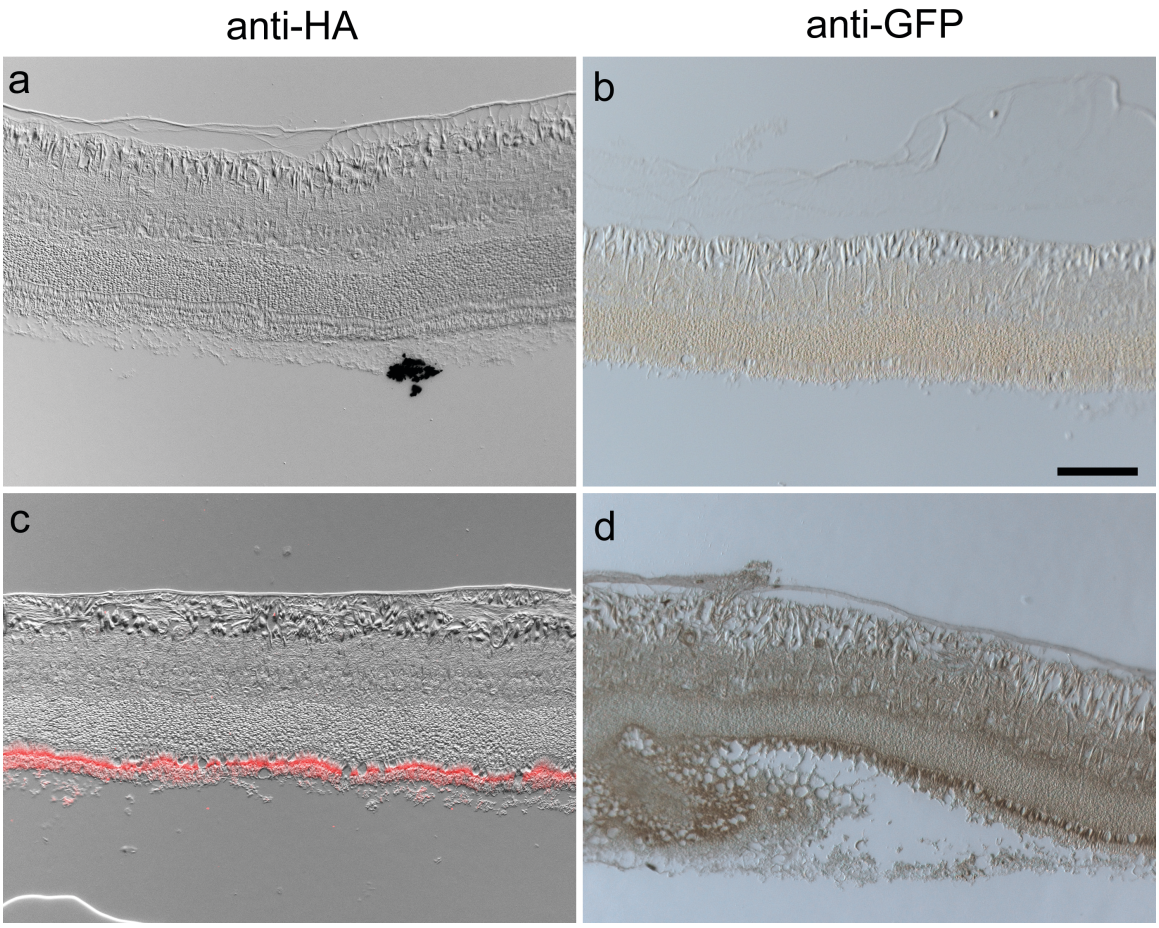

Supplemental Figure 4.6. Immunohistochemistry shows XIAP and GFP expression resulting from the viral injection.
(a,b) No primary antibody controls for the HA-tag and GFP, respectively. (c) The HA-tagged XIAP protein is detected in the inner and outer segments of the photoreceptors using an anti-HA antibody and a Cy3 secondary fluorophore. (d) Due to autofluorescence of the feline retina in the green channel, immunofluorescence detection of the GFP was not possible. A colorimetric (peroxidase activity) assay was used to localize GFP protein to the photoreceptor segments.

and quantification. Conversely, the animal with residual pathology (XIAP1) showed one of the lowest a-wave ERG trances. Since all animals with full retinal detachments (as well as the solid detachment and retinal hemorrhage animals described above) were removed from the analysis, the results did not reach significance due to the small numbers of animals remaining (n=3 for GFP and n=4 for XIAP).

Discussion

Retinal detachment has an incidence of approximately 12 in 100,000 in the general population, and this translates into a lifetime risk of 0.6% (up to the age of 60 years) (Haimann et al, 1982; Sodhi et al, 2008). This risk increases in patients with high myopia (Haimann et al., 1982). Despite successful surgical interventions to re-attach the retina, vision is often compromised in these patients, especially if the central retina (macula) is involved in the detachment.

Animal studies have shown that retinal detachment induces both photoreceptor apoptosis and necroptosis. When caspase inhibitors are used to block apoptosis, there is a switch to increased necrotic cell death to compensate for the block in apoptosis (Trichonas et al., 2010). Others have also shown that TNF-α is involved in cell death following retinal detachment, further implicating both apoptotic and necrotic pathways (Nakazawa et al., 2011). In the current study, over-expression of the X-linked Inhibitor of Apoptosis (XIAP) protects photoreceptor structure following retinal detachment. XIAP is able to protect photoreceptors because in addition to blocking caspases 3,7 and 9, it has been shown to interact with RIP kinases to reduce the formation of the

necroptosome and thus can impact both apoptotic and necrotic cell death pathways (Lawlor et al., 2015; Vince et al., 2012; Yabal and Jost, 2015; Yabal et al., 2014).

In this study, unimpeded activity of the animals resulted in complete detachments in 3 eyes, necessitating their removal from the study. In addition, further complications with the surgery, including a vitreal and subretinal hemorrhage and the presence of a solid detachment led to the removal of an additional two animals from the analysis. These complications lowered the power of our study. Nevertheless, we still found significant differences in photoreceptor thickness when treated with XIAP gene therapy. Importantly, we saw improved ERGs in 2 of the 4 XIAP-treated animals and these two animals also had preservation of their photoreceptor layer by histological analysis. There was also a correlation between a high ERG a-wave value (12.38 μV), un-affected histological analysis and the highest retinal to ONL ratio. The other two XIAP-treated animals with lower ERGs showed thicker ONL layer qualitatively and quantitatively (as compared to GFP treated animals), and only one of those two cats showed areas of retinal damage in the plane of the optic nerve. There may be several explanations for the imperfect preservation of the ONL in these animals. In one of these animals (XIAP1, Figure 4.3), the fundus image revealed that the retinotomy sites were quite far apart, suggesting that there was imperfect overlap between the viral vector injection and the retinal detachment site. Thus, there would have been detached retina that was not covered by the AAV-XIAP injection. Moreover, the presence of puckering in the histological sections (Figure 4.5) and the OCTs (see Supplemental Figure 4.3) would suggest that the re-attachment was not perfect and the photoreceptors might not have received the trophic support that they needed for their continued survival. This also correlated with lower

ERG a-wave results in XIAP1 (7.757 μV). In the clinical setting this would not be a problem, as retinal re-attachment surgery is very successful at ensuring good contact between the retina and the underlying retinal pigment epithelium (RPE). We therefore conclude that the improved surgical outcomes in the clinic, combined with XIAP therapy would likely result in robust structural and functional protection of the photoreceptors.

In the current study, we provide proof-of-principle for XIAP efficacy in protecting photoreceptors, but XIAP gene delivery preceded the retinal detachment, in order to allow the virus adequate time to over-express the transgene prior to the detachment. In the clinical setting, this would not be possible, and the swift onset of retinal damage following a detachment would necessitate rapid intervention to ensure a satisfactory visual outcome. Improved, rapid viral delivery systems would be required. Alternatively, XIAP protein delivery, potentially through the use of biodegradable microparticles (Rafat et al., 2010 Wassmer et al., 2013), would allow immediate delivery of XIAP to the damaged cells and improved outcomes in both retinal structure and function.

Materials and Methods

Animals

Twelve male cats aged 8 months and older were purchased from Liberty Research (Waverly, NY). Animals were housed together in large multi-level enclosures that provided an enriched environment and allowed free movement. Animal procedures were conducted in accordance with the University of Ottawa Animal Care Committee rules

and regulations and adhered to the ARVO statement for the Use of Animals in Ophthalmic and Vision Research.

Anaesthesia

Felines were given propofol (1mL/min; Fresenius Kabi, Richmond Hill, ON, Canada) intravenously or 5% isoflurane (Fresenius Kabi) by aerosol mask before surgery and during the administration of the anesthetic. Animals were administered 0.015 mg/kg medetomidine (Modern Veterinary Therapeutics, Miami, FL) and 0.1 mg/kg hydromorphone (Sandoz Canada, Boucherville, QC) by intramuscular injection and were kept under 2-3% isoflurane throughout all surgical procedures. Normosol fluids (Hospira Healthcare Corp., Saint Laurent, QC, Canada) were provided by intravenous infusion. The antiemetic medication, Cerenia (Zoetis Canada, Kirkland, QC), was used at a dosage of 0.5mg/Kg in susceptible animals, only when electroretinography was not being performed, as our previous studies showed that Cerenia interferes with the electroretinogram (Wassmer et al., 2016). Vital signs were monitored throughout the procedure, and an intramuscular injection of 0.02 mg glycopyrrolate (2mg/mL; Sandoz Canada) was administered if the heart rate significantly decreased during or after surgery. Five minutes before the end of the surgery, the medetomidine was reversed using 0.05-0.06 mg/Kg atipamezole hydrochloride (Modern Veterinary Therapeutics, Miami, FL, 5mg/mL). After the surgery, animals received 0.02 mg/Kg buprenorphine (0.3mg/mL; Sovegal UK Ltd, York, UK) subcutaneously for pain management.

Virus Vector Production

A cDNA construct encoding the full-length, open-reading frame of human XIAP was cloned into the pTR AAV vector. The construct had an N-terminal hemagglutinin (HA) tag and was under the control of the human rhodopsin kinase (RK) promoter. Transgene expression was enhanced by a woodchuck hepatitis virus posttranscriptional regulatory element in the 3' untranslated region of the construct. A RK-GFP construct was similarly generated for use as a control. Recombinant adeno-associated virus vector, serotype 5, was generated and purified as previously described (Hauswirth et al., 2000; Zolotukhin et al., 2002).

Surgeries

One drop each of mydriacyl (1%), mydfrin (2.5%) and alcaine (0.5%) (Alcon Canada, Mississauga, ON) were administered to the surgical eye. The 3-port pars plana phacofragmentation lensectomy followed by a vitrectomy were performed as previously described (Wassmer et al., 2016). These procedures gave unobstructed access to the central retina for the delivery of the AAV vector and the induction of the retinal detachment. The left eye of 6 cats received serotype 5 AAV carrying HA-tagged XIAP driven by the rhodopsin kinase promoter (AAV5.RK.XIAP). The virus was injected into the subretinal space of the superior retina, in close proximity to the optic nerve. A total volume of 100 µl was injected, containing $1x10^{11}$ vector genomes (vg). Another 6 animals received $1x10^{11}$ vg of AAV5.RK.GFP as a control. The posterior chamber was filled with sterile balanced saline salt (BSS) after the vector injection to maintain intraocular pressure.

Three weeks after vector delivery, a retinal detachment was created by administering 8% C_3F_8 gas as close as possible to the viral injection site. A 15-20% retinal detachment was created.

After each surgery, the eyes were treated with 5 to 10 drops of 1.0% w/v atropine sulphate (Chauvin Pharmaceuticals, Surrey, UK) and covered with Tobradex Ophthalmic Ointment (tobramycin 0.3%, dexamethasone 0.1%) (Alcon Canada, Mississauga, ON). The animals were treated 4 times daily with Tobradex for ten days post-surgery.

Enucleation

Nine or ten weeks post-detachment, left eyes of the animals were surgically removed. In addition to the anaesthesia regime described above, 10mL of 2% xylocaine was injected into the orbit. Buprenorphine and the NSAID Metacam (meloxicam, 0.1mg/Kg; Boehringer Ingelheim, Burlington, ON, Canada) were administered every day for a minimum of three days post-enucleation. Oral administration of the antibiotic clavamox (1mL containing 50mg amoxicillin and 12.5mg clavulanic acid; Zoetis, Kirkland, QC) was given to the cats twice daily post-enucleation, and oral gabapentin (10mg/kg) was given for pain relief, as needed, Following complete recovery, animals were adopted out.

Optical Coherence Tomography (OCT) and Electroretinography (ERG)

OCT was performed as previously reported (Wassmer et al., 2016). Eyes were imaged before injection of the vector and subsequently every three weeks post-detachment. After lens removal, a 10+ diopter lens was placed in front of the eye to gain access into the focusing range of the OCT machine. Photoreceptor function was assessed with an Espion

e3 (Diagnosys, USA) full-field flash ERG (3 cd·s/m^2 on a 30 cd/m^2 background luminance) presented at a rate of 1 Hz. An ERG-Jet (LKC Technologies) was placed on the corneal surface with appropriate corneal hydration. ERGs were recorded with bandpass filtering of .3-300 Hz and 50 sweeps were signal averaged.

Area Measurements

Images were taken of H&E sections using the 20X objective on the Zeiss Axio Imager M2 (Zeiss, Canada) through the plane of the optic nerve. Images were combined to obtain a collage of the full retina, and the final image was imported into ImageJ. The outer nuclear layer (ONL) was traced in the superior retina (where the detachment was located) from the optic nerve peripherally for a distance of ~8800 μm. The area encompassing the ONL was calculated. In the same region, the area of the whole retina was also measured. The ratio of the ONL area to the whole retinal area was calculated and compared between XIAP-treated and GFP-treated animals.

TNF-α Cell Death Assays

The transformed cone photoreceptor cell line, 661W was kindly provided by Dr. M. Al-Ubaiddi (Tan et al., 2004b). 661Ws were transfected with pCI-neo containing the full-length coding sequence of human XIAP which was generated from pCM-SPORT6-XIAP (Origene, Rockville, MD), digested with SalI and NotI to isolate XIAP coding sequence, and ligated into the pCI-neo vector (Promega, Madison, WI). Transfections were conducted using ExpressIn or Lipofectamine 2000 (ThermoFisher Scientific), according to the manufacturer's instructions. Control cell lines were transfected in a similar manner

with the pCI-neo empty vector (EV). Stably-expressing cells lines were grown under G418 selection. Three independent cell lines over-expressing XIAP were generated. The line with the highest expression of XIAP was used for the results described in the body of the paper. Results obtained with the other 2 lines are found in the supplemental material. All cell lines were used below passage 15, and XIAP expression was monitored in each assay by western blot or RT-qPCR.

For the death assays, cells were plated onto 6-well or 96-well plates at 60% confluency and incubated with mouse recombinant TNF-α at 5ng/mL (Roche) for four days, 1mM hydrogen peroxide (Sigma Aldrich, Oakville, ON, Canada) for 32 hours or 15μM menadione (Sigma Aldrich) for four hours. Cell viability was measured using Trypan Blue (Sigma Aldrich) or AlamarBlue ® Cell Viablity Reagent (Invitrogen, Carlsbad, CA) for 6-well and 96-well formats, respectively.

Western Blot

Twenty μg of retinal protein was separated by electrophoresis on 12% polyacrylamide gels, and transferred onto PVDF membranes. Membranes were blocked for 1 hour at 4°C in 5% powdered milk, and incubated overnight at 4°C with primary rabbit anti-GST-XIAP, rabbit anti-RIAP3 antibodies (1:5000 in blocking buffer; courtesy of Dr. Robert Korneluk, University of Ottawa). Membranes were washed and incubated for one hour at room temperature in anti-rabbit HRP or anti-rabbit IRDye 800 (Li-Cor, Lincoln, NE). Proteins were visualized using Pierce Chemiluminescence substrates (ThermoFisher Scientific) and film, or the Licor imaging system.

Immunohistochemistry

Prior to enucleation, a 3-0 Vicryl suture (Ethicon, Somerville, NJ) was used to mark the superior pole of the eye. Enucleated eyes were placed in modified Davidson's fixative and sent to Excalibur Pathology Inc., where they were embedded in wax and sectioned at 6 μm. A subset of the slides were stained by Excalibur Pathology Inc. with hematoxylin and eosin.

For immunohistochemical detection of HA-tagged XIAP, sections were dewaxed, then placed in citrate buffer (10 mM sodium citrate in water, pH 6) within the Biocare Medical Digital Decloaking Chamber (Biocare, Concord, CA). Slides were removed from the chamber, allowed to cool to room temperature, washed with PBS, permeabilized in 0.1% triton X-100 in PBS (wash buffer), blocked for two hours (10% normal goat serum in wash buffer) and incubated for two days at 4°C with HA primary antibody (1:100; Roche Canada, Mississauga, ON) diluted in blocking solution. Slides were then washed in wash buffer and incubated with Cy3 secondary antibody (1:500, Jackson ImmunoResearch, West Grove, PA) diluted in PBS. After precisely two hours, the sections were washed with wash buffer then PBS, and mounted in Prolong Gold antifade reagent (Life Technologies). For specific details for immunofluorescence staining, see Nayagam *et al*., 2003 (Nayagam et al., 2013).

To detect the GFP signal, autofluorescence in the retinal sections necessitated the use of a colorimetric assay (the ImmPRESS Detection System, Vector Laboratories, California). All manufacturer procedures were followed, with the exception that no counterstain was used. All sections were imaged using a Zeiss Axio Imager M2.

Acknowledgements

We wish to thank Dr. David Zacks (Kellogg Eye Institute) for helping with the detachment protocols and Lijun Fang for help with the surgeries. We are grateful to the Animal Care and Veterinary Service staff for their tremendous help with the surgeries and their wonderful and caring attitude towards the animals in this study. This work was supported by Canadian Institutes of Health Research and Foundation Fighting Blindness grants to CT, NIH grant P30-EY021721, MVRF and RPB Inc funding to WWH. CT is supported by the Don and Joy Maclaren Endowed Chair in Vision Research. SW was supported by the David S. Shillito Scholarship in Ophthalmology and by an Ontario Graduate Scholarship.

CHAPTER 5: CHITOSAN MICROPARTICLES FOR DELIVERY OF PROTEIN TO THE RETINA

Chitosan Microparticles for Delivery of Proteins to the Retina

Abbreviated title: Chitosan Microparticles for Delivery to the Retina

Wassmer S.,[a,b †] Rafat M.,[a,c†] Fong W.G.,[a] Baker A.,[a] and Tsilfidis C.[a,b*]

[a] Ottawa Hospital Research Institute, Ottawa, ON, K1H 8L6, Canada

[b] Department of Cellular and Molecular Medicine, University of Ottawa, Ottawa, ON, K1H 8M5, Canada

[c] Department of Clinical and Experimental Medicine, Linkoping University, Linkoping, 581 85, Sweden

† S. Wassmer and M. Rafat contributed equally to this work.

* Corresponding author: Dr. Catherine Tsilfidis,

Ottawa Hospital Research Institute,

Ottawa Hospital, General Division

501 Smyth Road, Ottawa, ON, K1H 8L6

Tel: 1-613-737-8233 Fax: 1-613-737-8836

Email: ctsilfidis@ohri.ca

Author Contributions

Wassmer S helped with experimental design, performed *in vitro* and *in vivo* analysis of chitosan microparticle efficacy and toxicity, and helped to write the manuscript.

Rafat M helped with experimental design, produced and evaluated chitosan microparticles (SEM/TEM and release kinetics).

Baker A performed subretinal injections and helped with the design of the figures.

Tsilfidis C funded the studies, was instrumental in experiment design and manuscript writing.

Manuscript published August 2013 in *Acta Biomaterialia*, Volume 9, Issue 8, pages 7855-7864.

Abstract

Chitosan microparticles (CMPs) have previously been developed for topical applications to the eye, but their safety and efficacy in delivering proteins to the retina have not been adequately evaluated. This study examines the release kinetics of CMPs *in vitro*, and assesses their biocompatibility and cytotoxicity on retinal cells *in vitro* and *in vivo*. Two proteins were used in the encapsulation and release studies: BSA (bovine serum albumen) and tat-EGFP (enhanced green fluorescent protein fused to the transactivator of transcription peptide). Not surprisingly, the *in vitro* release kinetics were dependent on the protein encapsulated, with BSA showing higher release than tat-EGFP. CMPs containing encapsulated tat-EGFP were tested for cellular toxicity in photoreceptor-derived 661W cells. They showed no signs of *in vitro* cell toxicity at a low concentration (up to 1 mg/mL) but at a higher concentration of 10 mg/mL they were associated with cytotoxic effects. *In vivo,* CMPs were found beneath the photoreceptor layer of the retina, and persisted for at least 8 weeks. Similar to the *in vitro* studies, the lower concentration of CMPs was generally well tolerated, but the higher concentration resulted in cytotoxic effects and in reduced electroretinogram amplitudes. Overall, this study suggests that CMPs are effective long-term delivery agents to the retina, but the concentration of chitosan may affect cytotoxicity.

Key words: Chitosan, Retina, Microparticles, Encapsulation, Biodegradation.

Introduction

Diseases of the retina such as glaucoma, age-related macular degeneration (AMD), and diabetic retinopathy are major causes of irreversible blindness. The development of efficient delivery systems for ocular therapeutic agents is critical for the treatment of these diseases. Topical agents are generally used for corneal and anterior problems of the eye, but are mostly ineffective in targeting the retina at the back of the eye. For retinal disease, adeno-associated viruses (AAVs) are currently being used in clinical trials (Bainbridge et al., 2008a; Cideciyan et al., 2009a, 2009b; Hauswirth et al., 2008b; Maguire et al., 2009; Simonelli et al., 2010). The viruses are safe and effective at delivering transgenes to the retina, and are long-lasting, making them ideal gene carriers for genetic forms of disease requiring long-term therapy. However, once AAV viruses are delivered to the retina, there is no way to disable the therapy if harmful side effects are discovered. Moreover, in cases such as retinal ischemia or retinal detachment, short term treatment is essential, but once the clinical problem is resolved, the therapeutic agent is no longer required. For this reason, there is still a vital need for safe, effective methods of short term or sustained delivery of therapeutic agents to the retina. Biodegradable and biocompatible nano- and microparticles are ideal vehicles for such a purpose.

We have previously reported the use of PEG-PLA microparticles as protein delivery vehicles to retinal cells (Rafat et al., 2010). PEG-PLA microparticles offered the advantages of controlled, sustained protein release, and biocompatibility. However, the amount of the protein released from PEG-PLA particles was somewhat low in

comparison to AAV expression levels. In addition, the percentage of the encapsulated protein that was released was quite low, ranging from 1% to 5% depending on the microparticle formulation. Although this may not be a concern in treatments where nanogram quantities of protein are sufficient for neuroprotection, PEG-PLA microparticles would not be useful when larger quantities of the therapeutic agent are required. In order to enhance the release profile of the particles, here we report the development and testing of chitosan microparticles (CMPs) for delivery of tat-EGFP protein to the retina.

Chitosan has been widely used in biomedical applications (e.g., for the development of scaffolds for artificial liver (Wang et al., 2003), for skin transplants (Gingras et al., 2003), as a wound dressing (Kratz et al., 1997), and as a drug delivery system (Aiedeh et al., 1997)). Chitosan makes a good biomimetic component for extracellular matrices (ECM) due to its structural similarity to proteoglycans (one of the main constituents of ECM). This is mostly attributed to its reactive amino and hydroxyl groups that can be chemically modified and also the fact that it can be easily manipulated for different pore structures (Madihally and Matthew, 1999; Yagi et al., 1997).

Chitosan is an amino polysaccharide (poly-1, 4-d-glucoamine) derived from chitin by deacetylation. Chitin is one of the most abundant polysaccharides found in nature. It is almost as common as cellulose, and possesses many of the structural and chemical characteristics of cellulose. Chitin is an important structural component of the exoskeleton of a great number of organisms such as insects, shrimp, and shellfish. It also serves as a cell wall component of fungi and of numerous plankton and other small marine organisms. Due to the different biological requirements of these various species,

chitin has proven to be an extremely versatile natural polymer. Chitin and its most important derivative, chitosan, have a number of useful physical and chemical properties, including strength, biodegradability, and lack of cytotoxicity. Chitosan has been shown to be effective in trans-cellular transport (Illum et al., 1994; Lee et al., 2001) (for example, in enhancing the transport of drugs across the cell membrane (Artursson et al., 1994; Thanou et al., 2001)), and has been reported to be nontoxic on several types of cells (Guang Liu and De Yao, 2002).

Despite the fact that chitosan is being widely used as a drug delivery vehicle for various medical applications, and has been extensively studied for topical application of drugs to the eye (see review (Başaran and Yazan, 2012)), its safety and efficacy has not been fully evaluated for intraocular ophthalmic drug delivery applications. To our knowledge, two studies have examined the effects of intraocular delivery of unmixed chitosan (Prow et al., 2008; Yang et al., 2008). In the first study, chitosan was used as in intravitreal tamponade material (Yang et al., 2008). The authors concluded that there were no significant effects on the histology of the eye, with only slight increases in inflammatory factors. In the second study (Prow et al., 2008), intravitreal delivery of chitosan particles was part of a larger analysis examining several types of nanoparticles. The authors reported a significant inflammatory response following an injection of chitosan microparticles into rabbit eyes. However, cytotoxicity can be influenced by the material purity and source, the fabrication process, the particle size, the morphology and concentration, the type of target cell and the mode of administration of the particles (e.g. intravitreal versus subretinal). Prow et al. (Prow et al., 2008) acknowledged that it was

possible that contaminants of the material were responsible for the immune response following intravitreal delivery.

Due to the different outcomes seen in these two studies, and the fact that neither of them examined subretinal delivery of the microparticles, a more detailed evaluation of ocular applications for chitosan particles is warranted. In the current study, we have developed chitosan microparticles for the encapsulation and release of tat-EGFP to the retina. We evaluated the release kinetics of these particles *in vitro* and assessed their toxicity on retinal cells *in vitro,* and *in vivo* following subretinal delivery into the eye.

Materials and Methods

Materials

Water-soluble chitosan powder was purchased from Jinan Haidebei Marine Bioengineering Co. Ltd (60 MESH). Tat-EGFP was synthesized as we previously reported (Rafat et al., 2010). Sodium triphosphate pentabasic (TPP; Cat# 72061) and Bovine Serum Albumin (BSA; Cat# A-3912) were purchased from Sigma Aldrich (St. Louis, MO).

Preparation of Chitosan Microparticles

Chitosan microparticles loaded with BSA or tat-EGFP proteins were prepared by a modified ionotropic gelification technique previously developed by Calvo et al. (Calvo et al., 1997) and de la Fuente et al. (de la Fuente et al., 2008). Briefly, 12mg BSA or 2.5 mg tat-EGFP (in 1 ml ddH_2O) were mixed with 4 ml of a 0.7% mg/ml solution of TPP. The

protein/TPP solution was then added to 15 ml of a 1 mg/ml chitosan in water solution under magnetic stirring using a drop-wise technique and a syringe pump (Baxter PCAIII) at a rate of 15 ml/hr. Agitation was maintained for 15 minutes to allow the complete formation of the particles. The solidified microparticles were collected by centrifugation, washed three times with sterile PBS, frozen overnight, lyophilized for 6 hours, and stored at 4 ºC until use.

Scanning Electron Microscopy (SEM)

Scanning electron microscopy (SEM) was used to assess the morphology and size of freeze-dried chitosan microparticles (SEM, Model S-2250N, Hitachi, Japan). In preparation for SEM, the particles were mounted on metal holders using conductive double-sided adhesive tape, and sputter coated with a gold layer for 60 seconds at 0.1 bar vacuum pressure (Cressington Sputter Coater, 108).

Transmission Electron Microscopy (TEM)

The morphology and size of the particles were further characterized by transmission electron microscopy (TEM) using a Tecnai G2 20 S-TWIN model TEM with 200kV acceleration voltage. 10 mg of the sample particles was dispersed in 10 ml of ddH2O in an ultrasonic bath. Approximately 200 µl of the dispersed particle suspension was placed on a copper grid coated with a carbon film.

In vitro Release from Chitosan Microparticles

Microparticles were dispersed in DMEM high glucose culture medium (HyClone, Thermo Scientific, Waltham, MA), supplemented with 10% heat-inactivated fetal bovine serum (HyClone), 10000 units/ml Penicillin,10 mg/ml Streptomycin, 2mM L-glutamine (Gibco, Invitrogen Life Technologies, Carlsbad, CA) and 1mM sodium pyruvate (Sigma). To follow protein release over time, dispersed particles were aliquoted into 2ml microcentrifuge tubes, and incubated at 37°C with agitation.

In vitro Release of BSA from Chitosan Microparticles

Protein release from BSA-loaded microparticles was assessed using two methods. In Method 1, microparticles were aliquoted into 3 identical tubes. At each timepoint, the tubes were centrifuged at 13,000 rpm in a microfuge for 10 minutes, and the supernatant was collected and frozen at -20°C. Microparticles were then resuspended in fresh media and returned to 37°C with agitation. After all the samples were collected, the presence of BSA in the supernatant was assessed using the Bovine Albumin Enzyme-linked Immunosorbent assay (ELISA) Quantitation Kit (Bethyl Laboratories, Montgomery, TX).

In order to avoid aggregation problems due to centrifugation and to cause minimal disruption of particles due to re-suspension, Method 2 involved the re-suspension and aliquoting of CMPs into 18 tubes (1 ml of media in each). At each timepoint, 3 tubes were sampled, and the supernatant was collected, frozen and processed as described above.

In vitro Release of Tat-EGFP from Chitosan Microparticles

Due to the limited amount of tat-EGFP protein available, *in vitro* release samples were collected using Method 1 above (involving centrifugation and media changes). Protein quantification in the samples was assessed using fluorescence and ELISA. For fluorescence measurements, 100μL of each sample was read at 509 nm following excitation at 480 nm using a BioTek® Synergy HT plate reader. Fluorescence readings were used to determine tat-EGFP protein concentration by comparing to a linear standard curve generated from known tat-EGFP concentrations. Tubes containing media free of microparticles, or containing a 0.5 μg/ml solution of tat-EGFP served as negative and positive controls, respectively.

Protein quantification obtained from fluorescence was confirmed by ELISA, as we have previously described (Rafat et al., 2010).

In Vitro Cell Culture and Toxicity Assays

Mouse photoreceptor derived 661W cells (kindly donated by Dr. Muayyad R. Al-Ubaidi, University of Oklahoma) were cultured to 30% confluency in 12-well and 96-well plates in supplemented DMEM medium (as described in section 2.5). Cells were treated with 2.5mg/mL of tat-EGFP or CMPs at 0.5, 1.0 or 10 mg/mL for 24 or 48 hours at 37°C (5% CO2).

Following the 24 and 48 hour incubation in the presence of CMPs, tat-EGFP or control medium, alamarBlue® solution (Invitrogen) was added to the 661W cells of a 96-well plate for 2 hours in order to assess cell viability. With this assay, the fluorescence intensity of the medium is proportional to the metabolic activity of living cells.

Fluorescence was quantified on a BioTek plate reader using 530/25-excitation and 590/35-emission filter settings. The mean value of the blank was subtracted from the sample value. The fluorescence for CMP-treated cells was compared to control cell values to calculate the percentage of viable cells in CMP-treated cultures. All cell death assays were conducted with three or more replicates.

Immunocytochemistry (ICC)

Following 24 and 48 hour incubations in the presence of CMPs, 661W cells plated on 12-well dishes at 30% confluency were washed with 1xPBS, fixed with 2% PFA for 10 minutes, and re-washed with PBS three times with gentle rocking. 200μL of blocking solution (1% BSA and 5% goat serum in PBS) was added to the cells for 20 minutes at room temperature. Cells were incubated with rabbit anti-GFP IgG primary antibody (Invitrogen), diluted 1/500 in blocking solution with 0.3% Triton-X 100. The plates were sealed with Parafilm (Pechiney Plastic Packaging Company, Chicago, IL), and incubated overnight at 4°C. The next day, cells were washed with PBS three times for two minutes each, and 200μL of Alexa Fluor 488 goat anti-rabbit IgG secondary antibody (Invitrogen; diluted 1/500) was added to each well for 60 minutes. Cells were then washed with PBS two times for three minutes and treated with 200uL of 1mg/mL DAPI diluted 1:10,000 in PBS for 3 minutes, followed by 200μl of N-propyl gallate (anti-fade solution). The plates were sealed with Parafilm and stored at 4°C. Images were taken under fluorescence on a Nikon Eclipse TE2000-E and a Zeiss Observer Z1 microscope.

In vivo Subretinal Injections of Chitosan Microparticles

Long Evans rats were purchased from Charles River Laboratories (Wilmington, MA) and maintained under standard laboratory conditions. All procedures were approved by the University of Ottawa Animal Care and Veterinary Service and conformed to the ARVO Statement for the Use of Animals in Ophthalmic and Vision Research. Subretinal injections were done in the temporal superior quadrant of the left eye of 26 animals, according to our previous methods (Zadro-Lamoureux et al., 2009). CMPs were suspended in 10% FBS supplemented DMEM. Ten rats received CMPs at a concentration of 1.0 mg/ml, and 12 rats received a concentration of 10 mg/ml. An additional 4 animals received an adeno-associated virus (AAV) expressing GFP driven by the chicken beta actin (CBA) promoter at a titre of $1x10^{12}$ particles/ml (injection control). In all cases, 2 μL of the CMP or viral suspension was delivered into the subretinal space.

Electroretinography

Electroretinograms (ERGs) were performed at 2, 4, 6 and 8 weeks following subretinal injection of microparticles. Rats were weighed and dark adapted overnight before full-field scotopic/photopic ERGs were conducted using the ESPION system (Diagnosys LLC). Animals were anesthetized with an intraperitoneal injection of ketamine hydrochloride (30mg/kg - Vetalar®) and medetomidine hydrochloride (0.5mg/kg - Domitor ®). Anesthesia was maintained for one hour, after which the medetomidine was reversed using atipamezole hydrochloride (1mg/kg - Antisedan ®). Eyes were dilated five minutes prior to the ERG test with one drop each of 1% tropicamide (Alcon) and 2.5% phenylephrine hydrochloride (Alcon). A topical anesthetic (0.5% proparacaine

hydrochloride; Alcon) was applied to each eye. The animals were placed on a water-circulating heated pad (Gaymar T/pump) to maintain body temperature during the ERG. Silver wire loop electrodes were placed on both corneas with 0.3% hypromellose (GenTeal). A reference electrode was placed on the tongue and a ground needle electrode was placed subcutaneously in the medial quadrant of the rat's tail. The rat's head was positioned under a Ganzfeld dome. Single flash stimuli (4 ms duration) were presented at 10 intensities of light, ranging from 0.0025cd.s/m2 to 25 cd.s/m2. Five traces were generated and averaged at each light intensity.

Fundus Photography

A Micron III fundus camera (Phoenix Research Laboratories Inc) was used to image the retina of each rat to assess injection site, spread of particles and retinal damage.

Sampling and Tissue Processing

For each of the microparticle injected groups, one third of the animals were sampled at 4 weeks after the subretinal injection of microparticles, and two thirds were sampled at 8 weeks. Prior to sampling, animals were intraperitoneally injected with 1mL or 2mL of Euthanyl at 65mg/mL, and transcardially perfused with 4% PFA. Eyes were sampled and sectioned as previously described (Renwick et al., 2005). Slides were washed for three minutes in Tris-buffered phosphate (TBS), followed by incubation for three minutes in DAPI (1mg/mL) diluted in TBS. The slides were rewashed in TBS for three minutes, concealed with a coverslip and Antifade.

Results

SEM and TEM Characterization

SEM images of tat-EGFP-loaded chitosan microparticles showed that chitosan spheres range in size from about 0.3-3.0 μm (Fig. 5.1A). Non-spherical stem-like particles are also formed. A TEM image of similar composition chitosan microparticles (Fig. 5.1B) confirmed the presence of sub-micron microspheres that would be difficult to detect by conventional light microscopy. The microparticle size and shape may have been affected by a number of factors. Chitosan is a positively charged biopolymer. In the presence of the crosslinker TPP, some of the positive charges are neutralized by the negatively charged TPP, but the extent of this may be variable. Thus, the overall shape and size of the microparticles may be dependent on the nature and concentration of the protein being encapsulated (as we showed previously with EGFP and PEG-PLA (Rafat et al., 2010), on the concentration of the chitosan biopolymers (Calija et al., 2011), and on the nature and concentration of the crosslinker.

Protein Release from Microparticles

Two in vitro methods were used to assess protein release from chitosan microparticles. In the first method, BSA- or GFP-encapsulated chitosan microparticles were suspended in medium, and at each sampling timepoint, the medium was centrifuged to pellet the microparticles and the supernatant was collected and analyzed for the presence of released protein. The microparticles were then re-suspended (with agitation) in fresh

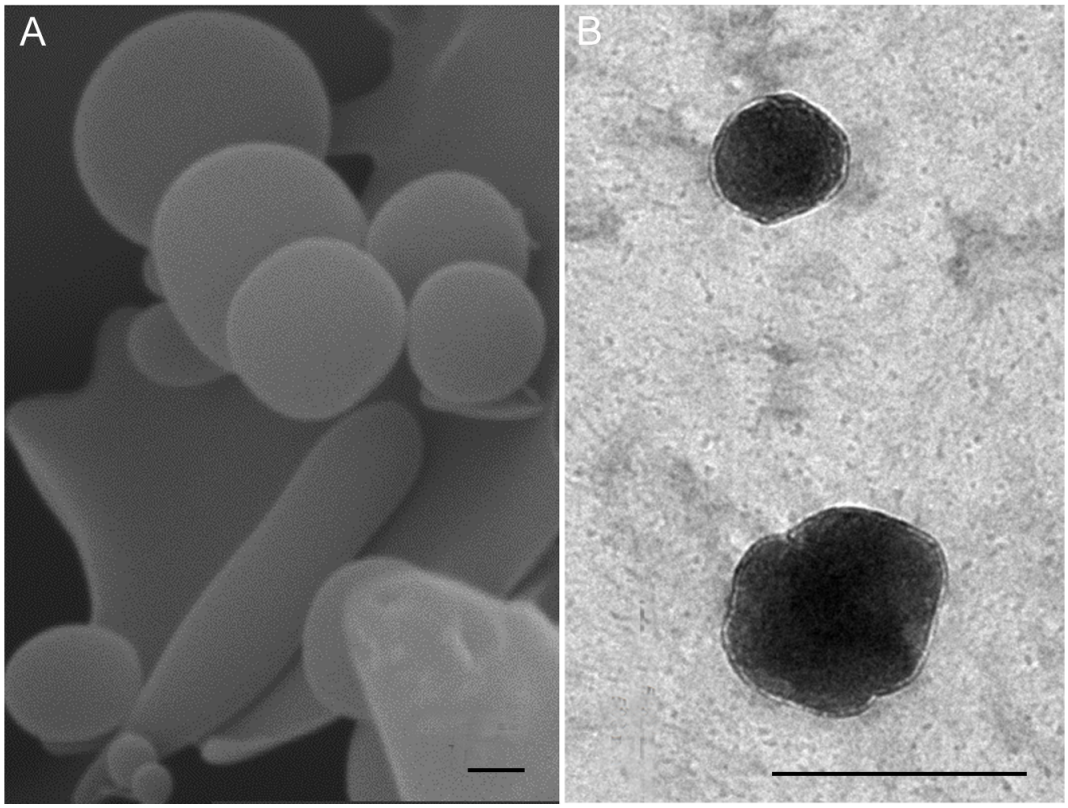

Fig. 5.1. **SEM (A) and TEM (B) images of chitosan microparticles**.
SEM shows chitosan spheres ranging in size from approximately 0.3-3.0 μm. Non-spherical stem-like particles are also visible. TEM confirms the presence of sub-micron microspheres. Bar = 0.5 μm.

medium, and returned to 37ºC until the next sampling timepoint. Using this method a biphasic release profile was obtained. There appeared to be an initial burst of protein release within the first 24 hours, and this was followed by a slower, sustained release over the next 20 days (Fig. 5.2A, B). The initial burst may have been due to the release of protein at, or close to, the particle surface, and was undoubtedly aided by the centrifugation and re-suspension of the particles, which would have aided in breaking them down and releasing their contents. The sustained release phase likely resulted from protein release through the slow degradation of the microparticles or through gradual diffusion of proteins from the microparticle core.

The second method of assessing protein release did not involve repeated centrifugation or re-suspension of the microparticles. With this method, there was a slow and steady release of protein from the microparticles, as opposed to the biphasic release observed with the first method (Fig. 5.2C).

BSA vs. Tat-EGFP release profiles

Both protein release methods resulted in approximately the same total release of BSA protein by the end of the 20-day period. However, the cumulative release for BSA was higher than that of tat-EGFP. As shown in Fig. 5.2, 11 μg BSA was released from each mg of CMPs over a period of 20 days, accounting for about 55 % of total BSA encapsulated. These numbers were 1.1 μg and 21%, respectively, for tat-EGFP release. The higher release for BSA may be attributed to the nature of the protein, but is most likely related to the higher initial ratio of BSA to chitosan used for the fabrication of

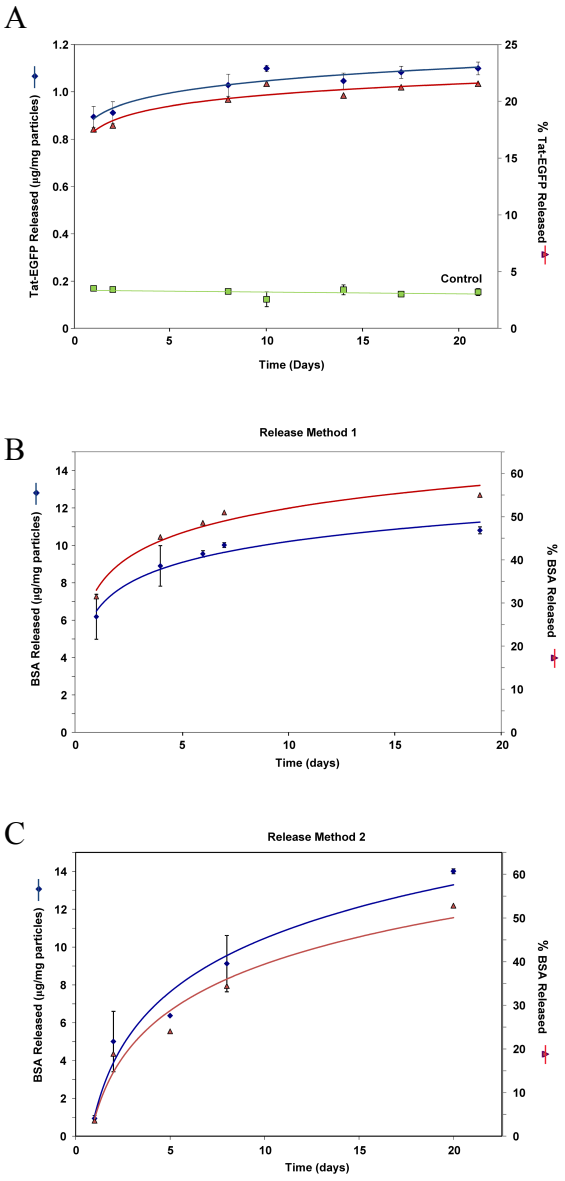

Fig. 5.2. **Release kinetics of chitosan microparticles.**
Total amount of protein release is shown on the left axis, and percentage of encapsulated protein released is shown on the right axis. For tat-EGFP (A), an initial burst of protein release is followed by a more gradual release over time. Control, non-encapsulated protein shows minimal degradation with time. BSA release (B, C) was assessed using 2 methods (see Materials and Methods). The first method (B) shows a biphasic release profile, similar to that obtained for tat-EGFP. The second method, which does not involve perturbation of the CMPs through multiple centrifugation and resuspension steps, shows a gradual protein release over time (C). Both methods resulted in approximately 50% release of encapsulated protein within 20 days.

particles (e.g. 0.8 for BSA compared to about 0.17 for Tat-EGFP). These results are in-line with our previous study using PEG-PLA in which we found that the cumulative protein released was directly proportional to the concentration of protein initially used for encapsulation (Rafat et al., 2010).

In vitro toxicity of CMPs

CMPs containing encapsulated tat-EGFP were tested for cellular toxicity in 661W cells, a transformed photoreceptor-derived mouse cell line. Tat-EGFP-encapsulated CMPs were used for this study (and for the in vivo subretinal injections described below) in order to allow tracking of the microparticles through fluorescence microscopy. Several concentrations of microparticles were tested (0.5 mg/mL medium, 1.0 mg/mL and 10 mg/mL). Cell viability was analyzed using alamarBlue assays after 24 and 48 hours in the presence of CMPs.

Chitosan microparticles adhered to the surface of 661W cells, and were seen to associate with cells after 24 hours in culture (Fig. 5.3A-D). The lower concentrations of CMPs (0.5 mg/mL and 1.0 mg/mL) were not toxic to the cells. Cell viability was >95% after 48 hours in the presence of the microparticles. However, 10 mg/mL of CMPs had significant impact on the viability of the cells. Approximately 50% of the cells were compromised within 24 hours, and there was approximately 90% cell death at 48 hours, as assessed by the alamarBlue colorimetric assay (Fig. 5.3E). It remains to be seen if this is due to the release of toxic factors from the CMPs or to the 'suffocation' of the cells because of the sheer number of CMPs adhering to their cell surface. Cellular toxicity by

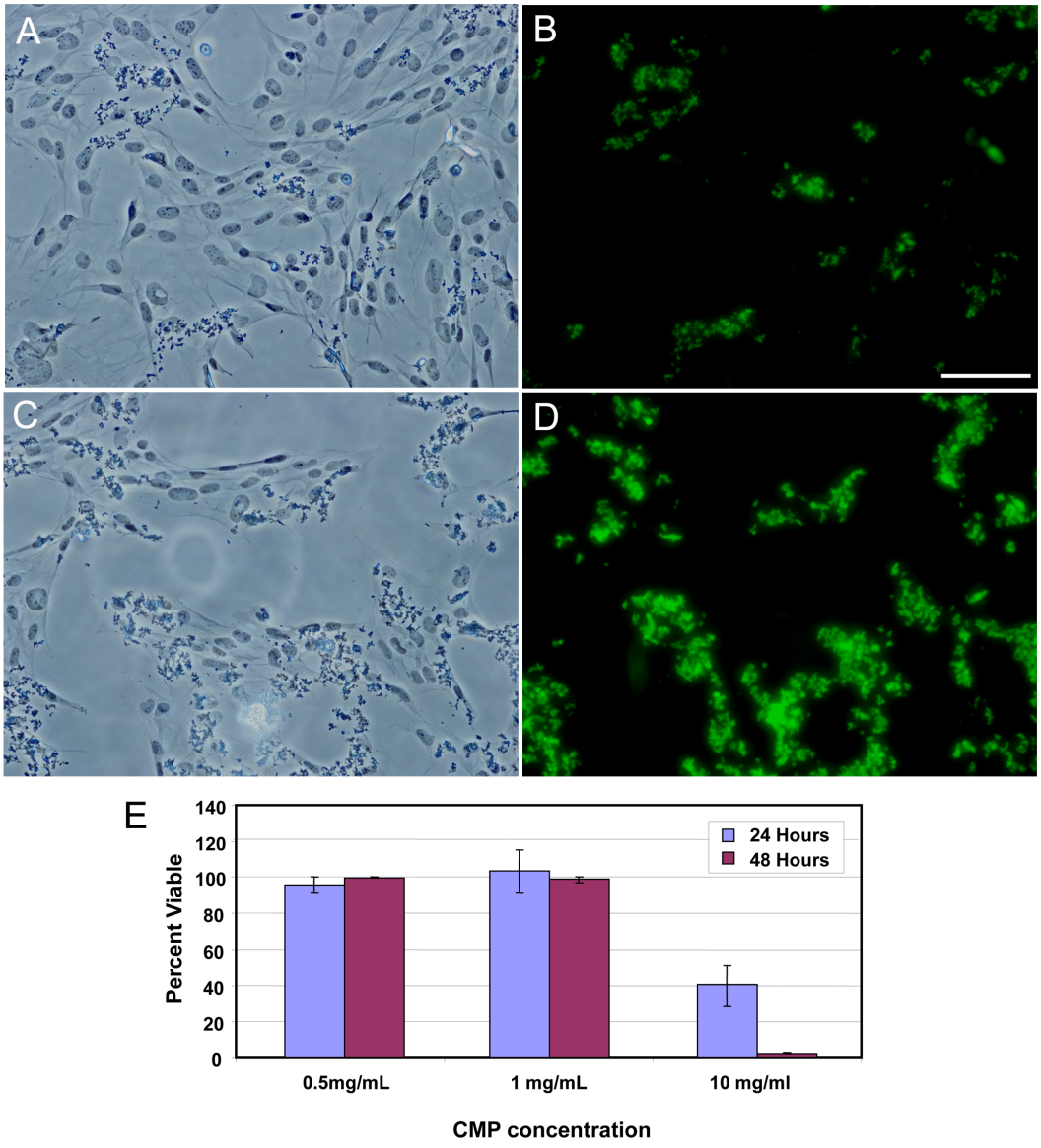

Fig. 5.3. **Phase contrast and fluorescence images of 661W cells showing cell surface localization of the eGFP-loaded microparticles after 24 hours in culture**.
(A, B) – 0.5 mg/mL. (C,D) – 1.0 mg/mL. (E) Cell viability, as assessed by AlamarBlue staining. There is no cellular toxicity at the low CMP concentrations of 0.5 and 1 mg/mL. However, there is significant cell death in the presence of 10 mg/mL CMPs, at both 24 hours and 48 hours in culture. Bar = 100 µm.

chitosan is not completely unexpected. Hu et al. (Hu et al., 2011) reported toxic effects on zebrafish embryos that were both concentration and size dependent, with smaller particles and higher concentrations having higher toxicity. Prego et al (Prego et al., 2005, 2006) reported toxic effects of chitosan nanoparticles on Caco-2 human epithelial colorectal adenocarcinoma cells at concentrations of 1 mg/mL.

In vivo injections of CMPs into the subretinal space of rats

In order to test the therapeutic potential of CMPs as drug delivery vehicles for the treatment of retinal diseases, the microparticles were injected into the subretinal space of Long Evans rats. Based on the *in vitro* toxicity assays, two concentrations of microparticles were injected: 1.0 mg/mL and 10 mg/mL in a volume of 2 μL. Animals were followed for a period of 8 weeks after the subretinal injection using bi-weekly electroretinograms to test effects on retinal function. Adeno-associated virus (AAV) carrying EGFP was injected as a positive control for the injection procedure and for the expression levels of EGFP. Fundus images were taken at each ERG timepoint using both regular illumination and fluorescence microscopy.

Subretinally injected CMPs were still present in the subretinal space at 8 weeks after delivery, making them ideal long-term therapeutic delivery agents. However, subretinal injections with CMPs were much more challenging than AAV-GFP injections. Due to the adhesive nature of the microparticles, CMPs would often obstruct the needle, thus increasing the injection pressure required to deliver them into the subretinal space. This increased pressure would often cause increased damage at the injection site.

Electroretinography

The electroretinogram (ERG) is a measure of retinal function. The a-wave of the ERG results from photoreceptor activation and the amplitude of the b-wave is indicative of overall retinal health. ERGs were conducted at 2, 4, 6 and 8 weeks after CMP injection. In order to test the effects of the CMPs on retinal function, the amplitudes of the a-wave and b-wave were compared between the CMP-injected left eyes of the animals and their uninjected control right eyes.

CMP-injected eyes showed a significant decrease in both a-wave and b-wave amplitudes at 2 weeks after the injection (Fig. 5.4A). Most of this decrease is probably attributable to the injection procedure itself. We and others have previously shown that it takes several weeks for the eye to fully recover from any subretinal injection (Leonard et al., 2007; Timmers et al., 2001). By 4 weeks, the eyes injected with 1mg/mL CMPs appeared to be recovering from the injection procedure, and their a-waves were no longer significantly different from the uninjected controls (Fig. 5.4B). At this timepoint, the ERGs of eyes injected with 10 mg/mL CMPs were still significantly decreased in comparison to their uninjected controls, and were now also significantly different from the eyes receiving 1 mg/mL CMPs. This trend persisted at 6 weeks; there were no significant differences between uninjected eyes and those receiving 1mg/mL CMPs, but significant decreases in both a- and b-wave amplitudes of 10 mg/mL-injected animals in comparison to the other 2 groups (Fig. 5.4C). By 8 weeks, there appeared to be some recovery in all injected eyes; however, the eyes injected with 10 mg/mL of CMPs still showed significantly reduced a- and b-waves in comparison to the uninjected controls (Fig. 5.4D). The ERG data suggest that CMPs may be toxic to the retina at higher

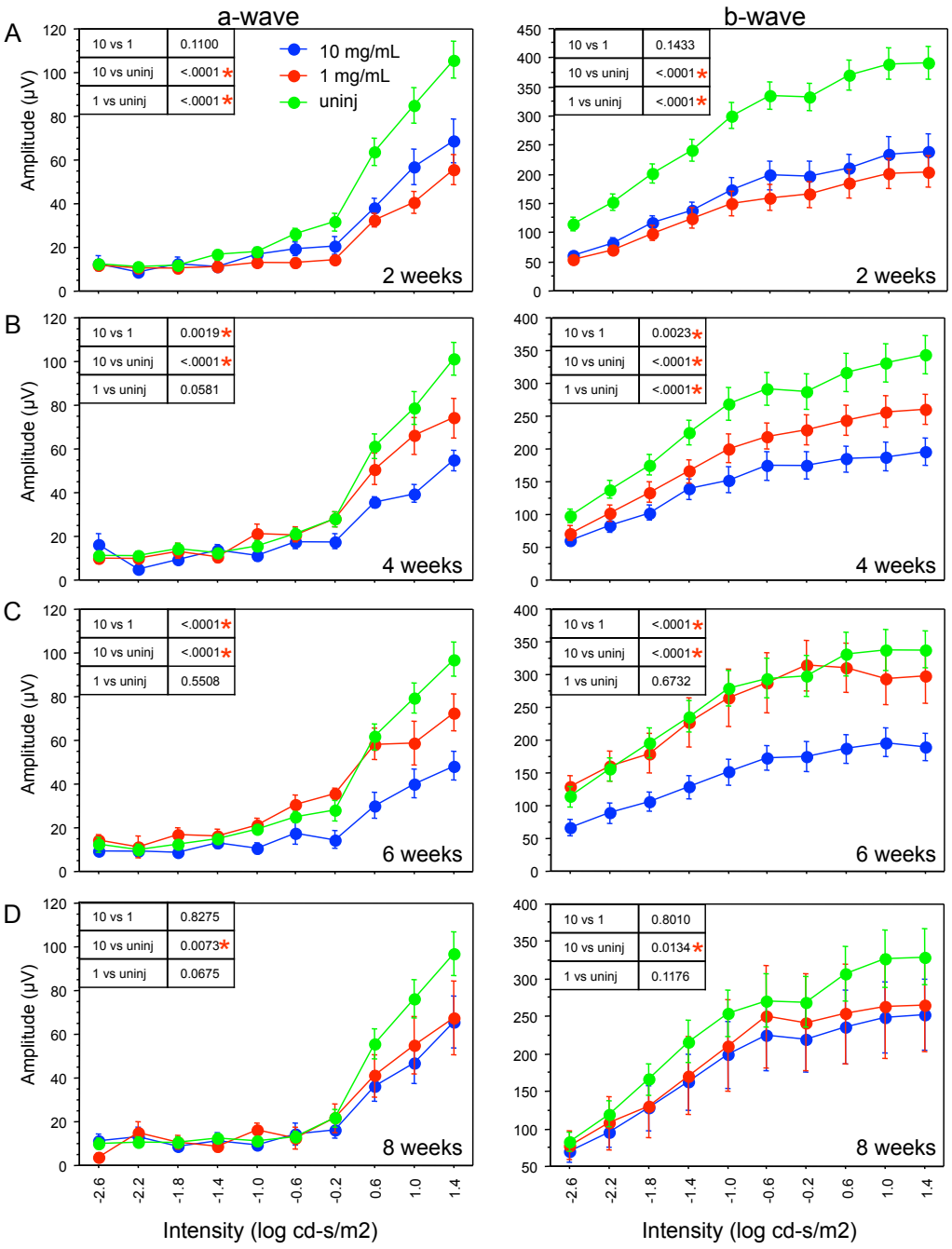

Fig 5.4. **ERG analysis of CMP treated retinas.** The injection procedure results in a depressed ERG amplitude in both CMP groups at 2 weeks. At 4 weeks, the animals injected with 1 mg/ml appear to be recovering from the injection and are statistically better than the 10 mg/ml group. By 6 weeks, there is no difference between control, uninjected eyes and those receiving 1 mg/ml CMPs, but the 10 mg/ml group continues to show reduced ERGs. Statistical analysis was conducted using StatView for Windows (vers. 4.5). Statistical significance between test groups was assessed using one-way ANOVA with a Scheffe post-hoc analysis. P-values are shown between test groups. Significance is indicated by a red asterisk.

concentrations. This is manifested in lower ERG amplitudes with higher concentrations of CMPs. This explanation seems to be supported by the *in vitro* data, which suggest that higher concentrations of chitosan microparticles are toxic to 661W cells. The ERGs also suggest that the degradation of the CMPs with time may allow some recovery of. function. This might account for the reduced significant differences in ERG amplitudes at 8 weeks after the CMP subretinal injections.

Fundus imaging and histology

In vivo imaging of the retina under light and fluorescence microscopy was used to assess the status of the retina following the subretinal injection, and to determine the 'spread' of the microparticles from the site of the injection (Fig. 5.5). CMPs appeared as particulate matter in the subretinal space. The fluorescent particles were often clearly seen in eyes injected with the higher concentration of CMPs, but were not as evident with the lower concentration. A few injections showed spread of the CMPs from the injection site, whereas others appeared to show clustering of CMPs at localized sites in the subretinal space (Fig. 5.5). By comparison, AAV-GFP-injected eyes showed beautiful spread of the injected material and widespread fluorescence in the subretinal space (Fig. 5.5J).

Histology was used to confirm the observations of the *in vivo* retinal imaging. Histological effects on the retina depended on the state of dispersion of the chitosan microparticles. For both concentrations, disruptions to the characteristic laminar structure of the retina were seen when microparticles clustered together in the subretinal

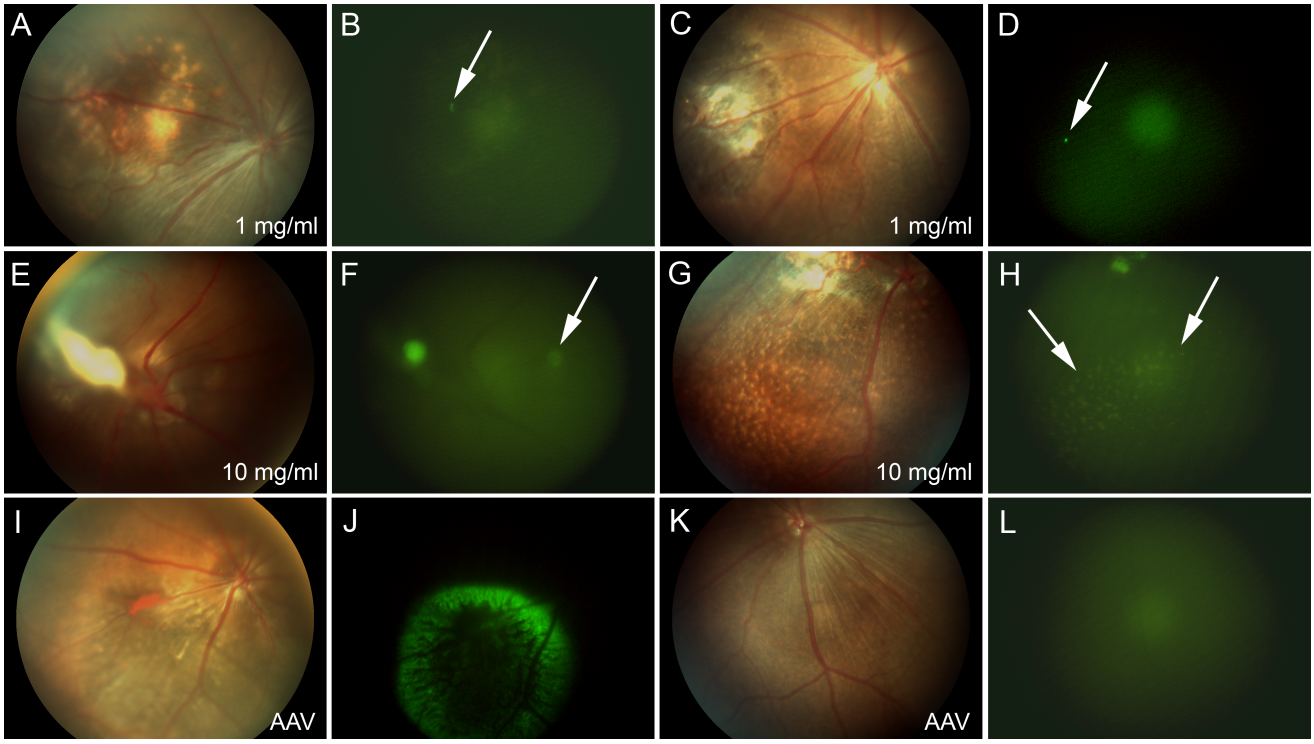

Fig. 5.5. Fundus images under bright field and fluorescence of animals injected with 1 mg/ml (A-D) or 10 mg/ml (E-H) of tat-EGFP encapsulated CMPs.
The CMPs are difficult to see in the subretinal space at the lower concentration except for a small number of clustered particles (arrows). At the higher concentration, the fundus images in E and F show clustered particles, whereas those of G and H show more dispersed particles in the subretinal space. (A, B, E, F) Fundus images at 2 weeks after the injection. (C, D, G, H) Fundus images at 6 weeks after the injection. An AAV-injected retina (at 4 weeks) shows higher levels of GFP fluorescence (I, J). In contrast, the uninjected control shows a complete lack of fluorescence (K, L). Fluorescent images were enhanced in Adobe Photoshop 7.0 to allow visualization of CMPs in the subretinal space.

space, inducing localized detachments of the retina and rosetting at the injection site (Fig. 5.6). When CMPs were adequately dispersed, the laminar structure of the retina was unaffected. By contrast, AAV-GFP injections were rarely disruptive of retinal structure (Fig.5. 6).

Discussion

Ocular therapy is a burgeoning industry, but most therapeutic agents are delivered topically onto the corneal surface of the eye. Therapeutic agents are quickly washed away by the tear film, limiting their therapeutic potential. Nanoparticle and microparticle research in anterior segment diseases aims to develop delivery vehicles that will prolong half-life and achieve a longer-term controlled release of the therapeutic agent. Numerous studies have been conducted on chitosan use in topical delivery of drugs to the cornea (for review, see (Başaran and Yazan, 2012)). These studies suggest that chitosan is well-tolerated and increases the drug retention time on the ocular surface, allowing greater permeation through the cornea. There are very few studies that have examined chitosan delivery intraocularly. Prow et al (Prow et al., 2008) suggest that chitosan microparticle delivery into the vitreous of the eye may be toxic to the retina; however, as previously stated, the authors acknowledged that the inflammatory response induced by chitosan may have been influenced by the purity of the material. Yang et al (Yang et al., 2008) examined the use of chitosan as a vitreous tamponade material, and concluded that there were no clinically significant effects caused by the material, with only slight increases in inflammatory factors. This would further suggest that the problems seen by Prow and

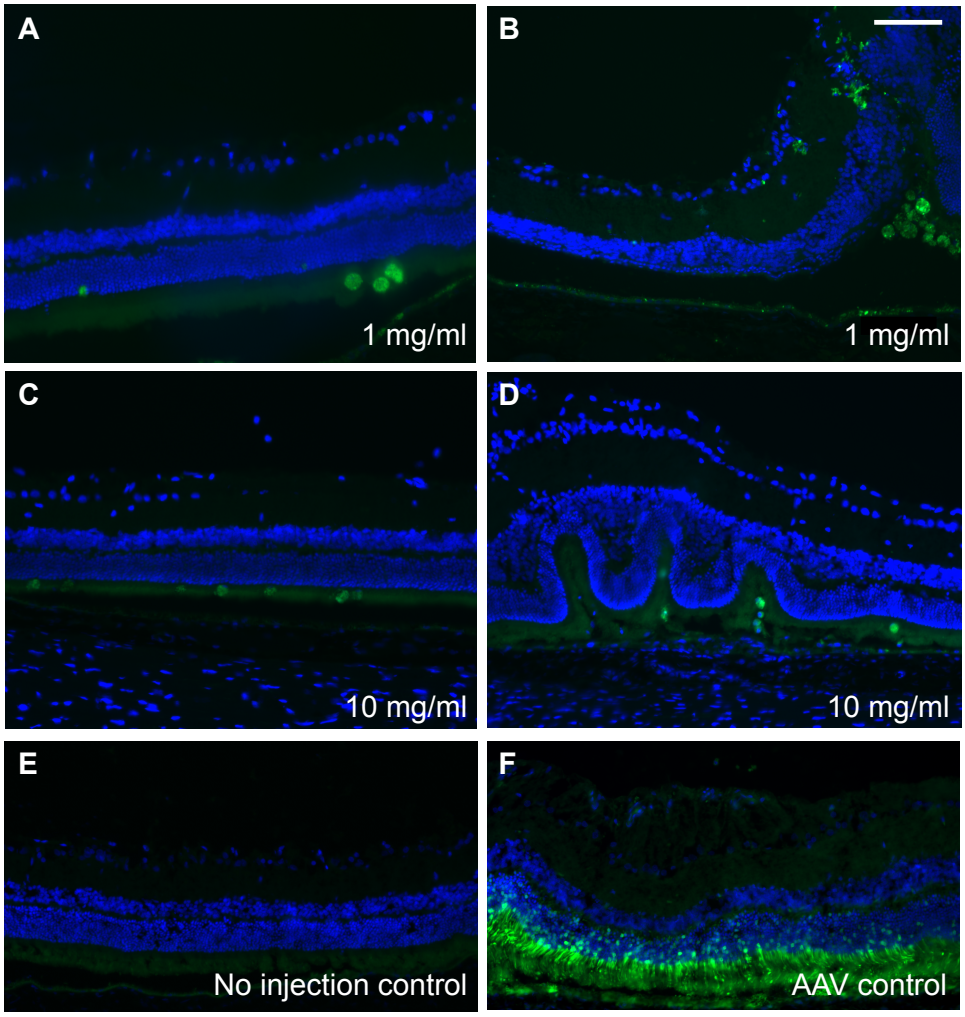

Fig. 5.6. ***In vivo*** **immunocytochemistry showing CMPs in the subretinal space.** Both concentrations showed minimal disruption of the retinal structure when CMPs were adequately dispersed (A, C). However, when there was aggregation of microparticles, retinal architecture was severely disrupted, irrespective of the concentration of the CMPs (B,D). An uninjected control (E) and an AAV-injected control (F) are shown for comparison. All images were taken at 4 weeks, except for (B) which was taken at 8 weeks. Bar = 100 μm.

colleagues might be related to the purity of the sample, and not the toxicity of chitosan. Importantly, both of these studies injected chitosan into the vitreous, and not the subretinal space.

In the current study, the *in vivo* results obtained with electroretinography, retinal imaging and histology suggest that the higher concentrations of microparticles are disruptive to the structure and function of the retina. The *in vitro* results appear to support the *in vivo* data. However, the effects observed may have two possible explanations. It is entirely possible that chitosan microparticles, at high concentrations, may be chemically toxic to retinal cells. The potential toxicity of chitosan in non-ocular tissues has been reported by others (Hu et al., 2011; Prego et al., 2005, 2006). Since it is difficult to determine the exact concentration of chitosan exposed to individual cells in all the current and previous studies, it is difficult to make a definitive conclusion. Due to the adhesive nature of the chitosan microparticles, and the resulting clustering of the particles, the effective concentration seen by some cells may be different than others. In our study, the clustering of particles caused localized disruptions in retinal structure. Where CMPs were nicely dispersed, no disruption in retinal structure was seen, irrespective of the initial concentration injected. In addition, the adhesive nature of the CMPs made subretinal injection challenging, and clumped particles were ejected from the syringe with greater pressure, increasing the damage at the injection site. For this reason, it is difficult to determine whether the toxic effects of CMPs resulted from the chemical nature of the particles or from the difficulties with injecting the adhesive particles. The *in vitro* toxic effects may also be attributed to the adhesive nature of the particles, which attached to the cells and were concentrated on the cell surface. The level of toxicity

found in our study, and in a few other studies, is difficult to reconcile with the numerous studies in the literature showing that chitosan is safe and well tolerated. The differences may be attributed to the cell types examined, the effective concentration of the chitosan seen by each of the cell types, or possibly the fabrication process used to generate the microparticles.

Conclusions

Overall, this study suggests that chitosan microparticles are effective long-term delivery agents to the outer segment of the retina. Chitosan microparticles exhibited enhanced encapsulation capacity and a better release profile than the PEG-PLA microparticles investigated in our previous study. The percentage of encapsulated tat-EGFP released from chitosan microparticles was 21% over 20 days, in comparison to 1-5% over 30 days for PEG-PLA. However, the concentration of chitosan microparticles may be critical in determining the extent of toxicity. It is also important to ensure that chitosan microparticles are adequately dispersed during the injection procedure in order to ensure minimal disruption to retinal structure and function.

Acknowledgements

The authors wish to thank William Hauswirth (University of Florida) for the AAV virus, and Herman Cheung for helpful advice with the cell death assays. This work was supported by grants to CT from the Canadian Institutes of Health Research (CIHR), the

Canadian Foundation Fighting Blindness, and the Ottawa Hospital Foundation. SW was supported by a Queen Elizabeth II Graduate Scholarship in Science and Technology (QE-II GSST). We would also like to thank the Medical Devices Bureau of Health Canada for allowing us to use their SEM system.

CHAPTER 6: GENERAL DISCUSSION

The work described in this thesis evaluated the potential for using XIAP as a therapeutic in both chronic and acute forms of retinal degeneration. In the second chapter, we evaluated the potential for XIAP gene therapy to protect against a genetic form of retinal degeneration, Leber's hereditary optic neuropathy (LHON). This form of retinal degeneration is amenable to gene therapy since it is a progressive disease requiring long-term interventions. In the third and fourth chapters of the thesis, we examined the potential for XIAP as a therapeutic in retinal detachment. We first developed the model (Chapter 3) and then examined the protective effects of XIAP gene therapy. Since retinal detachment is acute and often occurs without warning, the gene therapy studies outlined in Chapter 4 provide important proof-of-principle for XIAP efficacy but are not an ideal method for treatment, so in the fifth chapter, we examined an alternative strategy (chitosan microparticles) for delivering proteins to the retina. Each of the chapters is discussed in further detail below.

The first manuscript (in Chapter 2) entitled "XIAP over-expression protects optic nerve structure and function in the mutant ND4 mouse model of Leber's Hereditary Optic Neuropathy" firstly validated the work of Dr. John Guy and his group at the University of Miami, showing that the administration of an adeno-associated virus, packaged with the R340H mutant ND4, into the mouse vitreous can generate a dominant model of LHON. We found that this vector mediated approach produced a variable disease phenotype between animals and was slow acting (requiring greater than 4 months to ensure complete onset of disease). These features were also observed in the literature as the time points for disease onset typically ranged between 6 months and one year, and very large

cohorts of animals were necessary to study the disease (Guy et al., 2009; Koilkonda et al., 2014, 2010; Yu et al., 2012a).

Even though we did not see advanced disease in the LHON animals, in the second part of the manuscript, we were able to evaluate the potential of XIAP-mediated neuroprotection in the early stages of LHON disease. *In vitro* studies showed that XIAP is a potent inhibitor of apoptosis. A microarray was performed (Appendix A) to determine the genetic changes after over-expression of XIAP in 661W cone photoreceptor cells under control and apoptotic conditions. The results from this array showed hundreds of genes that were differentially regulated, and fell into the categories of cell proliferation, cell death and homeostasis, supporting studies in the literature that show that XIAP not only prevents cell death in a caspase-dependent manner, but is involved in multiple other caspase-independent pathways (Galbán and Duckett, 2010). *In vivo*, our studies showed that XIAP-treated axons within the optic nerve had a significantly greater cross-sectional area compared to GFP-injected mND4 axons and the architecture of the optic nerve was preserved. There was also evidence of functional protection by PERG.

These data are promising, but modifications to the experimental design are warranted in order to make the research more clinically applicable. Both in our study, and in the preclinical studies performed by others (Koilkonda et al., 2014, 2014), the therapeutic vector was delivered before the mutant ND4, which causes the disease. This strategy ensured that the therapeutic vector had a good opportunity to start expressing optimal levels of the transgene, and it provided proof-of-principal for the efficacy of the therapy. However, in the clinical setting, therapy would most likely only be initiated

after the onset of disease and thus, future studies examining the effect of XIAP therapy delivered after the onset of disease are warranted.

One of the reasons why the eye is an optimal tissue for gene therapy and why gene therapy has advanced so far in this model system is that the eye is considered to be immune privileged due to its physical barriers, inhibitory ocular microenvironment and its ability to regulate systemic immune responses (Zhou and Caspi, 2010). However, this does not necessarily make the ocular system resistant to antibodies produced by the immune system to neutralize viruses, such as AAV. In fact, anti-AAV antibodies are quite prevalent in humans as a result of preexisting humoral immunity due to natural exposure to AAV early in life (before the age of 2 years old) (Masat et al., 2013). Consequently, gene therapy intervention will be most effective in naïve patients on an immunosuppression (B cell depletion) drug regime before and after surgery (Corti et al., 2014). Neutralizing antibodies are also found in the sera of mice. Rapti *et al.* (2012) showed that naïve mice purchased directly from manufacturers had natural inhibitory AAV antibodies to AAV1 and AAV6. These results are quite striking as it was thought that only larger animals (non human primates (NHP) and humans) harbored antibodies against AAV serotypes. Furthermore, the murine AAV only contains ~50% amino acid identity to AAV1-9 used in scientific research which makes these results even more surprising (Rapti et al., 2012). In addition, Kotterman *et al*. (2015) found that an intravitreal injection with AAV2 capsids (even capsids with other mutations such as 7m8 and 4YF) elicited an humoral response in non-human primates who had no neutralizing antibodies before the injection and significant levels post-injection (Kotterman et al., 2015). Furthermore, in 2008 the Hauswirth group (University of Florida) found that an

intravitreal injection of AAV2 in one eye mounted a humoral response, which completely prevented transduction of AAV2 in the contralateral eye two months later (Li et al., 2008). These results show that the immune privileged eye is not completely protected from humoral antibodies generated in the vitreous body, which can travel to other organs. Although there does not seem to be a cell mediated response, anti-AAV antibodies are prevalent in the eye and need to be considered when conducing gene therapy clinical trials (Bennett, 2003; Kotterman et al., 2015; Wang et al., 2015).

These studies on neutralizing antibodies may be relevant to the current study. Guy et al. (2009) administered the wild-type ND4 into the vitreous, followed by the injection of mutant ND4, to generate the disease, three days later (Guy et al., 2009). Similarly, we also injected our therapeutic vector (XIAP or GFP) prior to the disease vector (mND4); however, in our study, the second virus was injected two weeks after the first to ensure optimal XIAP expression before the onset of disease. Thus, it may be argued that the reason for the slow disease progression or the variability in disease manifestation between animals may be attributed to neutralizing antibodies (ie. insufficient amounts of vector delivered to the retina). However, studies evaluating neutralizing antibodies of the mutant ND4 and wild-type ND4 vectors created at the University of Florida (where our preparations used for this thesis were generated) or the University of North Carolina, showed significantly increased neutralizing titres in only 2/5 rhesus monkeys, suggesting the vectors do not illicit a strong response in all animals. Furthermore, none of the monkeys showed an increase in stimulation index after T-cell proliferation assays (Koilkonda et al., 2014). Moreover, all preclinical studies from other groups using the ND4 subunit in rodents and rhesus monkeys which employed a double

injection of AAV2, did not present any reduction in transfection of the second virus correlated to neutralizing antibodies and there was no indication of viral spread outside the eye, with the exception of a few viral genomes found in the lymph nodes and the spleen (Koilkonda et al., 2014, 2010; Yu et al., 2012a). This may be because the mouse strain used, DBA1/J, may not produce a strong antibody response following AAV injection. However, it is most likely that the three mutations of the capsid proteins of the vector (Y444,500,730F) which were generated to evade intracellular degradation and thereby increase the transduction of the retina (Petrs-Silva et al., 2009) may be so effective at transducing the retina that fewer particles are necessary to obtain efficient transgene expression. Thus, even if some of the viruses are neutralized, the loss may not be sufficient to affect overall expression. In this thesis, immunostaining of the FLAG tagged mutant ND4 confirmed that the second injection of virus was still effective at promoting expression in the retina. There were some areas of the retina that were better transduced than others, but that is to be expected after an intravitreal injection of any vector. However, it is important to note that the best expression of the FLAG tag was seen during the first set of experiments that were used to characterize the disease, and where only one viral injection was conducted.

In the current study, even if neutralizing antibodies were present, this might affect the severity of the disease, but it would not negate the results obtained with XIAP, because any effects on disease progression would apply equally to both the GFP and XIAP-treated groups. However, in future studies, the contribution of neutralizing antibodies to the variability in phenotype between animals can be easily evaluated. Neutralization assays can be performed on the serum and vitreous of DBA/1J mice after a

first and second intravitreal injection. It would also be interesting to determine the time course at which a humoral response is mounted and to determine the optimal timing for subsequent injections. Furthermore, future studies can evaluate transgene expression after a second viral injection within 72 hours of the first, (likely completely evading any B-cell response) compared to the expression data after 2 weeks as presented here.

In terms of functional PERG results, despite efforts to reduce background noise (such as recording on evening and weekends when other machines in the area are not being used), the PERG traces were impacted by background noise and did not always show a typical waveform. Further studies must be conducted that include more controls and better insulation of the machine. Although, simply analyzing the crude N95 amplitude, XIAP treated animals show the strongest and often more typical waveforms.

Overall, the results of chapter 2 showed that XIAP was effective in protecting structure of the optic nerve. However, there will be inherited retinal diseases in which the mutation prevents the retinal cells from functioning properly. In this case, XIAP might be able to preserve retinal structure and function, but it would not **regenerate** retinal function. However, even in these situations, there might be a role for XIAP therapy. For example, in the current gene therapy trials for Leber's congenital amaurosis (LCA), the wild-type RPE65 gene is being administered to RPE cells in patients that lack the functional gene. These clinical trials have shown that despite an improvement in visual function, the results are not long-lasting and are followed by a decline in vision as a result of the underlying natural photoreceptor degeneration (Cideciyan et al., 2013a; Jacobson et al., 2015). In situations such as this, a combination therapy involving XIAP to protect the structure of the retina, in addition to the replacement of the defective gene

to restore function should provide improvements in vision that may be sustained for the long term.

The second and third manuscripts in this thesis (Chapter 3 and 4), further tested the ability of XIAP to protect the retina. Employing the LHON model of Chapter 2, I've tested the effects of XIAP in a chronic genetic model of retinal degeneration that affected retinal ganglion cells and the optic nerve. In Chapter 3 and 4, we examined the effects of XIAP gene therapy in a physically induced model of retinal detachment, which results in the acute death of the photoreceptors.

In a previous study in rats, we showed that XIAP could protect photoreceptor structure for up to 2 months following a retinal detachment. However, due to the technical challenges of performing surgery in the small rat eye, we were unable to re-attach the retina and examine the effects on retinal function. For this reason, we developed a cat model of retinal detachment (Chapter 3) and tested the effects of XIAP therapy in this model (Chapter 4).

XIAP was able to protect retinal structure in 4 of the 6 animals treated. The other two animals each suffered surgical complications that made it impossible to assess XIAP's efficacy (one had a complete retinal detachment and the other developed a vitreal hemorrhage). Despite the significant protection afforded by XIAP, the low number of animals in each of the experimental groups reduced the power of the study and resulted in a lack of significance in the functional analysis. We started with 6 animals in each group. Based on our previous studies, we determined that this was enough to provide enough power in the study to identify significant differences between experimental groups. However, 3 animals (2 GFP-treated and 1 XIAP-treated) suffered complete

detachments (caused by the gas bubble travelling around the retina due to the activity of the animals). Another two animals presented with surgical complications in the form of bleeding into the vitreous (vitreal hemorrhage) and fluid/cells entering the detached retina (solid detachment). As a result, all quantitative results were based on four XIAP-treated animals and three GFP-treated animals. These low numbers significantly reduced the statistical power of the study. As a result, we observed significant differences in the outer nuclear layer thickness analysis ($p=0.05$, by student's t-test) but no significance in the functional ERG test.

In terms of the functional assessment of the retina, a full-field ERG is not optimal. This test records the average function of the entire retina, which includes attached and detached portions, and areas that received the vector and those that did not. A more appropriate test would have been the multi-focal ERG (mfERG), which can study the function of specific areas of the retina, and in theory, could be positioned over the retinal detachment to assess the focal effects of the XIAP gene therapy. Although we were able to obtain a mfERG in one animal (Appendix B), and there was an observable reduction in waveforms in the superior pole (which is where the detachment was induced), we found that we were unable to reliably place the hexagonal array onto the feline retina in the region of the detachment every time. The fundus camera on the VERIS mfERG system, which is normally used to position the instrument over the desired location on the retina, did not function due to the tapetum lucidum of the cat retina, a reflective layer under the retina which allows incoming light that is not absorbed by the retina to be reflected and interact with the photoreceptor cells a second time. The tapetum lucidum allows felines to have superior night vision, but in the mfERG, the excess infrared light, which the fundus

imagining system uses to illuminate the retina, was reflected back to the camera, resulting in a loss of dynamic range and no fundus image. To solve this problem, we tried multiple LED sources with different wavelengths, which all failed. We also tried to use the OCT machine to image the retina, and without moving the animal's head to replace the OCT with the mfERG machine. However, since it was impossible to accurately show the position of the hexagons in relation to the detachment, and to image the same area with each subsequent ERG test, we were forced to use the full field ERG protocol. Consequently, we did not see a significant difference between XIAP and GFP treated animals, although there was a trend that the XIAP treated animals had higher waveforms compared to the GFP group.

Despite the limitations outlined above, a large animal study such as this is very important for the pre-clinical characterization of XIAP neuroprotection in the retina. It is noteworthy, however, that these studies provide important proof-of-principle for XIAP efficacy, but the gene therapy approach described here would not be suitable for the treatment of retinal detachment in the clinic. Since a detachment often occurs without warning, a therapy that quickly delivers anti-apoptotic agents to the retina would be ideal. In contrast, viral delivery of a transgene requires approximately approximately 7 days before expression is robust. Even with recent advances in the generation of self-complementary AAVs, the speed of transgene delivery would not be sufficient to preempt the rapid damage induced by a retinal detachment. As a result, alternative strategies for rapid delivery of XIAP to the retina are warranted. This need led to the studies in Chapter 5 of the thesis, where we examined the ability of biodegradable chitosan microparticles to deliver proteins directly to the retina. Chitosan is a natural

biocompatible and biodegradable polymer derived from crustaceans (Buranachai et al., 2010). We encapsulated EGFP protein into the microparticles and studied the release kinetics and the biocompatibility of the chitosan microparticles, with a future goal of encapsulating XIAP protein, and using it to treat acute insults in the retina.

Not surprisingly, the results obtained with the microparticles indicated that the concentration administered both *in vitro* and *in vivo* impacted the health of the surrounding cells. We found that lower concentrations (0.5mg/mL and 1.0mg/mL) of microparticles did not influence cell viability *in vitro* or *in vivo*, whereas the higher concentration (10mg/mL) induced cell death in 661W mouse photoreceptor cells and within the retina (confirmed by reductions in the amplitude of the full field ERG). Furthermore, irrespective of concentration, histological sections showed that areas where microparticles clumped together produced malformation/rosetting of the retina, and areas where the particles did not aggregate showed no changes in retinal architecture. These results suggest that the mucosal-adhesive nature of the chitosan microparticles impacts cell viability in culture by adhering to the surface of the cells. The 'sticky' particles also impact the subretinal injection procedure by adhering to the injection needle and requiring excess force to eject particles. Ultimately, the particles also affect the function, and histology of the retina (by adhering to one another and causing folding and rosettes in the retina).

After the publication of the fourth and final manuscript in this thesis, we evaluated alternative methods to rinse the particles once they were produced. The hypothesis was that we could possibly reduce the adherent properties of the particles. Interestingly, we found that washing the particles with distilled water instead of PBS

significantly reduced the ability of the particles to adhere to one another. We tested the high concentration (10mg/mL) of this new formulation in an *in vitro* cell death assay, and assessed the adhesive properties of the microparticles via immunofluorescence. There was no cell death after 24 and 48 hours in culture. Interestingly, despite fixing the cells treated with the microparticles for 48 hours, the particles all washed away during the staining process (Appendix B), further stressing their reduction in adhesive properties. Evidently, even small changes in the formulation process can affect the properties of the microparticles.

As stated in the manuscript, it is difficult to determine whether the *in vivo* toxic effects of microparticles was a function of their chemical nature (adhesivity) or due to the difficulties with injecting the adhesive particles, since slightly more force may have been used to eject the particles from the needle. Future studies can assess whether the new, less adhesive formulation can cause the microparticles to disperse within the confined space of the sub-retina, or if they will continue to aggregate. Furthermore, this new formulation can also be employed to encapsulate XIAP protein for future retinal detachment studies.

Altogether, the results presented in this thesis clearly show the potential of XIAP therapy in both chronic and acute forms of retinal degeneration. Future research in the laboratory will build on these studies and work to bring XIAP therapy closer to clinical trials.

REFERENCES

Abu-Amero, K. (2011). Leber′s hereditary optic neuropathy: The mitochondrial connection revisited. Middle East Afr. J. Ophthalmol. *18*, 17.

Acland, G.M., Aguirre, G.D., Ray, J., Zhang, Q., Aleman, T.S., Cideciyan, A.V., Pearce-Kelling, S.E., Anand, V., Zeng, Y., Maguire, A.M., et al. (2001). Gene therapy restores vision in a canine model of childhood blindness. Nat. Genet. *28*, 92–95.

Acland, G.M., Aguirre, G.D., Bennett, J., Aleman, T.S., Cideciyan, A.V., Bennicelli, J., Dejneka, N.S., Pearce-Kelling, S.E., Maguire, A.M., Palczewski, K., et al. (2005). Long-term restoration of rod and cone vision by single dose rAAV-mediated gene transfer to the retina in a canine model of childhood blindness. Mol. Ther. J. Am. Soc. Gene Ther. *12*, 1072–1082.

Adams, J.M., and Cory, S. (2001). Life-or-death decisions by the Bcl-2 protein family. Trends Biochem. Sci. *26*, 61–66.

Aiedeh, K., Gianasi, E., Orienti, I., and Zecchi, V. (1997). Chitosan microcapsules as controlled release systems for insulin. J. Microencapsul. *14*, 567–576.

Al-Enezi, M., Al-Saleh, H., and Nasser, M. (2008). Mitochondrial Disorders with Significant Ophthalmic Manifestations. Middle East Afr. J. Ophthalmol. *15*, 81–86.

Al-Ubaidi, M.R. (2014). RGC-5: ARE THEY REALLY 661W? THE SAGA CONTINUES. Exp. Eye Res. *119*, 115.

Al-Ubaidi, M.R., Matsumoto, H., Kurono, S., and Singh, A. (2008). Proteomics profiling of the cone photoreceptor cell line, 661W. Adv. Exp. Med. Biol. *613*, 301–311.

Alvarez-Saavedra, M., De Repentigny, Y., Lagali, P.S., Raghu Ram, E.V.S., Yan, K., Hashem, E., Ivanochko, D., Huh, M.S., Yang, D., Mears, A.J., et al. (2014). Snf2h-mediated chromatin organization and histone H1 dynamics govern cerebellar morphogenesis and neural maturation. Nat. Commun. *5*, 4181.

Arroyo, J.G., Yang, L., Bula, D., and Chen, D.F. (2005). Photoreceptor apoptosis in human retinal detachment. Am. J. Ophthalmol. *139*, 605–610.

Artursson, P., Lindmark, T., Davis, S.S., and Illum, L. (1994). Effect of chitosan on the permeability of monolayers of intestinal epithelial cells (Caco-2). Pharm. Res. *11*, 1358–1361.

Bainbridge, J.W.B., Smith, A.J., Barker, S.S., Robbie, S., Henderson, R., Balaggan, K., Viswanathan, A., Holder, G.E., Stockman, A., Tyler, N., et al. (2008a). Effect of gene therapy on visual function in Leber's congenital amaurosis. N. Engl. J. Med. *358*, 2231–2239.

Bainbridge, J.W.B., Smith, A.J., Barker, S.S., Robbie, S., Henderson, R., Balaggan, K., Viswanathan, A., Holder, G.E., Stockman, A., Tyler, N., et al. (2008b). Effect of Gene Therapy on Visual Function in Leber's Congenital Amaurosis. N. Engl. J. Med. *358*, 2231–2239.

Bainbridge, J.W.B., Mehat, M.S., Sundaram, V., Robbie, S.J., Barker, S.E., Ripamonti, C., Georgiadis, A., Mowat, F.M., Beattie, S.G., Gardner, P.J., et al. (2015). Long-term effect of gene therapy on Leber's congenital amaurosis. N. Engl. J. Med. *372*, 1887–1897.

Baracca, A., Solaini, G., Sgarbi, G., Lenaz, G., Baruzzi, A., Schapira, A.H.V., Martinuzzi, A., and Carelli, V. (2005). Severe impairment of complex I-driven adenosine triphosphate synthesis in leber hereditary optic neuropathy cybrids. Arch. Neurol. *62*, 730–736.

Başaran, E., and Yazan, Y. (2012). Ocular application of chitosan. Expert Opin. Drug Deliv. *9*, 701–712.

Bauler, L.D., Duckett, C.S., and O'Riordan, M.X.D. (2008). XIAP regulates cytosol-specific innate immunity to Listeria infection. PLoS Pathog. *4*, e1000142.

Bennett, J. (2003). Immune response following intraocular delivery of recombinant viral vectors. Gene Ther. *10*, 977–982.

Bennett, J., Wellman, J., Marshall, K.A., McCague, S., Ashtari, M., DiStefano-Pappas, J., Elci, O.U., Chung, D.C., Sun, J., Wright, J.F., et al. (2016). Safety and durability of effect of contralateral-eye administration of AAV2 gene therapy in patients with childhood-onset blindness caused by RPE65 mutations: a follow-on phase 1 trial. The Lancet *388*, 661–672.

Bennicelli, J., Wright, J.F., Komaromy, A., Jacobs, J.B., Hauck, B., Zelenaia, O., Mingozzi, F., Hui, D., Chung, D., Rex, T.S., et al. (2008). Reversal of Blindness in Animal Models of Leber Congenital Amaurosis Using Optimized AAV2-mediated Gene Transfer. Mol. Ther. *16*, 458–465.

Berghe, T.V., Vanlangenakker, N., Parthoens, E., Deckers, W., Devos, M., Festjens, N., Guerin, C.J., Brunk, U.T., Declercq, W., and Vandenabeele, P. (2010). Necroptosis, necrosis and secondary necrosis converge on similar cellular disintegration features. Cell Death Differ. *17*, 922–930.

Berghe, T.V., Linkermann, A., Jouan-Lanhouet, S., Walczak, H., and Vandenabeele, P. (2014). Regulated necrosis: the expanding network of non-apoptotic cell death pathways. Nat. Rev. Mol. Cell Biol. *15*, 135–147.

Berthelet, J., and Dubrez, L. (2013). Regulation of Apoptosis by Inhibitors of Apoptosis (IAPs). Cells *2*, 163–187.

Bertrand, M.J.M., and Vandenabeele, P. (2011). The Ripoptosome: Death Decision in the Cytosol. Mol. Cell *43*, 323–325.

Bertrand, M.J.M., Milutinovic, S., Dickson, K.M., Ho, W.C., Boudreault, A., Durkin, J., Gillard, J.W., Jaquith, J.B., Morris, S.J., and Barker, P.A. (2008). cIAP1 and cIAP2 facilitate cancer cell survival by functioning as E3 ligases that promote RIP1 ubiquitination. Mol. Cell *30*, 689–700.

Bhatia, B., Singhal, S., Jayaram, H., Khaw, P.T., and Limb, G.A. (2010). Adult Retinal Stem Cells Revisited. Open Ophthalmol. J. *4*, 30–38.

Bo, Q., Ma, S., Han, Q., Wang, F.E., Li, X., and Zhang, Y. (2015). Role of autophagy in photoreceptor cell survival and death. Crit. Rev. Eukaryot. Gene Expr. *25*, 23–32.

Boye, S.E., Boye, S.L., Lewin, A.S., and Hauswirth, W.W. (2013). A Comprehensive Review of Retinal Gene Therapy. Mol. Ther. *21*, 509–519.

Bragadóttir, R., and Narfström, K. (2003). Lens sparing pars plana vitrectomy and retinal transplantation in cats. Vet. Ophthalmol. *6*, 135–139.

Buch, P.K., Bainbridge, J.W., and Ali, R.R. (2008). AAV-mediated gene therapy for retinal disorders: from mouse to man. Gene Ther. *15*, 849–857.

Bull, N.D., Johnson, T.V., Welsapar, G., DeKorver, N.W., Tomarev, S.I., and Martin, K.R. (2011). Use of an Adult Rat Retinal Explant Model for Screening of Potential Retinal Ganglion Cell Neuroprotective Therapies. Invest. Ophthalmol. Vis. Sci. *52*, 3309–3320.

Buranachai, T., Praphairaksit, N., and Muangsin, N. (2010). Chitosan/polyethylene glycol beads crosslinked with tripolyphosphate and glutaraldehyde for gastrointestinal drug delivery. AAPS PharmSciTech *11*, 1128–1137.

Caffé, A.R., Ahuja, P., Holmqvist, B., Azadi, S., Forsell, J., Holmqvist, I., Söderpalm, A.K., and van Veen, T. (2001). Mouse retina explants after long-term culture in serum free medium. J. Chem. Neuroanat. *22*, 263–273.

Calija, B., Cekić, N., Savić, S., Krajišnik, D., Daniels, R., and Milić, J. (2011). An investigation of formulation factors affecting feasibility of alginate-chitosan microparticles for oral delivery of naproxen. Arch. Pharm. Res. *34*, 919–929.

Calvo, P., Remu[illegible]n-L[illegible]pez, C., Vila-Jato, J.L., and Alonso, M.J. (1997). Novel hydrophilic chitosan-polyethylene oxide nanoparticles as protein carriers. J. Appl. Polym. Sci. *63*, 125–132.

Carelli, V., Ross-Cisneros, F.N., and Sadun, A.A. (2002). Optic nerve degeneration and mitochondrial dysfunction: genetic and acquired optic neuropathies. Neurochem. Int. *40*, 573–584.

Carelli, V., Ross-Cisneros, F.N., and Sadun, A.A. (2004a). Mitochondrial dysfunction as a cause of optic neuropathies. Prog. Retin. Eye Res. *23*, 53–89.

Carelli, V., Rugolo, M., Sgarbi, G., Ghelli, A., Zanna, C., Baracca, A., Lenaz, G., Napoli, E., Martinuzzi, A., and Solaini, G. (2004b). Bioenergetics shapes cellular death pathways in Leber's hereditary optic neuropathy: a model of mitochondrial neurodegeneration. Biochim. Biophys. Acta *1658*, 172–179.

Carelli, V., Morgia, C.L., Valentino, M.L., Rizzo, G., Carbonelli, M., Negri, A.M.D., Sadun, F., Carta, A., Guerriero, S., Simonelli, F., et al. (2011). Idebenone Treatment In Leber's Hereditary Optic Neuropathy. Brain *134*, e188–e188.

Carvalho, L.S., and Vandenberghe, L.H. (2015). Promising and delivering gene therapies for vision loss. Vision Res. *111, Part B*, 124–133.

Cederlund, M., Ghosh, F., Arnér, K., Andréasson, S., and Akerström, B. (2013). Vitreous levels of oxidative stress biomarkers and the radical-scavenger α1-microglobulin/A1M in human rhegmatogenous retinal detachment. Graefes Arch. Clin. Exp. Ophthalmol. Albrecht Von Graefes Arch. Für Klin. Exp. Ophthalmol. *251*, 725–732.

Chang, G.Q., Hao, Y., and Wong, F. (1993). Apoptosis: final common pathway of photoreceptor death in rd, rds, and rhodopsin mutant mice. Neuron *11*, 595–605.

Chaudhary, A.K., Yadav, N., Bhat, T.A., O'Malley, J., Kumar, S., and Chandra, D. (2015). A potential role of X-linked inhibitor of apoptosis protein in mitochondrial membrane permeabilization and its implication in cancer therapy. Drug Discov. Today.

Chen, A.C.-H., Arany, P.R., Huang, Y.-Y., Tomkinson, E.M., Sharma, S.K., Kharkwal, G.B., Saleem, T., Mooney, D., Yull, F.E., Blackwell, T.S., et al. (2011). Low-level laser therapy activates NF-kB via generation of reactive oxygen species in mouse embryonic fibroblasts. PloS One *6*, e22453.

Cheung, H.H., LaCasse, E.C., and Korneluk, R.G. (2006). X-linked inhibitor of apoptosis antagonism: strategies in cancer treatment. Clin. Cancer Res. Off. J. Am. Assoc. Cancer Res. *12*, 3238–3242.

Cheung, H.H., Plenchette, S., Kern, C.J., Mahoney, D.J., and Korneluk, R.G. (2008). The RING Domain of cIAP1 Mediates the Degradation of RING-bearing Inhibitor of Apoptosis Proteins by Distinct Pathways. Mol. Biol. Cell *19*, 2729–2740.

Chinskey, N.D., Zheng, Q.-D., and Zacks, D.N. (2014). Control of photoreceptor autophagy after retinal detachment: the switch from survival to death. Invest. Ophthalmol. Vis. Sci. *55*, 688–695.

Cideciyan, A.V., Aleman, T.S., Boye, S.L., Schwartz, S.B., Kaushal, S., Roman, A.J., Pang, J.-J., Sumaroka, A., Windsor, E.A.M., Wilson, J.M., et al. (2008). Human gene therapy for RPE65 isomerase deficiency activates the retinoid cycle of vision but with slow rod kinetics. Proc. Natl. Acad. Sci. U. S. A. *105*, 15112–15117.

Cideciyan, A.V., Hauswirth, W.W., Aleman, T.S., Kaushal, S., Schwartz, S.B., Boye, S.L., Windsor, E.A.M., Conlon, T.J., Sumaroka, A., Roman, A.J., et al. (2009a). Vision 1 year after gene therapy for Leber's congenital amaurosis. N. Engl. J. Med. *361*, 725–727.

Cideciyan, A.V., Hauswirth, W.W., Aleman, T.S., Kaushal, S., Schwartz, S.B., Boye, S.L., Windsor, E.A.M., Conlon, T.J., Sumaroka, A., Pang, J.-J., et al. (2009b). Human RPE65 gene therapy for Leber congenital amaurosis: persistence of early visual improvements and safety at 1 year. Hum. Gene Ther. *20*, 999–1004.

Cideciyan, A.V., Jacobson, S.G., Beltran, W.A., Sumaroka, A., Swider, M., Iwabe, S., Roman, A.J., Olivares, M.B., Schwartz, S.B., Komáromy, A.M., et al. (2013a). Human retinal gene therapy for Leber congenital amaurosis shows advancing retinal degeneration despite enduring visual improvement. Proc. Natl. Acad. Sci. *110*, E517–E525.

Cideciyan, A.V., Jacobson, S.G., Beltran, W.A., Sumaroka, A., Swider, M., Iwabe, S., Roman, A.J., Olivares, M.B., Schwartz, S.B., Komáromy, A.M., et al. (2013b). Human retinal gene therapy for Leber congenital amaurosis shows advancing retinal degeneration despite enduring visual improvement. Proc. Natl. Acad. Sci. U. S. A. *110*, E517–E525.

Cook, B., Lewis, G.P., Fisher, S.K., and Adler, R. (1995). Apoptotic photoreceptor degeneration in experimental retinal detachment. Invest. Ophthalmol. Vis. Sci. *36*, 990–996.

Corti, M., Elder, M., Falk, D., Lawson, L., Smith, B., Nayak, S., Conlon, T., Clément, N., Erger, K., Lavassani, E., et al. (2014). B-cell depletion is protective against anti-AAV capsid immune response: a human subject case study. Mol. Ther. — Methods Clin. Dev. *1*, 14033.

Creagh, E.M., Murphy, B.M., Duriez, P.J., Duckett, C.S., and Martin, S.J. (2004). Smac/Diablo antagonizes ubiquitin ligase activity of inhibitor of apoptosis proteins. J. Biol. Chem. *279*, 26906–26914.

Crescitelli, F. (1972). The Visual Cells and Visual Pigments of the Vertebrate Eye. In Photochemistry of Vision, H.J.A. Dartnall, ed. (Springer Berlin Heidelberg), pp. 245–363.

Cruz-Bermúdez, A., Vicente-Blanco, R.J., Hernández-Sierra, R., Montero, M., Alvarez, J., González Manrique, M., Blázquez, A., Martín, M.A., Ayuso, C., Garesse, R., et al. (2016). Functional Characterization of Three Concomitant MtDNA LHON Mutations Shows No Synergistic Effect on Mitochondrial Activity. PloS One *11*, e0146816.

Cullen, S.P., Henry, C.M., Kearney, C.J., Logue, S.E., Feoktistova, M., Tynan, G.A., Lavelle, E.C., Leverkus, M., and Martin, S.J. (2013). Fas/CD95-induced chemokines can serve as "find-me" signals for apoptotic cells. Mol. Cell *49*, 1034–1048.

Dalkara, D., and Sahel, J.-A. (2014). Gene therapy for inherited retinal degenerations. C. R. Biol. *337*, 185–192.

Degli Esposti, M., Carelli, V., Ghelli, A., Ratta, M., Crimi, M., Sangiorgi, S., Montagna, P., Lenaz, G., Lugaresi, E., and Cortelli, P. (1994). Functional alterations of the mitochondrially encoded ND4 subunit associated with Leber's hereditary optic neuropathy. FEBS Lett. *352*, 375–379.

Dong, K., Zhu, Z.-C., Wang, F.-H., Ke, G.-J., Yu, Z., and Xu, X. (2014). Activation of autophagy in photoreceptor necroptosis after experimental retinal detachment. Int. J. Ophthalmol. *7*, 745–752.

Doonan, F., and Cotter, T.G. (2004). Apoptosis: a potential therapeutic target for retinal degenerations. Curr. Neurovasc. Res. *1*, 41–53.

Dyer, M.A., and Cepko, C.L. (2001). Regulating proliferation during retinal development. Nat. Rev. Neurosci. *2*, 333–342.

Erickson, P.A., Fisher, S.K., Anderson, D.H., Stern, W.H., and Borgula, G.A. (1983). Retinal detachment in the cat: the outer nuclear and outer plexiform layers. Invest. Ophthalmol. Vis. Sci. *24*, 927–942.

Ezzeddine, Z.D., Yang, X., DeChiara, T., Yancopoulos, G., and Cepko, C.L. (1997). Postmitotic cells fated to become rod photoreceptors can be respecified by CNTF treatment of the retina. Dev. Camb. Engl. *124*, 1055–1067.

Farrar, G.J., Chadderton, N., Kenna, P.F., and Millington-Ward, S. (2013). Mitochondrial disorders: aetiologies, models systems, and candidate therapies. Trends Genet. TIG *29*, 488–497.

Feoktistova, M., Geserick, P., Kellert, B., Dimitrova, D.P., Langlais, C., Hupe, M., Cain, K., MacFarlane, M., Häcker, G., and Leverkus, M. (2011). cIAPs Block Ripoptosome Formation, a RIP1/Caspase-8 Containing Intracellular Cell Death Complex Differentially Regulated by cFLIP Isoforms. Mol. Cell *43*, 449–463.

Feuer, W.J., Schiffman, J.C., Davis, J.L., Porciatti, V., Gonzalez, P., Koilkonda, R.D., Yuan, H., Lalwani, A., Lam, B.L., and Guy, J. (2015). Gene Therapy for Leber Hereditary Optic Neuropathy: Initial Results. Ophthalmology.

Fisher, S.K., and Lewis, G.P. (2003). Müller cell and neuronal remodeling in retinal detachment and reattachment and their potential consequences for visual recovery: a review and reconsideration of recent data. Vision Res. *43*, 887–897.

Fitzgerald, J.B., Malykhina, A.P., Al-Ubaidi, M.R., and Ding, X.-Q. (2008). Functional expression of cone cyclic nucleotide-gated channel in cone photoreceptor-derived 661W cells. Adv. Exp. Med. Biol. *613*, 327–334.

de la Fuente, M., Seijo, B., and Alonso, M.J. (2008). Novel hyaluronic acid-chitosan nanoparticles for ocular gene therapy. Invest. Ophthalmol. Vis. Sci. *49*, 2016–2024.

Fulda, S., and Vucic, D. (2012). Targeting IAP proteins for therapeutic intervention in cancer. Nat. Rev. Drug Discov. *11*, 109–124.

Galbán, S., and Duckett, C.S. (2010). XIAP as a ubiquitin ligase in cellular signaling. Cell Death Differ. *17*, 54–60.

Gentle, I.E., Wong, W.W.-L., Evans, J.M., Bankovacki, A., Cook, W.D., Khan, N.R., Nachbur, U., Rickard, J., Anderton, H., Moulin, M., et al. (2011). In TNF-stimulated cells, RIPK1 promotes cell survival by stabilizing TRAF2 and cIAP1, which limits induction of non-canonical NF-kappaB and activation of caspase-8. J. Biol. Chem. *286*, 13282–13291.

Gingras, M., Paradis, I., and Berthod, F. (2003). Nerve regeneration in a collagen-chitosan tissue-engineered skin transplanted on nude mice. Biomaterials *24*, 1653–1661.

Giordano, C., Montopoli, M., Perli, E., Orlandi, M., Fantin, M., Ross-Cisneros, F.N., Caparrotta, L., Martinuzzi, A., Ragazzi, E., Ghelli, A., et al. (2011). Oestrogens ameliorate mitochondrial dysfunction in Leber's hereditary optic neuropathy. Brain J. Neurol. *134*, 220–234.

Gómez-Vicente, V., Donovan, M., and Cotter, T.G. (2005). Multiple death pathways in retina-derived 661W cells following growth factor deprivation: crosstalk between caspases and calpains. Cell Death Differ. *12*, 796–804.

Grozdanov, V., Müller, A., Sengottuvel, V., Leibinger, M., and Fischer, D. (2010). A method for preparing primary retinal cell cultures for evaluating the neuroprotective and neuritogenic effect of factors on axotomized mature CNS neurons. Curr. Protoc. Neurosci. Editor. Board Jacqueline N Crawley Al *Chapter 3*, Unit3.22.

Guang Liu, W., and De Yao, K. (2002). Chitosan and its derivatives--a promising non-viral vector for gene transfection. J. Control. Release Off. J. Control. Release Soc. *83*, 1–11.

Gueven, N. (2014). Optic Neurodegeneration: Time to Act. Biol. Med. *1*, 1–6.

Guy, J., Qi, X., Koilkonda, R.D., Arguello, T., Chou, T.-H., Ruggeri, M., Porciatti, V., Lewin, A.S., and Hauswirth, W.W. (2009). Efficiency and Safety of AAV-Mediated Gene Delivery of the Human ND4 Complex I Subunit in the Mouse Visual System. Invest. Ophthalmol. Vis. Sci. *50*, 4205–4214.

Gyrd-Hansen, M., Darding, M., Miasari, M., Santoro, M.M., Zender, L., Xue, W., Tenev, T., da Fonseca, P.C.A., Zvelebil, M., Bujnicki, J.M., et al. (2008). IAPs contain an evolutionarily conserved ubiquitin-binding domain that regulates NF-κB as well as cell survival and oncogenesis. Nat. Cell Biol. *10*, 1309–1317.

Hamacher-Brady, A., and Brady, N.R. (2015). Bax/Bak-dependent, Drp1-independent Targeting of X-linked Inhibitor of Apoptosis Protein (XIAP) into Inner Mitochondrial

Compartments Counteracts Smac/DIABLO-dependent Effector Caspase Activation. J. Biol. Chem. *290*, 22005–22018.

Hamacher-Brady, A., Choe, S.C., Krijnse-Locker, J., and Brady, N.R. (2014). Intramitochondrial recruitment of endolysosomes mediates Smac degradation and constitutes a novel intrinsic apoptosis antagonizing function of XIAP E3 ligase. Cell Death Differ. *21*, 1862–1876.

Hauswirth, W.W., Lewin, A.S., Zolotukhin, S., and Muzyczka, N. (2000). Production and purification of recombinant adeno-associated virus. Methods Enzymol. *316*, 743–761.

Hauswirth, W.W., Aleman, T.S., Kaushal, S., Cideciyan, A.V., Schwartz, S.B., Wang, L., Conlon, T.J., Boye, S.L., Flotte, T.R., Byrne, B.J., et al. (2008a). Treatment of Leber Congenital Amaurosis Due to *RPE65* Mutations by Ocular Subretinal Injection of Adeno-Associated Virus Gene Vector: Short-Term Results of a Phase I Trial. Hum. Gene Ther. *19*, 979–990.

Hauswirth, W.W., Aleman, T.S., Kaushal, S., Cideciyan, A.V., Schwartz, S.B., Wang, L., Conlon, T.J., Boye, S.L., Flotte, T.R., Byrne, B.J., et al. (2008b). Treatment of leber congenital amaurosis due to RPE65 mutations by ocular subretinal injection of adeno-associated virus gene vector: short-term results of a phase I trial. Hum. Gene Ther. *19*, 979–990.

He, C., and Klionsky, D.J. (2009). Regulation Mechanisms and Signaling Pathways of Autophagy. Annu. Rev. Genet. *43*, 67–93.

Hofer-Warbinek, R., Schmid, J.A., Stehlik, C., Binder, B.R., Lipp, J., and de Martin, R. (2000). Activation of NF-kappa B by XIAP, the X chromosome-linked inhibitor of apoptosis, in endothelial cells involves TAK1. J. Biol. Chem. *275*, 22064–22068.

Holcik, M., and Korneluk, R.G. (2001). XIAP, the guardian angel. Nat. Rev. Mol. Cell Biol. *2*, 550–556.

Holder, G.E. (2001). Pattern Electroretinography (PERG) and an Integrated Approach to Visual Pathway Diagnosis. Prog. Retin. Eye Res. *20*, 531–561.

Howell, N. (1998). Leber hereditary optic neuropathy: respiratory chain dysfunction and degeneration of the optic nerve. Vision Res. *38*, 1495–1504.

Hu, Y.-L., Qi, W., Han, F., Shao, J.-Z., and Gao, J.-Q. (2011). Toxicity evaluation of biodegradable chitosan nanoparticles using a zebrafish embryo model. Int. J. Nanomedicine *6*, 3351–3359.

Huang, W., Li, G., Qiu, J., Gonzalez, P., and Challa, P. (2013). Protective effects of resveratrol in experimental retinal detachment. PloS One *8*, e75735.

Huckfeldt, R.M., and Vavvas, D.G. (2013). Neuroprotection for retinal detachment. Int. Ophthalmol. Clin. *53*, 105–117.

Hudson, G., Keers, S., Yu Wai Man, P., Griffiths, P., Huoponen, K., Savontaus, M.-L., Nikoskelainen, E., Zeviani, M., Carrara, F., Horvath, R., et al. (2005). Identification of an X-chromosomal locus and haplotype modulating the phenotype of a mitochondrial DNA disorder. Am. J. Hum. Genet. *77*, 1086–1091.

Hunter, A.M., LaCasse, E.C., and Korneluk, R.G. (2007). The inhibitors of apoptosis (IAPs) as cancer targets. Apoptosis Int. J. Program. Cell Death *12*, 1543–1568.

Igci, M., Baysan, M., Yigiter, R., Ulasli, M., Geyik, S., Bayraktar, R., Bozgeyik, İ., Bozgeyik, E., Bayram, A., and Cakmak, E.A. (2016). Gene expression profiles of autophagy-related genes in multiple sclerosis. Gene *588*, 38–46.

Illum, L., Farraj, N.F., and Davis, S.S. (1994). Chitosan as a novel nasal delivery system for peptide drugs. Pharm. Res. *11*, 1186–1189.

Imre, G., Larisch, S., and Rajalingam, K. (2011). Ripoptosome: a novel IAP-regulated cell death-signalling platform. J. Mol. Cell Biol. *3*, 324–326.

Jacobson, S.G., Cideciyan, A.V., Ratnakaram, R., Heon, E., Schwartz, S.B., Roman, A.J., Peden, M.C., Aleman, T.S., Boye, S.L., Sumaroka, A., et al. (2012). Gene therapy for leber congenital amaurosis caused by RPE65 mutations: safety and efficacy in 15 children and adults followed up to 3 years. Arch. Ophthalmol. Chic. Ill 1960 *130*, 9–24.

Jacobson, S.G., Cideciyan, A.V., Roman, A.J., Sumaroka, A., Schwartz, S.B., Heon, E., and Hauswirth, W.W. (2015). Improvement and decline in vision with gene therapy in childhood blindness. N. Engl. J. Med. *372*, 1920–1926.

Jalali, S. (2003). Retinal Detachment. Community Eye Health *16*, 25–26.

Kaur, S., Wang, F., Venkatraman, M., and Arsura, M. (2005). X-linked inhibitor of apoptosis (XIAP) inhibits c-Jun N-terminal kinase 1 (JNK1) activation by transforming growth factor beta1 (TGF-beta1) through ubiquitin-mediated proteosomal degradation of the TGF-beta1-activated kinase 1 (TAK1). J. Biol. Chem. *280*, 38599–38608.

Kirches, E. (2011). LHON: Mitochondrial Mutations and More. Curr. Genomics *12*, 44–54.

Kirkman, M.A., Yu-Wai-Man, P., Korsten, A., Leonhardt, M., Dimitriadis, K., De Coo, I.F., Klopstock, T., and Chinnery, P.F. (2009). Gene-environment interactions in Leber hereditary optic neuropathy. Brain J. Neurol. *132*, 2317–2326.

Klopstock, T., Yu-Wai-Man, P., Dimitriadis, K., Rouleau, J., Heck, S., Bailie, M., Atawan, A., Chattopadhyay, S., Schubert, M., Garip, A., et al. (2011). A randomized placebo-controlled trial of idebenone in Leber's hereditary optic neuropathy. Brain awr170.

Koilkonda, R., Tse, D., Hauswirth, W., Chiodo, V., Boye, S., Neuringer, M., Stout, T., and Guy, J. (2013). Mitochondrial Gene Therapy for G11778A LHON: Safety of Human

ND4 in Nonhuman Primates and Expression in Ex Vivo Human Eyes. Invest. Ophthalmol. Vis. Sci. *54*, 2738–2738.

Koilkonda, R., Yu, H., Talla, V., Porciatti, V., Feuer, W.J., Hauswirth, W.W., Chiodo, V., Erger, K.E., Boye, S.L., Lewin, A.S., et al. (2014). LHON gene therapy vector prevents visual loss and optic neuropathy induced by G11778A mutant mitochondrial DNA: biodistribution and toxicology profile. Invest. Ophthalmol. Vis. Sci. *55*, 7739–7753.

Koilkonda, R.D., Chou, T.-H., Porciatti, V., Hauswirth, W.W., and Guy, J. (2010). Induction of Rapid and Highly Efficient Expression of the Human ND4 Complex I Subunit in the Mouse Visual System by Self-complementary Adeno-Associated Virus. Arch. Ophthalmol. *128*, 876–883.

Koilkonda RD, Yu H, Chou T, and et al (2014). SAfety and effects of the vector for the leber hereditary optic neuropathy gene therapy clinical trial. JAMA Ophthalmol. *132*, 409–420.

Kotterman, M.A., Yin, L., Strazzeri, J.M., Flannery, J.G., Merigan, W.H., and Schaffer, D.V. (2015). Antibody Neutralization Poses a Barrier to Intravitreal Adeno-Associated Viral Vector Gene Delivery to Non-Human Primates. Gene Ther. *22*, 116–126.

Kovács, G.G., Höftberger, R., Majtényi, K., Horváth, R., Barsi, P., Komoly, S., Lassmann, H., Budka, H., and Jakab, G. (2005). Neuropathology of white matter disease in Leber's hereditary optic neuropathy. Brain J. Neurol. *128*, 35–41.

Kratz, G., Arnander, C., Swedenborg, J., Back, M., Falk, C., Gouda, I., and Larm, O. (1997). Heparin-chitosan complexes stimulate wound healing in human skin. Scand. J. Plast. Reconstr. Surg. Hand Surg. Nord. Plast. Foren. Nord. Klubb Handkirurgi *31*, 119–123.

Krishnamoorthy, R.R., Crawford, M.J., Chaturvedi, M.M., Jain, S.K., Aggarwal, B.B., Al-Ubaidi, M.R., and Agarwal, N. (1999). Photo-oxidative stress down-modulates the activity of nuclear factor-kappaB via involvement of caspase-1, leading to apoptosis of photoreceptor cells. J. Biol. Chem. *274*, 3734–3743.

Krishnamoorthy, R.R., Agarwal, P., Prasanna, G., Vopat, K., Lambert, W., Sheedlo, H.J., Pang, I.H., Shade, D., Wordinger, R.J., Yorio, T., et al. (2001). Characterization of a transformed rat retinal ganglion cell line. Brain Res. Mol. Brain Res. *86*, 1–12.

Krishnamoorthy, R.R., Clark, A.F., Daudt, D., Vishwanatha, J.K., and Yorio, T. (2013). A forensic path to RGC-5 cell line identification: lessons learned. Invest. Ophthalmol. Vis. Sci. *54*, 5712–5719.

Lam, B.L., Feuer, W.J., Schiffman, J.C., Porciatti, V., Vandenbroucke, R., Rosa, P.R., Gregori, G., and Guy, J. (2014). Trial end points and natural history in patients with G11778A Leber hereditary optic neuropathy : preparation for gene therapy clinical trial. JAMA Ophthalmol. *132*, 428–436.

Lamba, D., Karl, M., and Reh, T. (2008). Neural regeneration and cell replacement: a view from the eye. Cell Stem Cell *2*, 538–549.

Larsson, J., Bauer, B., and Andréasson, S. (2000). The 30-Hz flicker cone ERG for monitoring the early course of central retinal vein occlusion. Acta Ophthalmol. Scand. *78*, 187–190.

Lawlor, K.E., Khan, N., Mildenhall, A., Gerlic, M., Croker, B.A., D'Cruz, A.A., Hall, C., Kaur Spall, S., Anderton, H., Masters, S.L., et al. (2015). RIPK3 promotes cell death and NLRP3 inflammasome activation in the absence of MLKL. Nat. Commun. *6*, 6282.

Lee, M., Nah, J.W., Kwon, Y., Koh, J.J., Ko, K.S., and Kim, S.W. (2001). Water-soluble and low molecular weight chitosan-based plasmid DNA delivery. Pharm. Res. *18*, 427–431.

Lenhausen, A.M., Wilkinson, A.S., Lewis, E.M., Dailey, K.M., Scott, A.J., Khan, S., and Wilkinson, J.C. (2016). Apoptosis Inducing Factor Binding Protein PGAM5 Triggers Mitophagic Cell Death That Is Inhibited by the Ubiquitin Ligase Activity of X-Linked Inhibitor of Apoptosis. Biochemistry (Mosc.) *55*, 3285–3302.

Leonard, K.C., Petrin, D., Coupland, S.G., Baker, A.N., Leonard, B.C., LaCasse, E.C., Hauswirth, W.W., Korneluk, R.G., and Tsilfidis, C. (2007). XIAP Protection of Photoreceptors in Animal Models of Retinitis Pigmentosa. PLoS ONE *2*.

Levitan, B., and Buchsbaum, G. (1993). Signal sampling and propagation through multiple cell layers in the retina: modeling and analysis with multirate filtering. J. Opt. Soc. Am. A *10*, 1463–1480.

Lewis, G.P., and Fisher, S.K. (2000). Müller cell outgrowth after retinal detachment: association with cone photoreceptors. Invest. Ophthalmol. Vis. Sci. *41*, 1542–1545.

Li, Q., Miller, R., Han, P.-Y., Pang, J., Dinculescu, A., Chiodo, V., and Hauswirth, W.W. (2008). Intraocular route of AAV2 vector administration defines humoral immune response and therapeutic potential.

Lin, F., Ghislat, G., Luo, S., Renna, M., Siddiqi, F., and Rubinsztein, D.C. (2015). XIAP and cIAP1 amplifications induce Beclin 1-dependent autophagy through NFκB activation. Hum. Mol. Genet. *24*, 2899–2913.

Lin, S.-L., Shiu, W.-C., Liu, P.-C., Cheng, F.-P., Lin, Y.-C., and Wang, W.-S. (2009). The Effects of Different Anesthetic Agents on Short Electroretinography Protocol in Dogs. J. Vet. Med. Sci. *71*, 763–768.

Liston, P., Fong, W.G., and Korneluk, R.G. (2003). The inhibitors of apoptosis: there is more to life than Bcl2. Oncogene *22*, 8568–8580.

Liu, L., Sakai, T., Sano, N., and Fukui, K. (2004). Nucling mediates apoptosis by inhibiting expression of galectin-3 through interference with nuclear factor kappaB signalling. Biochem. J. *380*, 31–41.

Livesey, F.J., and Cepko, C.L. (2001). Vertebrate neural cell-fate determination: Lessons from the retina. Nat. Rev. Neurosci. *2*, 109–118.

van Loo, G., van Gurp, M., Depuydt, B., Srinivasula, S.M., Rodriguez, I., Alnemri, E.S., Gevaert, K., Vandekerckhove, J., Declercq, W., and Vandenabeele, P. (2002). The serine protease Omi/HtrA2 is released from mitochondria during apoptosis. Omi interacts with caspase-inhibitor XIAP and induces enhanced caspase activity. Cell Death Differ. *9*, 20–26.

Lu, M., Lin, S.-C., Huang, Y., Kang, Y.J., Rich, R., Lo, Y.-C., Myszka, D., Han, J., and Wu, H. (2007). XIAP induces NF-kappaB activation via the BIR1/TAB1 interaction and BIR1 dimerization. Mol. Cell *26*, 689–702.

Madihally, S.V., and Matthew, H.W. (1999). Porous chitosan scaffolds for tissue engineering. Biomaterials *20*, 1133–1142.

Mafei, L., and Fiorentini, A. (1981). Electroretinographic responses to alternating gratings before and after section of the optic nerve. Science *211*, 953–955.

Maguire, A.M., Simonelli, F., Pierce, E.A., Pugh, E.N.J., Mingozzi, F., Bennicelli, J., Banfi, S., Marshall, K.A., Testa, F., Surace, E.M., et al. (2008). Safety and Efficacy of Gene Transfer for Leber's Congenital Amaurosis. N. Engl. J. Med. *358*, 2240–2248.

Maguire, A.M., High, K.A., Auricchio, A., Wright, J.F., Pierce, E.A., Testa, F., Mingozzi, F., Bennicelli, J.L., Ying, G., Rossi, S., et al. (2009). Age-dependent effects of RPE65 gene therapy for Leber's congenital amaurosis: a phase 1 dose-escalation trial. Lancet Lond. Engl. *374*, 1597–1605.

Man, P.Y.W., Griffiths, P.G., Brown, D.T., Howell, N., Turnbull, D.M., and Chinnery, P.F. (2003). The Epidemiology of Leber Hereditary Optic Neuropathy in the North East of England. Am. J. Hum. Genet. *72*, 333–339.

Marieb, E. (2007). THE SPECIAL SENSES. Human Anatomy and Physiology. (San Francisco: Pearson).

Masat, E., Pavani, G., and Mingozzi, F. (2013). Humoral immunity to AAV vectors in gene therapy: challenges and potential solutions. Discov. Med. *15*, 379–389.

Mascialino, B., Leinonen, M., and Meier, T. (2011). Meta-analysis of the prevalence of Leber hereditary optic neuropathy mtDNA mutations in Europe. Eur. J. Ophthalmol. *22*, 461–465.

Matsumoto, H., Miller, J.W., and Vavvas, D.G. (2013). Retinal detachment model in rodents by subretinal injection of sodium hyaluronate. J. Vis. Exp. JoVE.

Matsumoto, H., Kataoka, K., Tsoka, P., Connor, K.M., Miller, J.W., and Vavvas, D.G. (2014). Strain Difference in Photoreceptor Cell Death After Retinal Detachment in Mice. Invest. Ophthalmol. Vis. Sci. *55*, 4165–4174.

McKinnon, S.J., Lehman, D.M., Tahzib, N.G., Ransom, N.L., Reitsamer, H.A., Liston, P., LaCasse, E., Li, Q., Korneluk, R.G., and Hauswirth, W.W. (2002). Baculoviral IAP repeat-containing-4 protects optic nerve axons in a rat glaucoma model. Mol. Ther. J. Am. Soc. Gene Ther. *5*, 780–787.

Miura, G., Wang, M.H., Ivers, K.M., and Frishman, L.J. (2009). Retinal pathway origins of the pattern ERG of the mouse. Exp. Eye Res. *89*, 49–62.

Mohan, K., Harper, M.M., Kecova, H., Ye, E.-A., Lazic, T., Sakaguchi, D.S., Kardon, R.H., Grozdanic, S.D., and CR: BioMed Vision Technologies, N.I. (2012). Characterization of structure and function of the mouse retina using pattern electroretinography, pupil light reflex, and optical coherence tomography. Vet. Ophthalmol. *15*, 94–104.

Nair, U., and Klionsky, D.J. (2011). Activation of autophagy is required for muscle homeostasis during physical exercise. Autophagy *7*, 1405–1406.

Nakazawa, T., Kayama, M., Ryu, M., Kunikata, H., Watanabe, R., Yasuda, M., Kinugawa, J., Vavvas, D., and Miller, J.W. (2011). Tumor necrosis factor-alpha mediates photoreceptor death in a rodent model of retinal detachment. Invest. Ophthalmol. Vis. Sci. *52*, 1384–1391.

Nayagam, D.A.X., McGowan, C., Villalobos, J., Williams, R.A., Salinas-LaRosa, C., McKelvie, P., Lo, I., Basa, M., Tan, J., and Williams, C.E. (2013). Techniques for processing eyes implanted with a retinal prosthesis for localized histopathological analysis. J. Vis. Exp. JoVE.

Nelson, C.M., Ackerman, K.M., O'Hayer, P., Bailey, T.J., Gorsuch, R.A., and Hyde, D.R. (2013). Tumor necrosis factor-alpha is produced by dying retinal neurons and is required for Muller glia proliferation during zebrafish retinal regeneration. J. Neurosci. Off. J. Soc. Neurosci. *33*, 6524–6539.

Newman, E., and Reichenbach, A. (1996). The Müller cell: a functional element of the retina. Trends Neurosci. *19*, 307–312.

Ng, C.-P., Zisman, A., and Bonavida, B. (2002). Synergy is achieved by complementation with Apo2L/TRAIL and actinomycin D in Apo2L/TRAIL-mediated apoptosis of prostate cancer cells: Role of XIAP in resistance. The Prostate *53*, 286–299.

Nickells, R.W., and Zack, D.J. (1996). Apoptosis in ocular disease: a molecular overview. Ophthalmic Genet. *17*, 145–165.

Nielsen, O.H., and LaCasse, E.C. (2016). How genetic testing can lead to targeted management of XIAP deficiency-related inflammatory bowel disease. Genet. Med.

Norman, J.C., Narfström, K., and Barrett, P.M. (2008). The effects of medetomidine hydrochloride on the electroretinogram of normal dogs. Vet. Ophthalmol. *11*, 299–305.

Nuñez, G., Benedict, M.A., Hu, Y., and Inohara, N. (1998). Caspases: the proteases of the apoptotic pathway. Oncogene *17*, 3237–3245.

Owens, T.W., Foster, F.M., Valentijn, A., Gilmore, A.P., and Streuli, C.H. (2010). Role for X-linked Inhibitor of Apoptosis Protein Upstream of Mitochondrial Permeabilization. J. Biol. Chem. *285*, 1081–1088.

Petrin, D., Baker, A., Coupland, S.G., Liston, P., Narang, M., Damji, K., Leonard, B., Chiodo, V.A., Timmers, A., Hauswirth, W., et al. (2003). Structural and functional protection of photoreceptors from MNU-induced retinal degeneration by the X-linked inhibitor of apoptosis. Invest. Ophthalmol. Vis. Sci. *44*, 2757–2763.

Petrs-Silva, H., Dinculescu, A., Li, Q., Min, S.-H., Chiodo, V., Pang, J.-J., Zhong, L., Zolotukhin, S., Srivastava, A., Lewin, A.S., et al. (2009). High-efficiency Transduction of the Mouse Retina by Tyrosine-mutant AAV Serotype Vectors. Mol. Ther. J. Am. Soc. Gene Ther. *17*, 463–471.

Plati, J., Bucur, O., and Khosravi-Far, R. (2011). Apoptotic cell signaling in cancer progression and therapy. Integr. Biol. *3*, 279–296.

Porciatti, V. (2015). Electrophysiological assessment of retinal ganglion cell function. Exp. Eye Res. *141*, 164–170.

Pourcho, R.G., and Goebel, D.J. (1988). Substance P-like immunoreactive amacrine cells in the cat retina. J. Comp. Neurol. *275*, 542–552.

Prego, C., García, M., Torres, D., and Alonso, M.J. (2005). Transmucosal macromolecular drug delivery. J. Control. Release Off. J. Control. Release Soc. *101*, 151–162.

Prego, C., Torres, D., Fernandez-Megia, E., Novoa-Carballal, R., Quiñoá, E., and Alonso, M.J. (2006). Chitosan-PEG nanocapsules as new carriers for oral peptide delivery. Effect of chitosan pegylation degree. J. Control. Release Off. J. Control. Release Soc. *111*, 299–308.

Prow, T.W., Bhutto, I., Kim, S.Y., Grebe, R., Merges, C., McLeod, D.S., Uno, K., Mennon, M., Rodriguez, L., Leong, K., et al. (2008). Ocular nanoparticle toxicity and transfection of the retina and retinal pigment epithelium. Nanomedicine Nanotechnol. Biol. Med. *4*, 340–349.

Qi, X., Sun, L., Lewin, A.S., Hauswirth, W.W., and Guy, J. (2007). The Mutant Human ND4 Subunit of Complex I Induces Optic Neuropathy in the Mouse. Invest. Ophthalmol. Vis. Sci. *48*, 1–10.

Rafat, M., Cléroux, C.A., Fong, W.G., Baker, A.N., Leonard, B.C., O'Connor, M.D., and Tsilfidis, C. (2010). PEG-PLA microparticles for encapsulation and delivery of Tat-EGFP to retinal cells. Biomaterials *31*, 3414–3421.

Rajalingam, K., and Dikic, I. (2009). Inhibitors of apoptosis catch ubiquitin. Biochem. J. *417*, e1–e3.

Rapti, K., Louis-Jeune, V., Kohlbrenner, E., Ishikawa, K., Ladage, D., Zolotukhin, S., Hajjar, R.J., and Weber, T. (2012). Neutralizing antibodies against AAV serotypes 1, 2, 6, and 9 in sera of commonly used animal models. Mol. Ther. J. Am. Soc. Gene Ther. *20*, 73–83.

Raymond, P.A., Barthel, L.K., Bernardos, R.L., and Perkowski, J.J. (2006). Molecular characterization of retinal stem cells and their niches in adult zebrafish. BMC Dev. Biol. *6*, 36.

Remé, C.E., Grimm, C., Hafezi, F., Wenzel, A., and Williams, T.P. (2000). Apoptosis in the Retina: The Silent Death of Vision. News Physiol. Sci. Int. J. Physiol. Prod. Jointly Int. Union Physiol. Sci. Am. Physiol. Soc. *15*, 120–124.

Renwick, J., Narang, M.A., Coupland, S.G., Xuan, J.Y., Baker, A.N., Brousseau, J., Petrin, D., Munger, R., Leonard, B.C., Hauswirth, W.W., et al. (2005). XIAP-mediated neuroprotection in retinal ischemia. Gene Ther. *13*, 339–347.

Roh, M.I., Murakami, Y., Thanos, A., Vavvas, D.G., and Miller, J.W. (2011). Edaravone, an ROS scavenger, ameliorates photoreceptor cell death after experimental retinal detachment. Invest. Ophthalmol. Vis. Sci. *52*, 3825–3831.

Roll, P., Reich, M.E., and Hofmann, H. (1975). [The course of zonular fibers in the area of pars plicata corporis cilaris pars plana, ora serrata and retina. Eectron microsocpic study]. Albrecht Von Graefes Arch. Für Klin. Exp. Ophthalmol. Albrecht Von Graefes Arch. Clin. Exp. Ophthalmol. *194*, 109–123.

Sabet-Peyman, E.J., Khaderi, K.R., and Sadun, A.A. (2012). Is Leber hereditary optic neuropathy treatable? Encouraging results with idebenone in both prospective and retrospective trials and an illustrative case. J. Neuro-Ophthalmol. Off. J. North Am. Neuro-Ophthalmol. Soc. *32*, 54–57.

Sadun, A.A., La Morgia, C., and Carelli, V. (2011). Leber's Hereditary Optic Neuropathy. Curr. Treat. Options Neurol. *13*, 109–117.

Sakai, T., Tsuneoka, H., Lewis, G.P., and Fisher, S.K. (2014). Remodelling of retinal on- and off-bipolar cells following experimental retinal detachment. Clin. Experiment. Ophthalmol. *42*, 480–485.

Savill, J., Dransfield, I., Gregory, C., and Haslett, C. (2002). A blast from the past: clearance of apoptotic cells regulates immune responses. Nat. Rev. Immunol. *2*, 965–975.

Schile, A.J., García-Fernández, M., and Steller, H. (2008). Regulation of apoptosis by XIAP ubiquitin-ligase activity. Genes Dev. *22*, 2256–2266.

Schneider, C.A., Rasband, W.S., and Eliceiri, K.W. (2012). NIH Image to ImageJ: 25 years of image analysis. Nat. Methods *9*, 671–675.

Schuler, M., Bossy-Wetzel, E., Goldstein, J.C., Fitzgerald, P., and Green, D.R. (2000). p53 induces apoptosis by caspase activation through mitochondrial cytochrome c release. J. Biol. Chem. *275*, 7337–7342.

Semeraro, F., Morescalchi, F., Duse, S., Gambicorti, E., Russo, A., and Costagliola, C. (2015). Current Trends about Inner Limiting Membrane Peeling in Surgery for Epiretinal Membranes. J. Ophthalmol. *2015*, 671905.

Shankar, S.P., Fingert, J.H., Carelli, V., Valentino, M.L., King, T.M., Daiger, S.P., Salomao, S.R., Berezovsky, A., Belfort, R., Braun, T.A., et al. (2008). Evidence for a novel x-linked modifier locus for leber hereditary optic neuropathy. Ophthalmic Genet. *29*, 17–24.

Silke, J., and Meier, P. (2013). Inhibitor of Apoptosis (IAP) Proteins–Modulators of Cell Death and Inflammation. Cold Spring Harb. Perspect. Biol. *5*, a008730.

Silke, J., and Vucic, D. (2014). IAP family of cell death and signaling regulators. Methods Enzymol. *545*, 35–65.

Silke, J., Kratina, T., Ekert, P.G., Pakusch, M., and Vaux, D.L. (2004). Unlike Diablo/smac, Grim promotes global ubiquitination and specific degradation of X chromosome-linked inhibitor of apoptosis (XIAP) and neither cause apoptosis. J. Biol. Chem. *279*, 4313–4321.

Simonelli, F., Maguire, A.M., Testa, F., Pierce, E.A., Mingozzi, F., Bennicelli, J.L., Rossi, S., Marshall, K., Banfi, S., Surace, E.M., et al. (2010). Gene therapy for Leber's congenital amaurosis is safe and effective through 1.5 years after vector administration. Mol. Ther. J. Am. Soc. Gene Ther. *18*, 643–650.

Stockton, R.A., and Slaughter, M.M. (1989). B-wave of the electroretinogram. A reflection of ON bipolar cell activity. J. Gen. Physiol. *93*, 101–122.

Strauss, O. (2005). The Retinal Pigment Epithelium in Visual Function. Physiol. Rev. *85*, 845–881.

Sun, S.-C. (2011). Non-canonical NF-κB signaling pathway. Cell Res. *21*, 71–85.

Suzuki, Y., Imai, Y., Nakayama, H., Takahashi, K., Takio, K., and Takahashi, R. (2001). A serine protease, HtrA2, is released from the mitochondria and interacts with XIAP, inducing cell death. Mol. Cell *8*, 613–621.

Tait, S.W.G., Oberst, A., Quarato, G., Milasta, S., Haller, M., Wang, R., Karvela, M., Ichim, G., Yatim, N., Albert, M.L., et al. (2013). Widespread mitochondrial depletion via mitophagy does not compromise necroptosis. Cell Rep. *5*, 878–885.

Takahashi, R., Deveraux, Q., Tamm, I., Welsh, K., Assa-Munt, N., Salvesen, G.S., and Reed, J.C. (1998). A Single BIR Domain of XIAP Sufficient for Inhibiting Caspases. J. Biol. Chem. *273*, 7787–7790.

Tan, E., Ding, X.-Q., Saadi, A., Agarwal, N., Naash, M.I., and Al-Ubaidi, M.R. (2004a). Expression of Cone-Photoreceptor–Specific Antigens in a Cell Line Derived from Retinal Tumors in Transgenic Mice. Invest. Ophthalmol. Vis. Sci. *45*, 764–768.

Tan, E., Ding, X.-Q., Saadi, A., Agarwal, N., Naash, M.I., and Al-Ubaidi, M.R. (2004b). Expression of Cone-Photoreceptor-Specific Antigens in a Cell Line Derived from Retinal Tumors in Transgenic Mice. Invest. Ophthalmol. Vis. Sci. *45*, 764–768.

Taylor, R.C., Cullen, S.P., and Martin, S.J. (2008). Apoptosis: controlled demolition at the cellular level. Nat. Rev. Mol. Cell Biol. *9*, 231–241.

Tenev, T., Bianchi, K., Darding, M., Broemer, M., Langlais, C., Wallberg, F., Zachariou, A., Lopez, J., MacFarlane, M., Cain, K., et al. (2011). The Ripoptosome, a Signaling Platform that Assembles in Response to Genotoxic Stress and Loss of IAPs. Mol. Cell *43*, 432–448.

Testa, F., Maguire, A.M., Rossi, S., Pierce, E.A., Melillo, P., Marshall, K., Banfi, S., Surace, E.M., Sun, J., Acerra, C., et al. (2013). Three-year follow-up after unilateral subretinal delivery of adeno-associated virus in patients with Leber congenital Amaurosis type 2. Ophthalmology *120*, 1283–1291.

Thanou, M., Verhoef, J.C., and Junginger, H.E. (2001). Chitosan and its derivatives as intestinal absorption enhancers. Adv. Drug Deliv. Rev. *50 Suppl 1*, S91–S101.

Timmers, A.M., Zhang, H., Squitieri, A., and Gonzalez-Pola, C. (2001). Subretinal injections in rodent eyes: effects on electrophysiology and histology of rat retina. Mol. Vis. *7*, 131–137.

Torres-Bacete, J., Sinha, P.K., Matsuno-Yagi, A., and Yagi, T. (2011). Structural contribution of C-terminal segments of NuoL (ND5) and NuoM (ND4) subunits of complex I from Escherichia coli. J. Biol. Chem. *286*, 34007–34014.

Towers, C.G., and Thorburn, A. (2016). Therapeutic Targeting of Autophagy. EBioMedicine.

Tran, S.E., Holmstrom, T.H., Ahonen, M., Kahari, V.M., and Eriksson, J.E. (2001). MAPK/ERK overrides the apoptotic signaling from Fas, TNF, and TRAIL receptors. J. Biol. Chem. *276*, 16484–16490.

Travis, G.H. (1998). Mechanisms of cell death in the inherited retinal degenerations. Am. J. Hum. Genet. *62*, 503–508.

Trichonas, G., Murakami, Y., Thanos, A., Morizane, Y., Kayama, M., Debouck, C.M., Hisatomi, T., Miller, J.W., and Vavvas, D.G. (2010). Receptor interacting protein kinases mediate retinal detachment-induced photoreceptor necrosis and compensate for inhibition of apoptosis. Proc. Natl. Acad. Sci. U. S. A. *107*, 21695–21700.

Tuohy, G., Millington-Ward, S., Kenna, P.F., Humphries, P., and Farrar, G.J. (2002). Sensitivity of photoreceptor-derived cell line (661W) to baculoviral p35, Z-VAD.FMK, and Fas-associated death domain. Invest. Ophthalmol. Vis. Sci. *43*, 3583–3589.

Uva, M.G., Di Pietro, M., Longo, A., Lauretta, K., Reibaldi, M., and Reibaldi, A. (2013). Pattern ERG and RNFL thickness in hypertensive eyes with normal blue-yellow visual field. Graefes Arch. Clin. Exp. Ophthalmol. Albrecht Von Graefes Arch. Für Klin. Exp. Ophthalmol. *251*, 839–845.

Varfolomeev, E., Blankenship, J.W., Wayson, S.M., Fedorova, A.V., Kayagaki, N., Garg, P., Zobel, K., Dynek, J.N., Elliott, L.O., Wallweber, H.J.A., et al. (2007). IAP antagonists induce autoubiquitination of c-IAPs, NF-kappaB activation, and TNFalpha-dependent apoptosis. Cell *131*, 669–681.

Veleri, S., Lazar, C.H., Chang, B., Sieving, P.A., Banin, E., and Swaroop, A. (2015). Biology and therapy of inherited retinal degenerative disease: insights from mouse models. Dis. Model. Mech. *8*, 109–129.

Vince, J.E., Wong, W.W.-L., Khan, N., Feltham, R., Chau, D., Ahmed, A.U., Benetatos, C.A., Chunduru, S.K., Condon, S.M., McKinlay, M., et al. (2007). IAP antagonists target cIAP1 to induce TNFalpha-dependent apoptosis. Cell *131*, 682–693.

Vince, J.E., Wong, W.W.-L., Gentle, I., Lawlor, K.E., Allam, R., O'Reilly, L., Mason, K., Gross, O., Ma, S., Guarda, G., et al. (2012). Inhibitor of Apoptosis Proteins Limit RIP3 Kinase-Dependent Interleukin-1 Activation. Immunity *36*, 215–227.

Vincent, A., Robson, A.G., and Holder, G.E. (2013). Pathognomonic (diagnostic) ERGs. A review and update. Retina Phila. Pa *33*, 5–12.

Vucic, D., Dixit, V.M., and Wertz, I.E. (2011). Ubiquitylation in apoptosis: a post-translational modification at the edge of life and death. Nat. Rev. Mol. Cell Biol. *12*, 439–452.

Wang, M., Crosby, A., Hastie, E., Samulski, J.J., McPhee, S., Joshua, G., Samulski, R.J., and Li, C. (2015). Prediction of adeno-associated virus neutralizing antibody activity for clinical application. Gene Ther. *22*, 984–992.

Wang, X.H., Li, D.P., Wang, W.J., Feng, Q.L., Cui, F.Z., Xu, Y.X., Song, X.H., and van der Werf, M. (2003). Crosslinked collagen/chitosan matrix for artificial livers. Biomaterials *24*, 3213–3220.

Wassmer, S., Leonard, B.C., Coupland, S.G., Baker, A., Hamilton, J., Torlone, R., Zacks, D.N., and Tsilfidis, C. (2016). The Development of a Cat Model of Retinal Detachment and Re-attachment. Adv. Exp. Med. Biol. *854*, 315–321.

Weleber, R.G., Pennesi, M.E., Wilson, D.J., Kaushal, S., Erker, L.R., Jensen, L., McBride, M.T., Flotte, T.R., Humphries, M., Calcedo, R., et al. (2016). Results at 2 Years after Gene Therapy for RPE65-Deficient Leber Congenital Amaurosis and Severe Early-Childhood–Onset Retinal Dystrophy. Ophthalmology *123*, 1606–1620.

Wilkinson, J.C., Wilkinson, A.S., Galbán, S., Csomos, R.A., and Duckett, C.S. (2008). Apoptosis-Inducing Factor Is a Target for Ubiquitination through Interaction with XIAP. Mol. Cell. Biol. *28*, 237–247.

Wong, A., and Cortopassi, G. (1997). mtDNA mutations confer cellular sensitivity to oxidant stress that is partially rescued by calcium depletion and cyclosporin A. Biochem. Biophys. Res. Commun. *239*, 139–145.

Wong, A., Cavelier, L., Collins-Schramm, H.E., Seldin, M.F., McGrogan, M., Savontaus, M.-L., and Cortopassi, G.A. (2002). Differentiation-specific effects of LHON mutations introduced into neuronal NT2 cells. Hum. Mol. Genet. *11*, 431–438.

World Health Organization (2010). WHO | What is VISION 2020?

Yabal, M., and Jost, P.J. (2015). XIAP as a regulator of inflammatory cell death: the TNF and RIP3 angle. Mol. Cell. Oncol. *2*, e964622.

Yabal, M., Müller, N., Adler, H., Knies, N., Groß, C.J., Damgaard, R.B., Kanegane, H., Ringelhan, M., Kaufmann, T., Heikenwälder, M., et al. (2014). XIAP restricts TNF- and RIP3-dependent cell death and inflammasome activation. Cell Rep. *7*, 1796–1808.

Yagi, K., Michibayashi, N., Kurikawa, N., Nakashima, Y., Mizoguchi, T., Harada, A., Higashiyama, S., Muranaka, H., and Kawase, M. (1997). Effectiveness of fructose-modified chitosan as a scaffold for hepatocyte attachment. Biol. Pharm. Bull. *20*, 1290–1294.

Yang, H., Wang, R., Gu, Q., and Zhang, X. (2008). Feasibility study of chitosan as intravitreous tamponade material. Graefes Arch. Clin. Exp. Ophthalmol. Albrecht Von Graefes Arch. Für Klin. Exp. Ophthalmol. *246*, 1097–1105.

Yang, L., Bula, D., Arroyo, J.G., and Chen, D.F. (2004). Preventing retinal detachment-associated photoreceptor cell loss in Bax-deficient mice. Invest. Ophthalmol. Vis. Sci. *45*, 648–654.

Yang, Q.-H., Church-Hajduk, R., Ren, J., Newton, M.L., and Du, C. (2003). Omi/HtrA2 catalytic cleavage of inhibitor of apoptosis (IAP) irreversibly inactivates IAPs and facilitates caspase activity in apoptosis. Genes Dev. *17*, 1487–1496.

Yang, Y., Fang, S., Jensen, J.P., Weissman, A.M., and Ashwell, J.D. (2000). Ubiquitin protein ligase activity of IAPs and their degradation in proteasomes in response to apoptotic stimuli. Science *288*, 874–877.

Yao, J., Feathers, K.L., Khanna, H., Thompson, D., Tsilfidis, C., Hauswirth, W.W., Heckenlively, J.R., Swaroop, A., and Zacks, D.N. (2011). XIAP Therapy Increases Survival of Transplanted Rod Precursors in a Degenerating Host Retina. Invest. Ophthalmol. Vis. Sci. *52*, 1567–1572.

Yao, J., Jia, L., Khan, N., Zheng, Q.-D., Moncrief, A., Hauswirth, W.W., Thompson, D.A., and Zacks, D.N. (2012). Caspase inhibition with XIAP as an adjunct to AAV vector gene-replacement therapy: improving efficacy and prolonging the treatment window. PloS One *7*, e37197.

Yao, J., Jia, L., Feathers, K., Lin, C., Khan, N.W., Klionsky, D.J., Ferguson, T.A., and Zacks, D.N. (2016). Autophagy-mediated catabolism of visual transduction proteins prevents retinal degeneration. Autophagy *12*, 2439–2450.

Yap, G.H., Chen, L.Y., Png, R., Loo, J.L., Tow, S., Mathur, R., and Chia, A. (2015). Clinical value of electrophysiology in determining the diagnosis of visual dysfunction in neuro-ophthalmology patients. Doc. Ophthalmol. Adv. Ophthalmol.

Yokoyama, T., Liou, G.I., Caldwell, R.B., and Overbeek, P.A. (1992). Photoreceptor-specific activity of the human interphotoreceptor retinoid-binding protein (IRBP) promoter in transgenic mice. Exp. Eye Res. *55*, 225–233.

Yorimitsu, T., and Klionsky, D. (2005). Autophagy: molecular machinery for self-eating. Cell Death Differ. *12*, 1542–1552.

Yu, H., Koilkonda, R.D., Chou, T.-H., Porciatti, V., Ozdemir, S.S., Chiodo, V., Boye, S.L., Boye, S.E., Hauswirth, W.W., Lewin, A.S., et al. (2012a). Gene delivery to mitochondria by targeting modified adenoassociated virus suppresses Leber's hereditary optic neuropathy in a mouse model. Proc. Natl. Acad. Sci. U. S. A. *109*, E1238–E1247.

Yu, H., Ozdemir, S.S., Koilkonda, R.D., Chou, T.-H., Porciatti, V., Chiodo, V., Boye, S.L., Hauswirth, W.W., Lewin, A.S., and Guy, J. (2012b). Mutant NADH dehydrogenase subunit 4 gene delivery to mitochondria by targeting sequence-modified adeno-associated virus induces visual loss and optic atrophy in mice. Mol. Vis. *18*, 1668.

Yu, H., Koilkonda, R.D., Chou, T.-H., Porciatti, V., Ozdemir, S.S., Chiodo, V., Boye, S.L., Boye, S.E., Hauswirth, W.W., Lewin, A.S., et al. (2012c). Gene delivery to mitochondria by targeting modified adenoassociated virus suppresses Leber's hereditary optic neuropathy in a mouse model. Proc. Natl. Acad. Sci. U. S. A. *109*, E1238–E1247.

Yu, H., Koilkonda, R.D., Chou, T.-H., Porciatti, V., Mehta, A., Hentall, I.D., Chiodo, V.A., Boye, S.L., Hauswirth, W.W., Lewin, A.S., et al. (2015). Consequences of zygote injection and germline transfer of mutant human mitochondrial DNA in mice. Proc. Natl. Acad. Sci. U. S. A. *112*, E5689–E5698.

Yurco, P., and Cameron, D.A. (2005). Responses of Müller glia to retinal injury in adult zebrafish. Vision Res. *45*, 991–1002.

Yu-Wai-Man, P., Votruba, M., Moore, A.T., and Chinnery, P.F. (2014). Treatment strategies for inherited optic neuropathies: past, present and future. Eye *28*, 521–537.

Zacks, D.N., Hänninen, V., Pantcheva, M., Ezra, E., Grosskreutz, C., and Miller, J.W. (2003). Caspase Activation in an Experimental Model of Retinal Detachment. Invest. Ophthalmol. Vis. Sci. *44*, 1262–1267.

Zacks, D.N., Zheng, Q.-D., Han, Y., Bakhru, R., and Miller, J.W. (2004). FAS-mediated apoptosis and its relation to intrinsic pathway activation in an experimental model of retinal detachment. Invest. Ophthalmol. Vis. Sci. *45*, 4563–4569.

Zadro-Lamoureux, L.A., Zacks, D.N., Baker, A.N., Zheng, Q.-D., Hauswirth, W.W., and Tsilfidis, C. (2009). XIAP effects on retinal detachment-induced photoreceptor apoptosis [corrected]. Invest. Ophthalmol. Vis. Sci. *50*, 1448–1453.

Zamzami, N., and Kroemer, G. (2001). The mitochondrion in apoptosis: how Pandora's box opens. Nat. Rev. Mol. Cell Biol. *2*, 67–71.

Zarnegar, B.J., Wang, Y., Mahoney, D.J., Dempsey, P.W., Cheung, H.H., He, J., Shiba, T., Yang, X., Yeh, W.-C., Mak, T.W., et al. (2008). Noncanonical NF-kappaB activation requires coordinated assembly of a regulatory complex of the adaptors cIAP1, cIAP2, TRAF2 and TRAF3 and the kinase NIK. Nat. Immunol. *9*, 1371–1378.

Zeng, H., Tso, M.O.M., Lai, S., and Lai, H. (2008). Activation of nuclear factor-κB during retinal degeneration in rd Mice. Mol. Vis. *14*, 1075–1080.

Zhang, L., and Fang, B. (2004). Mechanisms of resistance to TRAIL-induced apoptosis in cancer. Cancer Gene Ther. *12*, 228–237.

Zhao, S., Chen, Q., Hung, F.-C., and Overbeek, P.A. (2002). BMP signaling is required for development of the ciliary body. Development *129*, 4435–4442.

Zhou, R., and Caspi, R.R. (2010). Ocular immune privilege. F1000 Biol. Rep. *2*.

Zolotukhin, S., Potter, M., Zolotukhin, I., Sakai, Y., Loiler, S., Fraites, T.J., Chiodo, V.A., Phillipsberg, T., Muzyczka, N., Hauswirth, W.W., et al. (2002). Production and purification of serotype 1, 2, and 5 recombinant adeno-associated viral vectors. Methods San Diego Calif *28*, 158–167.

APPENDICES

APPENDIX A: Microarray

In 661W cone photoreceptor cells, there were 226 genes up-regulated and 206 genes down-regulated when XIAP was over-expressed by plasmid transfection. When the same cell lines are treated with TNF-α for 24 hours to induce apoptosis, there were 175 genes up-regulated and 143 genes down-regulated. As is evident by the heat-map below, about half of the genes completely change expression patterns when treated with TNF-α. Differentially expressed genes, such as the pro-apoptotic BCL2 family member, Bim, were validated and showed that reduced expression levels as the level of XIAP increased. An apoptosis array also revealed novel targets for future work such as neuronal apoptosis inhibitor family 1 (NAIP1) and Akt1 (serine-threonine protein kinase).

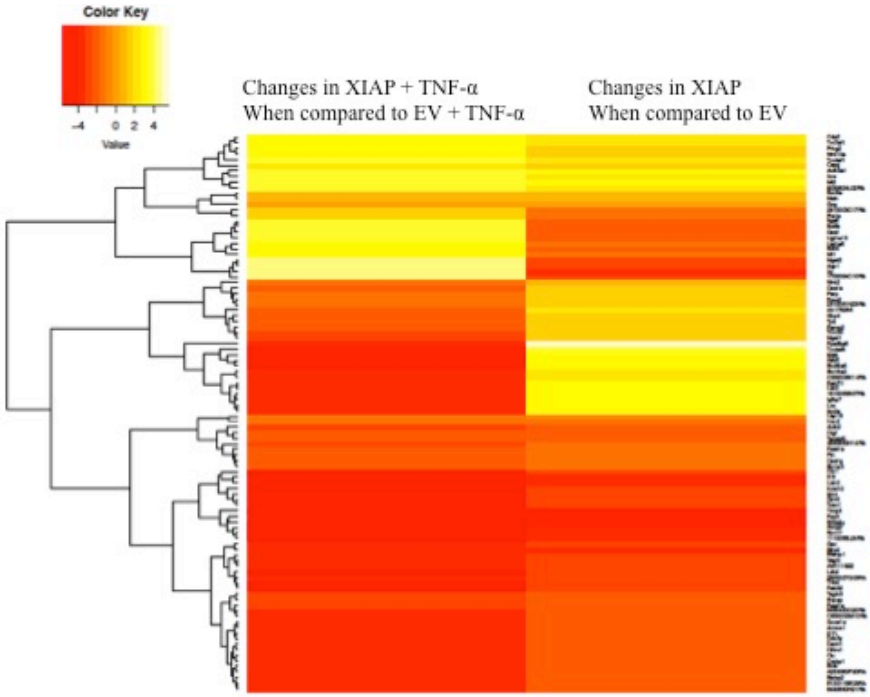

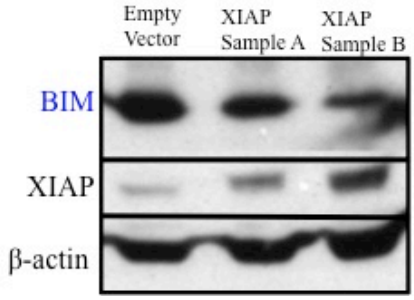

APPENDIX A PROTOCOL.

The microarray experiment was conducted as described in (Alvarez-Saavedra et al., 2014). RNA samples (XIAP/EV and XIAP+TNF/EV+TNF) were first labeled with Cy5 or Cy3 by use of 3DNA Array 900 kits (Genisphere) according to manufacturers protocols. MEEBO 38.5K arrays (mouse microarray slides) were then pre-washed in warmed 2xSSC/0.2% SDS buffer, warm blocking solution (water, 5xSSC, SDS and BSA) for 30 minutes, followed by a rinse with distilled water. The arrays were spun (800RPM, 3 min), prewarmed to 42 degrees and incubated with 50ul of cDNA in the hybridization chamber overnight. The next day, the microarray slides were washed with 2xSSC/0.2% SDS and 0.2xSSC/0.2%SSC, rinsed in water, and spun at 800RPM for 5 minutes. The second part of the 3DNA hybridization protocol was conducted, followed by washing of the slides (similar to above), and the slides were then scanned using the ScanArray express (Perkin Elmer). Results were analyzed with global loess, inter-array normalization with the quantile method and statistical analysis by Web Array (http://www.webarraydb.org/webarray/index.html). In each experiment, two arrays were used, one with Cy3 for the control and Cy5 for the treated cells, and the second using the reverse (Cy5 for the control and Cy3 for the treated) in order to prevent any false positives. These results were then normalized to the control. M ($\log_2$ ratio of XIAP/EV signal) and A values ($\log_2$ average signal strength) were then determined for all genes. A gene was scored as differentially expressed on an array if it demonstrated a *P*-value <0.01, an A value >8 and M (fold change) >2. In addition to microarray experiments, we also analyzed the results of XIAP-661W and EV-661W in an apoptotic qPCR-array (SABioscience).

APPENDIX B: Microparticles

Following the same protocols found in Chapter 5, a new batch of chitosan microparticles encapsulated with TAT-eGFP was generated. Microparticles were rinsed in water to remove their adhesive properties, and incubated with 661W cells for 24 and 48 hours, at the high concentration of 10 mg/mL (A). Cell viability was assessed after 24 and 48 hours. There was no cell death at either time-point, and 48 hours of incubation is shown here (B). Furthermore, the immunofluorescence protocol appears to have washed away most of the particles as very little fluorescence was seen in the brightfield (C) and GFP (D) images. This suggests that the rinsing reduced the adhesive nature of the particles.